Mn - DOPED $BaTiO_3$

A Thesis Submitted
In Partial Fulfilment of the Requirements
for the Degree of
MASTER OF TECHNOLOGY

By
L. M. ARUNACHALAM

to the
INTERDISCIPLINARY PROGRAMME IN MATERIALS SCIENCE
INDIAN INSTITUTE OF TECHNOLOGY, KANPUR
JANUARY, 1983

MS-1903-M-ARU-DOP

CERTIFICATE

Certified that this work on 'Mn-doped $BaTiO_3$' by Mr. L.M. Arunachalam has been carried out under my supervision and that this has not been submitted elsewhere for a degree.

E.C. Subbarao
Professor
Department of Metallurgical Engineering
Indian Institute of Technology
KANPUR.

ACKNOWLEDGEMENTS

I am grateful to Professor E.C. Subbarao for his excellent guidence and encouragement throughout the course of this work. It is a great pleasure to work under such a dextrous person who has shown me the path of perfect research.

I am indebted to Professor D. Chakravorthy for his excellent guidence during the earlier stages of this work.

I am thankful to Professor K.P. Gupta for his timely advices and suggestions during the final stages of this work.

I sincerely acknowledge the help of Mrs. Padmavati Shankar, for doing the chemical analysis, and Mr. K. Umesh Kumar for his cooperation and suggestions, and their timely help towards the last stage of this work.

I wish to express my appreciation towards Mr. V.P. Srivastava for his help in setting-up various systems of this work and the useful advices provided at different stages of this work.

I am thankful to Mr. B. Sharma, Mr. S.R. Chaurasia, Mr. U.S. Lal, Mr. A.N. Prasad, Mr. S.N. Muddukrishna, Mr. K.S. Kesava Murthi, Mr. B.A.R.C. Murthy, Mr. S.C. Barthwal, Mr. K. Rajagopalan, Mr. V. Srikant, and Mr. S.K. Mukherjee for their timely help throughtout the course of this work.

I wish to thank my friend Dr. S. Shankar for the valuable discussions during the sample preparation of this work.

I wish to express my gratitude towards Mr. R.N. Srivastava, Mr. Vishwanath Singh and Mr. V.P. Gupta for their help in getting this thesis in the printed form. Their unselfish cooperation is never forgettable.

The financial support of the Department of Electronics, Government of India is gratefully acknowledged.

Finally, I would like to thank my friends Dr. E.M.T. Velu, Mr. U. Ramakrishna, Mr. S. Bhattacharji, Mr. R. Chowdary, Mr. S. Pandian and Mr. T. Arul Mozhi for their cooperation and kind company.

L.M. ARUNACHALAM

To

MY PARENTS,

BROTHERS and SISTER.

" SCIENTIFIC INVESTIGATION BEGINS

WITH SIMPLE OBSERVATIONS "

CONTENTS

LIST OF TABLES

LIST OF FIGURES

ABSTRACT

A reasonably good dielectric composition of Mn-doped $BaTiO_3$ for Base Metal Electrode (BME) technology had been developed by oxalate method. An explanation was given for the suspected mechanism involved with doping of Mn into the Barium Titanyl compound. Detailed domain stabilization studies were done. It was found that the stabilization has got improved by quenching from the higher temperatures and heat treating in the low partial pressure of oxygen. The influence of Mn on the decomposition of Barium Titanyl oxalate was studied by simultaneous DTA and TGA. Successful use of IR technique to detect the Mn in the Barium Titanyl oxalate was done. Variation of the resistivity with the various partial pressure of oxygen was studied with the application of the BME multilayer capacitor in mind. Nickel electroded BME disc capacitors were produced with good properties. A dielectric composition i.e. $BaTiO_3$ having 0.6 cationic mole percent of Mn of the developed sample and 2.0 cationic mole percent of the coprecipitated sample were found to be most suitable for making BME capacitors, the same 0.6 mole percent could be used to produce multilayer capacitor with base metals.

I. INTRODUCTION

The ferroelectric nature of the ceramic materials has been extensively exploited in making ceramic capacitor which appeared nearly four decades ago. The principal reason is due to the presence of high dielectric constant in these materials. Barium Titanate, an important representative of a family of ferroelectric materials, was the first ferroelectric ceramic developed and is still used widely. Obviously the reasons for this are, apart from its high dielectric constant, (i) it is chemically and mechanically stable, (ii) it has a wide temperature range of operation i.e. it exhibits ferroelectric properties at and above room temperature, and (iii) it has the advantage of easy manufacturing technique in the form of polycrystalline ceramic samples.

We know that the capacitance of a parallel plate condensor is directly proportional to the electrode area and inversely proportional to the sample thickness. So by increasing the electrode area and by decreasing the dielectric material thickness a high value capacitor could be achieved. But due to the brittle nature of the ceramic materials the capacitors with a large area and small thickness are very fragile and cannot be used without any mechanical support. The drive towards the miniaturization led to the development of (i) multilayer capacitors and (ii) internal boundary layer capacitors.

I.1. MULTILAYER CAPACITORS:

A multilayer capacitor consists of alternating layers of insulating ceramic of 25 μm thickness and conducting electrodes of 2 μm thickness. Such thin ceramic layers can be processed because the mechanical stability is assured by stacking the layers upon each other in the form of plastic foils with metal paste printed on them before the unit is sintered as a whole. Figure I.1 shows a schematic representation of a multilayer capacitor. These are generally rectangular in shape with parallel electrodes brought out at the narrow ends of the rectangle. To prevent the edge breakdown a margin of bare dielectric is allowed around each plate. The whole arrangement is very compact and has high volumetric efficiency. The whole stack is sintered around 1350°C, which necessitates the use of high melting point metals like Pd, Pt or their alloys as the electrodes.

The most common and important characteristics of a multilayer capacitor to be appreciated are capacitance value, rated voltage, the stability of capacitance with respect to temperature and voltage and lastly the dielectric aging.

I.2. INTERNAL BOUNDARY LAYER (IBL) CAPACITORS:

Commercial capacitors are usually manufactured from titanate based materials of the perovskite (ABX_3) family, which are made semiconducting (n-type) by aliovalent chemical substitution, gaseous reduction, cr combination thereof. Resistivity distributions are developed within the microstructure by boundary counter diffusion, or by sintering in

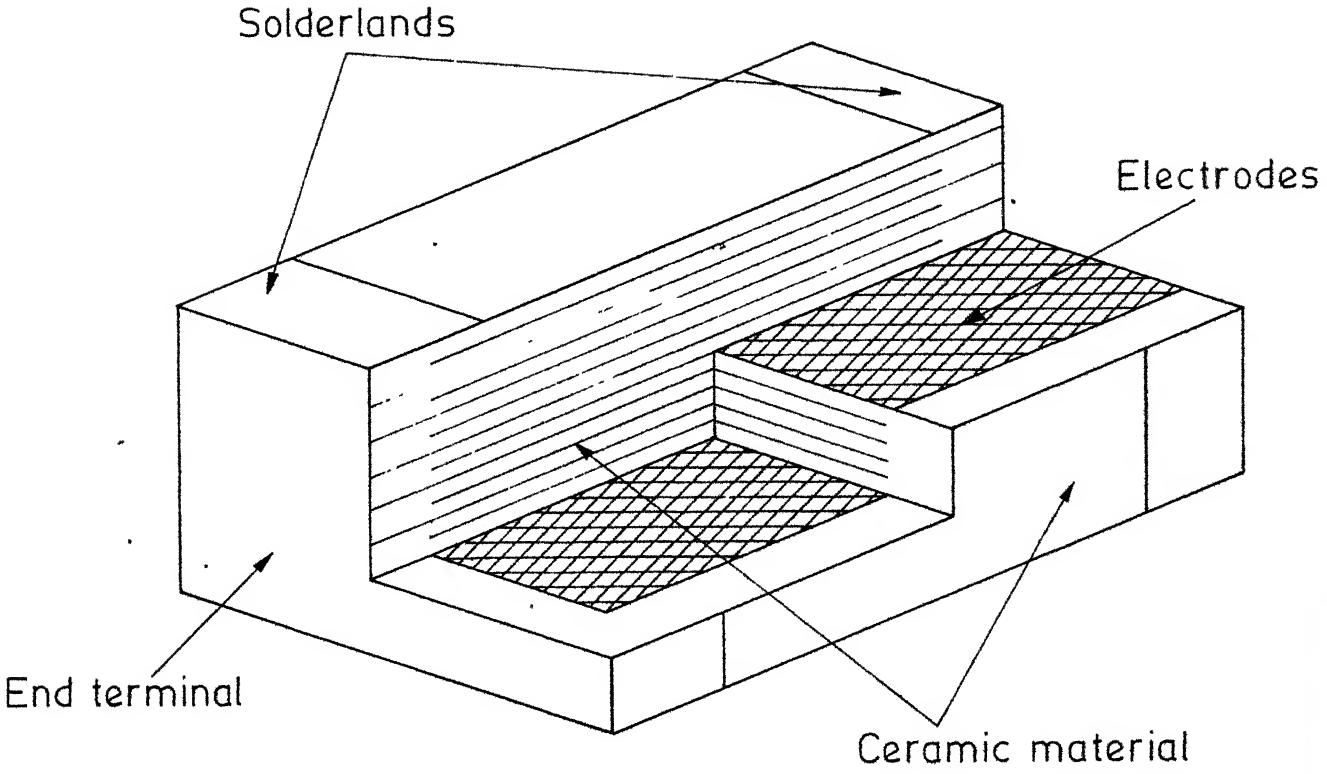

Fig. I .1. Schematic representation of a multilayer capacitor.

the presence of a liquid phase which solidifies on cooling into an insulator. Ideally, the former method is characterized by grain to grain contact, with interfacial compensation states, and the latter by grain to grain separation with an insulating intergrannular phase. Anomalously high apparent dielectric constants (over 20,000) calculated for IBL capacitors are generally attributed to enhanced space charge polarization processes taking place between semiconducting grains and resistive boundaries.

There are certain problems to be tackled in the development of these capacitors (1).

I.3. ELECTRODE PROBLEMS:

The usability of a metal as an electrode material in monolithics is determined by two properties: (i) its melting point and this should be higher than the sintering temperature of the ceramic and (ii) its metal/metal oxide equilibrium oxygen vapour pressure and this should be higher than that of the oxygen partial pressure during firing.

Normally the capacitor is sintered in air at temperatures higher than 1300°C, and therefore only high melting noble metals like Pd (m.p. 1552°C), Pt (m.p. 1769°C) or alloys thereof can be used for the electrodes. Consequently any multilayer capacitors must be an inherently expensive device.

There are two possible technological solutions to tackle this problem and they are (i) liquid phase sintering and (ii) base metal electrodes.

I.3.1. Liquid Phase Sintering:

In this the technique involved is by using a transient liquid phase, the sintering temperature of the ceramic dielectric can be lowered from the usual 1300-1400°C to below the melting temperature of Ag or one of the low melting Ag-Pd alloys and thereby the noble metals like Pt and Pd as the electrode material could be avoided. The liquid phase should possess the properties viz.

(i) it should not react with the dielectric composition,

(ii) it should melt at or below 800-900°C,

(iii) the crystalline phase, formed on cooling, should preferably have a relatively high dielectric constant, so that the dielectric constant of the composite is not too greatly decreased, and

(iv) the viscosity of the liquid should be low at the sintering temperature so that the amount of liquid phase is kept to a minimum. Lead germanate (2), CuO (3) and Bismuth Borate systems (4) have been used as liquid phase materials.

Generally the disadvantages involved are that the liquid phase diffuses into the $BaTiO_3$ lattice and thereby decreases the dielectric constant value at room temperature and poor densification of the ceramic dielectric at the temperatures that required to avoid the oxidation of Ag (m. p. 961°C).

I.3.2. Base Metal Electrodes:

In the BME technology, a base metal, such as nickel, has a melting point higher than the sintering temperatures employed in capacitor manufacture and is much cheaper than Pd or even Ag. However, at the sintering temperatures, Ni oxidizes to NiO and in the process reduces $BaTiO_3$ by converting a corresponding number of Ti^{4+} ions to the Ti^{3+} state. The presence of Ti in two valence states on crystallographically equivalent sites lead to large electronic conductivity and the ceramic is no longer useful as a dielectric. The oxidation of Ni may be prevented by sintering the multilayer capacitors in a reducing atmosphere, but this again causes the reduction of the titanate ceramic.

The incorporation of manganese ions into the barium titanate lattice has been found to prevent reduction of barium titanate, when it is fired in an atmosphere reducing enough to inhibit the oxidation of nickel. It was found that the Mn-doped barium titanate is the most effective dielectric composition that can be applied with base metals (5, 6, 10-13).

By using the BME technology, not only the multilayer chips but also the disc capacitors could be produced at relatively low cost. One of the most significant aspects of base metal electrode capacitors is the possibility of building very large capacitance values economically. Since the total electrode area and thus the metal content of a capacitor increases in direct proportion to capacitance,

precious metal costs quickly become prohibitive as capacitance values increase (Table I.1).

Thus it is obvious from Table I.1 that BME technology can extend the range of capacitance values that can be economically produced by at least two orders of magnitude.

TABLE I.1. Variation of the cost of the electrode material with capacitance value(6)

Capacitance	Metal cost				
	Pt ₹ 140	75Pd 25Pt ₹ 106	Pd ₹ 41	70Pd 30Ag ₹ 15.10	Ni ₹ 0.15
0.01 μF	0.006	0.005	0.002	0.001	0.000
0.10 μF	0.060	0.045	0.018	0.006	0.000
1.00 μF	0.600	0.454	0.176	0.064	0.001
10.00 μF	6.000	4.540	1.760	0.647	0.006
100.00 μF	60.000	45.400	17.600	6.470	0.064

The other advantages of using base metals such as nickel over conventional electrode materials such as silver are: (i) their non-migratory nature; (ii) lack of dissolution in soft solders; (iii) greater resistance towards humidity; (iv) extension of the life of the capacitor and (v) possibility of sintering dielectric with the base metal (since melting points are higher compared to silver). This obviates the electrode firing step which has to be carried out separately in case of silver electrodes whereas the obvious

disadvantage is that the base metals have higher resistivity values compared to precious metals, thus increasing the series resistance and in turn dissipation factor of the capacitor, but this can be easily compensated by their advantages.

I.4. PROCESSES TO MAKE BME CAPACITORS:

Essentially there are three different processes currently being used:

1. Electroless deposition of nickel on the fired samples of dielectric;
2. Applying Ni-glass frit electrode paste on sintered sample of modified composition and firing at about 900°C in reducing atmospheres.
3. Coating nickel to green samples of dielectric of modified composition and sintering them in controlled reducing atmospheres.

I.4.1. Electroless Nickel Deposition:

In this process the composition of the dielectric need not be modified. The air fired samples can be used directly. The nickel deposited in this way is not pure nickel but it is a nickel phosphorous alloy, containing 4 to 8 percent phosphorous. The presence of latter makes the deposit more corrosion resistant, and less magnetic than electrodeposited nickel.

The essential chemicals are simple nickel salt, hypophosphite ion, which is the reducing agent and a salt

usually of an organic acid which acts both as a buffer and complexing agent for nickel. The overall equation is

$$H_2PO_2^- + Ni^{++} + H_2O \rightarrow N_i + H_3PO_3^- + 2H^+ \qquad (I.1)$$

There is also some side reaction which wastes some of the hypophosphite ion;

$$H_2PO_2^- + H_2O \rightarrow H_3PO_3^- + H_2 \qquad (I.2)$$

There are two different types of baths, ammoniacal (pH, 8--11) and acidic (pH, 4-7). Vessels for electroless plating bath may consist of glass, passivated stainless steel etc. The bath should be heated in a manner that obviates local over heating which may lead to spontaneous decomposition. The procedure to deposit on dielectrics and insulators is,

(i) Degreasing by immersion in an alkaline properietery solution,

(ii) Chemical etching in solutions suitable for nonconductors,

(iii) Seeding the surface, and

(iv) Electroless nickel plating.

Degreasing and etching solutions vary with the nonconductor. The end result will be a surface that will be chemically clean and uniformly etched. The seeding solution will be 150 g/l solution of hypophosphite operated at 90°C. Eisenberg et al (7) deposited electroless nickel on alumina in an acid bath of composition,

Nickel sulphate	:	30 g/l
Sodium acetate	:	10 g/l
Sodium hypophosphite	:	10 g/l
pH	:	4-6
Temperature	:	80-90°C

This process will lower the processing costs because of the elimination of the electrode firing step.

I.4.2. Electrode Firing in Reducing Atmospheres:

Recently, Burn (8) has reported a method of producing BME capacitors with little change in processing procedure, except that the nickel glass frit electrodes should be fired in mildly reducing conditions and the composition of dielectric should also be changed slightly such that one can get high resistivity samples even after firing in reducing atmospheres. The atmospheres of firing electrodes should be such that the electrodes should not get oxidized; for firing temperatures around 900°C, the partial pressure of oxygen should be around 10^{-12} atm, if nickel is the electrode. Under this atmosphere, Pb and Bi which are usually present in the conventional glass frits, will also be reduced. For this purpose borosilicate glasses having composition 4BaO, Al_2O_3 $2B_2O_3$ are used.

This is a simple process of producing BME ceramic disc capacitors but this may not be a useful process in producing BME multilayer capacitor for which single step of firing is preferred.

I.4.3. Sintering in Reducing Atmospheres:

This method which is being widely used in producing multilayer capacitors with nickel as electrode consists of depositing nickel by casting under doctor blade or by spraying, on green samples of modified dielectric composition, and sintering them in reducing atmospheres.

Herbert (9) reported a general procedure for getting BME multilayer capacitors in the 100-10000 pF range with losses less than 0.001 and very low temperature coefficient. But he did not specify the dielectric composition.

Here the process consists of a single step of firing to produce the capacitors compared to two firings needed to produce conventional capacitors. Thus the processing costs also favour the substitution of silver by nickel.

I.5. LITERATURE SURVEY:

I.5.1. Development of Dielectric Composition for BME Capacitors:

As discussed in the previous section that there are three different processes of making BME capacitors, out of which two processes require a firing step in reducing atmosphere. This necessiates the use of modified $BaTiO_3$ composition which would not get reduced in reducing atmospheres.

In reducing atmospheres $BaTiO_3$ will become a conductive body due to the Ti^{3+} ions formed, accompanying the formation of oxygen ion vacancies. This can be prevented by adding an additive which can either act as an acceptor

thus compensating for the oxygen vacancies or can act as effective electron trap.

Various elements (10-13) were tried as reduction-inhibiting dopants such as Cr, Mn, Fe, Co, Ni, Mg, Zn, Al, Ga and Li which are capable of having a valency +4 with similar ionic size as Ti^{4+} and it was observed (10-13) that Mn is the most effective dopant in producing reduction inhibiting ceramic and the order of efficiency was found to be Mn > Co > Mg > Cr > Ga > Fe. Desu (6,12) suggested a plausible explanation for the above observed trend by the calculation of energy loss or gain when an ion present in $BaTiO_3$ lattice - traps electrons. The idea is that the probability of electron trapping will be highest in the case that leads to maximum decrease in the lattice energy. The order of effectiveness of the ions calculated based on this calculation very well compares with the observed trend.

Herbert (11) observed that when more than 2 mole per cent of oxides of Co, Ni and Fe are mixed with $BaTiO_3$ and fired above 1000°C in hydrogen, they are reduced to metallic state, whereas Mn yields a stable oxide MnO even in H_2 and at sintering temperatures of $BaTiO_3$.

To understand the behaviour of acceptors during the process of producing BME capacitors Daniels (13) has carried out some theoretical as well as experimental studies in a simple system like Ga doped $BaTiO_3$, where, there is little chancefor dopant to change its oxidation state during the process, and he found out that more than 0.4 mol per cent

of Ga is needed to prevent reduction of $BaTiO_3$ and to be sintered in reducing atmospheres.

I.5.2. Manganese Doped Barium Titanate:

We know, now, that manganese is the most effective dopant to prevent the reduction of barium titanate in the low partial pressure of oxygen. The present work is on this subject to understand more this dielectric composition because of its technological and scientific importance. Let us see now, briefly, the dielectric and electrical properties of this material based on the earlier research on this material.

It was found that MnO was the only oxide found to protect $BaTiO_3$ from reduction under strongly reducing conditions (10). Mn_2O_3 in excess of 5 atom per cent lowers the transition point of technical preparations of $BaTiO_3$ and it has been found that a solid solution of Mn_2O_3 in hexagonal $BaTiO_3$ is formed with a solubility limit of approximately 46 atom per cent Mn at 1100°C (10). The Mn was found analytically to be largely in the trivalent state in these solutions. Some quadrivalent Mn was also present when the total quantity of Mn was less than 5 atom per cent; here the structure was of the imperfect tetragonal type. Increasing amounts of Mn_2O_3 cause the shrinkage of the lattice of hexagonal $BaTiO_3$. It was reported, that, when such a hexagonal solution was sintered at 1200° to 1300°C in H_2 the Mn was reduced to the divalent state and some of it appeared as a separate phase of MnO while the $BaTiO_3$ was converted to the cubic form. The colour and

resistivity of the resulting body indicated that it did not contain Ti^{3+} ions (10).

Herbert (11) shown that 0.5 mol per cent Mn will be sufficient to prevent the reduction of $BaTiO_3$. Desu's calculations (6, 12), on the minimum concentration of various acceptor ions needed to prevent reduction of $BaTiO_3$ for two different conditions: (i) 900°C in H_2 and (ii) 1350°C in H_2, show that 0.25 for the condition (i) and 0.4 for the condition (ii) of the Mn^{3+}. These conditions are of importance because, the former is where, Ni electrode glass frits are fixed on dielectric samples to make BME ceramic disc capacitors, and the latter condition is being used as a sintering condition for making BME capacitors.

Generally doping of Mn at Ti^{4+} site in $BaTiO_3$ (prepared from $BaCO_3$ + TiO_2) reduces the permittivity and loss factor and they decrease further with larger Mn concentrations (6) upto 1 mol per cent of Mn (14). Desu's work on the Mn-doped $BaTiO_3$ (6), prepared from $BaCO_3$ and TiO_2 with different Ba/Ti ratio showed that the barium excess composition (Ba/Ti = 1.0/0.98) has very good dielectric properties over other compositions 1.0/1.0 and 1.0/1.02. Also it showes that there is no effect of Ba/Ti ratio on the Curie temperature of $BaTiO_3$. Sintering in Argon (low partial pressure of oxygen) always resulted in higher densities, high dielectric constants and low dissipation factors.

Just like other acceptors Mn also was found (15) to decrease the Curie point of $BaTiO_3$. This difference in Curie point was found to increase with increasing amounts of Mn (in $BaTiO_3$ prepared from $BaCO_3$ + TiO_2) and annealing in atmospheres of lower oxygen content; the latter fact is attributed to the change of oxidation state of Mn. But the Mn-doped material which was prepared by oxalate method (6) does not show decrease of the permittivity. Rather they show high dielectric constant compared to the undoped material. Also there is no remarkable decrease in Curie point (not more than $5^{o}C$ for 2 mol per cent of Mn addition).

To understand clearly the effect of a dopant in a particular lattice one should know its defect chemistry. The defect chemistry of $BaTiO_3$ was studied by several researchers (16-18) on polycrystalline and flux grown samples at temperatures above $500^{o}C$. All of these studies

indicate that there is an extensive range at low oxygen partial pressure (P_{O_2}) where conductivity increases with decreasing P_{O_2}, characteristic of 'n' type conduction related to oxygen deficiency, whereas in the P_{O_2} range near 1 atm. the conductivity increases with increasing P_{O_2} characteristic of P-type conduction related to stoichiometric excess of oxygen. Mn-doped $BaTiO_3$ has important applications in that they can be used as a dielectric material, in producing low cost multilayer capacitors by sintering in a low P_{O_2} atmosphere. With this idea in mind Hagemann's studies on the electrical properties of Mn-doped $BaTiO_3$ ceramic (19) revealed that the regime of high conductivity is shifted to lower partial pressures of oxygen by acceptors such as Mn i.e. only the Mn-doped samples are insulating whereas undoped $BaTiO_3$ exhibits relatively high conductivity after annealing in low P_{O_2} at 1100°C. Also his work on the electrical conductivity as a function of the annealing temperature showed that there exists a threshold temperature for the transition from low to high conductivity (which depends critically on the ratio of oxygen vacancy donors to Mn acceptors) and this threshold is shifted to higher temperatures as the acceptor concentration or the oxygen partial pressure is increased.

Desu's work on the electrical resistivity of Mn-doped $BaTiO_3$ (20) revealed the following: (i) the resistivity at any temperature was found to decrease with Mn content for the compositions with Ba/Ti ratio 1.0/0.98, 1.0/1.0 and 1.0/1.02 which were sintered in air and measured in air.

Similar results were obtained for samples sintered in oxygen and purified argon (this indicates that acceptors are more or less fully ionized). Samples which were prepared from oxalate method did not show any regular behaviour like samples prepared from $BaCO_3$ and TiO_2; (ii) the atmosphere during sintering has been found to affect the resistivity of Mn-doped $BaTiO_3$ samples with Ba/Ti ratio 1.0/0.98; (iii) at a given temperature and Mn concentration, the resistivity increases with decreasing P_{O_2} (as already indicated, this is because the incorporation of Mn extends the p-type behaviour to lower P_{O_2} at a given temperature or to higher temperatures at a given P_{O_2}); (iv) the work on the H_2 annealing at different temperatures (500, 700, 900 and 1100°C) showed that the undoped compositions exhibit a steep decrease of resistivity with increasing temperature of H_2 annealing, but the compositions doped with Mn, enables $BaTiO_3$ to resist reduction in H_2 at temperatures upto 900°C but not at 1100°C. Samples which were heat treated in less reducing atmosphere such as 75 per cent N_2 and 25 per cent H_2 (which is sufficient to prevent the oxidation of Ni) showed the resistivity which is nearly two orders of magnitude higher compared to the strong reducing atmosphere.

The material which is prepared by oxalate method does not fit into the model of acceptor doped $BaTiO_3$. Desu assumed this is due to the occupation of Mn at both Ba and Ti sites. Even though this material does not show any regular trend like the compositions which were prepared from $BaCO_3$ and TiO_2, but the EPR work (20) showed that the

distribution of Mn is nonuniform when manganese oxides are mixed with $BaCO_3$ and TiO_2, while coprecipitation of manganese oxalate with barium titanyl oxalate ensures homogeneous distribution.

Hagemann's studies on the domain stabilisation and loss mechanism in doped $BaTiO_3$ with La, Fe and Mn (14) showed that the permittivity and the loss factor are independent of the external Ac field upto the existing threshold field for Mn and Fe doped samples. The threshold field is less than 20 V cm^{-1} in La doped $BaTiO_3$ and is upto 5000 V cm^{-1} in Fe or Mn doped samples and the threshold field is the measure of the domain stabilization. In Mn-doped $BaTiO_3$ the threshold field increased by annealing at low partial pressures of oxygen. He hypothesised that the domain stabilisation in $BaTiO_3$ involves an orientation parallel to P_S of axial defect centres which consist of acceptor-type doping ions like Fe or Mn and neighbouring oxygen vacancies.

Little or no studies have been done to understand the Mn-doped $BaTiO_3$ prepared from oxalate method where Mn has a chance to occupy both Ba and Ti sites and also the grain boundary with variety of oxidation states (+2, +3 and +4) depending upon the doping technique and heat treatments in different atmospheres.

II. STATEMENT OF THE PROBLEM

It is clear from the Chapter I that Mn is a preferred additive in the production of Base Metal Electrode capacitors. Mn-doped $BaTiO_3$ prepared from $BaCO_3$ and TiO_2 shows the regular trend of dielectric and resistivity behaviours whereas the composition prepared from oxalate method does not, even though they retained their supremacy (good dielectric properties, highest purity, uniformity etc.) over the composition prepared from conventional oxide technique (6). This clearly shows that the doping procedure has a marked influence on the properties of Mn-doped $BaTiO_3$. We know that when Manganese is substituted at Titanium site its efficiency in preventing the reduction of $BaTiO_3$ sintered under reducing conditions is much more compared to its occupancy at Barium or grain boundary positions. That is one can see the usefulness of Mn-doped $BaTiO_3$ for BME technology when most of the Manganese sits at the Titanium site. Now the question is how Mn is going to prevent the reduction of $BaTiO_3$ sintered in reducing atmosphere when this composition prepared from oxalate method and the mechanism by which Mn will accomplish this role. The present work is undertaken basically to address these problems.

More specifically, the aims of the present investigations are:

(i) To study the Mn-doped $BaTiO_3$ prepared by oxalate method (when Manganese added to the Barium and Titanyl solutions and then precipitated as Mn-doped BTO) in order to understand the role of Mn in this material.

(ii) To attempt to develop a reasonably good dielectric composition by studying the role of Mn when precipitating along with the Barium Titanyl oxalates.

(iii) To investigate the influence of Mn on the decomposition of Barium Titanyl oxalates by simultaneous DTA and TGA studies. Also the influence of Mn on the infra-red spectra of the Barium Titanyl oxalates or in other words, detecting the Mn acceptance by the compound BTO by using IR technique.

(iv) To study the loss mechanism and domain stabilization in the Mn-doped $BaTiO_3$ by sintering them in air, purified argon (low partial pressure of oxygen) and oxygen; annealing the air sintered samples in purified argon; annealing and quenching in air, purified argon and oxygen; and measuring their permittivity and loss factor variation with external ac field and measuring the change of loss factor with frequency.

(v) To investigate the electrical resistivity behaviour of the Mn-doped $BaTiO_3$ with the application of BME disk and multilayer capacitors in mind by

(a) annealing the material in hydrogen over a wide range of temperatures;

(b) annealing and quenching the material from 1100^{o}C in the various partial pressures of oxygen (P_{O_2}); and

(c) the behaviour of the nickel electroded capacitors.

And to study the resistivity of the samples with temperature in air atmosphere.

III. EXPERIMENTAL TECHNIQUES

III.1. SAMPLE PREPARATION:

III.1.1. Raw Materials:

Raw materials used for the sample preparation are Barium chloride dihydrate, oxalic acid dihydrate (Sarabhai Chemicals, India), Titanium tetrachloride and Manganese carbonate (Reidel de Haven, Germany). All the chemicals are A.R. grade and more than 99.5 percent purity. Either pure distilled water or deionized water is used to make the Barium chloride and oxalic acid solutions.

By using DTA and TGA, the amount of hydrate present in $MnCO_3 \cdot XH_2O$ was found out (at 125°C) and the observed weight loss was compensated while making the compositions. Manganese was added either in the form of $MnCO_3$ or in the form of $MnCl_2$. $MnCl_2$ was prepared from $MnCO_3$, by the following reaction:

$$MnCO_3 + 2HCl \dashrightarrow MnCl_2 + H_2O + CO_2 \qquad \text{(III.1)}$$

III.1.2. Preparation of Mn-doped and Undoped Barium Titanyl Oxalates (BTO):

Depending upon the preparatory way there are three different groups in the preparation of the Mn-doped BTO.

GROUP I:

Manganous chloride solution was added to the Barium and Titanyl solutions and then Barium Titanyl oxalate doped with manganese was prepared. Two different compositions were made depending upon the manganese concentration.

BTO(B): Concentration of Mn is 1 mol percent and 1 mol percent of Ti was removed to facilitate Mn doping ($Ti_{1-x}Mn_x$, where 'x' is the concentration of the dopant in mole percent).

BTO(C): Concentration of Mn is 2 mol percent and 2 mol percent of Ti was removed.

In this 1 mol percent barium chloride and 10 mol percent oxalic acid were taken in excess of stoichiometric requirement.

GROUP II:

This group mainly consists of pilot or sample compositions to obtain a reasonably good Mn doped BTO. Manganese carbonate or manganous chloride was added to the oxalic acid solution and then the precipitate was made. Three different compositions were made depending upon the way of preparation involved.

BTO(E): Concentration of Mn is 2 mol percent and 2 mol percent of Ti was removed. No barium chloride excess was taken. Mn added in the form of $MnCO_3$.

BTO(F): Concentration of Mn is 2 mol percent and 2 mol percent of Ti was removed. 2 mol percent excess of barium chloride was added along with $MnCO_3$ to the oxalic acid.

BTO(G): Concentration of Mn is 2 mol percent and 2 mol percent of Ti was removed. 2 mol percent excess of barium chloride was added along with $MnCl_2$ solution to the oxalic acid.

GROUP III:

Manganese carbonate was added to the oxalic acid along with barium chloride; the amount of barium is equal to the manganese amount taken for doping. No titanium removal was done to facilitate manganese doping. Five different compositions were made depending upon the manganese concentration.

BTO(M_1): Concentration of Mn is 0.2 mol percent.

BTO(M_2): Concentration of Mn is 0.6 mol percent.

BTO(M_3): Concentration of Mn is 1.0 mol percent.

BTO(M_4): Concentration of Mn is 1.4 mol percent.

BTO(M_5): Concentration of Mn is 2.0 mol percent.

These are the . samples produced with good Mn doping into the compound BTO.

UNDOPED BTO:

BTO(A): Concentration of Mn is 0 mole percent.
The preparation of the BTO was done as follows:

III.1.2.a. General Procedure of Preparation:

The general procedure of preparation of Barium Titanyl Oxalate (BTO) is that of Clabaugh et al. (21) with some changes. They are (i) the titanium tetrachloride solution was made in 1 NHCl solution instead of in distilled water, to improve the stability towards temperature changes, and (ii) the amount of titanium solution taken for analysis of 'Ti' was weighed rather than pipetting out; then after dilution of the same, Ti was precipitated as hydroxides of titanium with ammonium hydroxide and then it was heated upto 900 to 1000°C and weighed as TiO_2. Weighing of the solution was preferred to pipetting out, since the error involved in the latter case is comparatively more due to the viscous nature of the titanium tetrachloride solution (6). Figure III.1 shows the systems used to transfer and dilute titanium tetrachloride solution in 1 NHCl solution.

A mixed solution of barium chloride and titanium tetrachloride is allowed to drip slowly into a hot (80°-85°C) vigorously stirred solution of oxalic acid. The apparatus used for this purpose is shown in Figure III.2.

The precipitated oxalate was filtered hot, to avoid the possibility of a different composition on

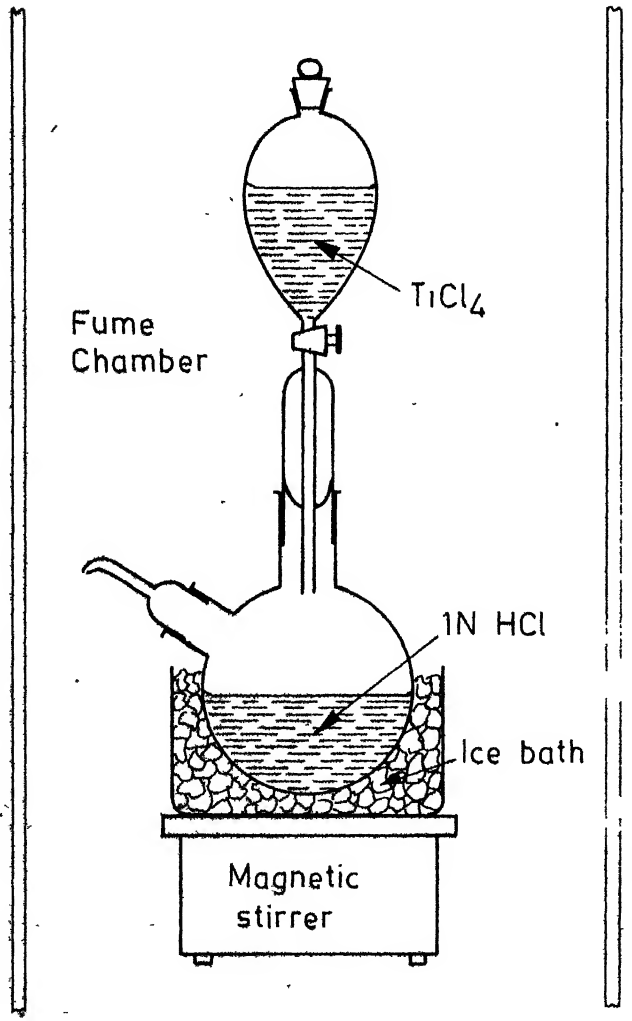

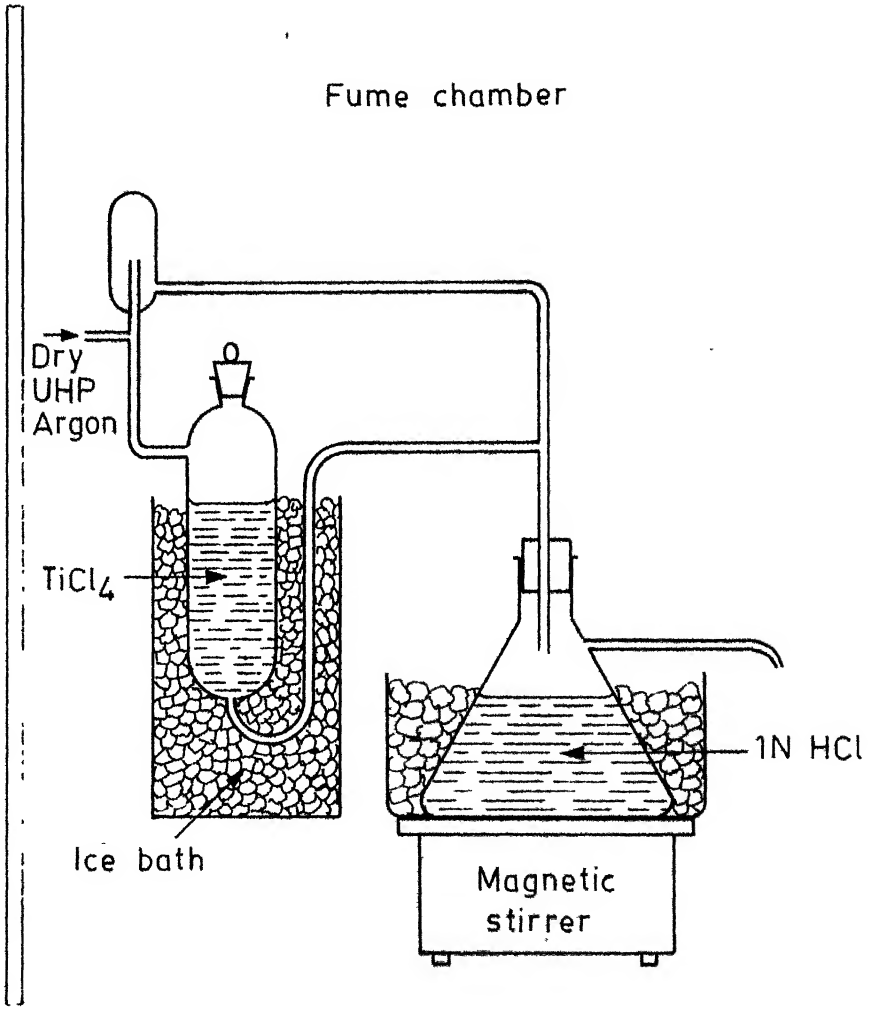

Fig. III.1. Systems used to transfer and dilute $TiCl_4$.

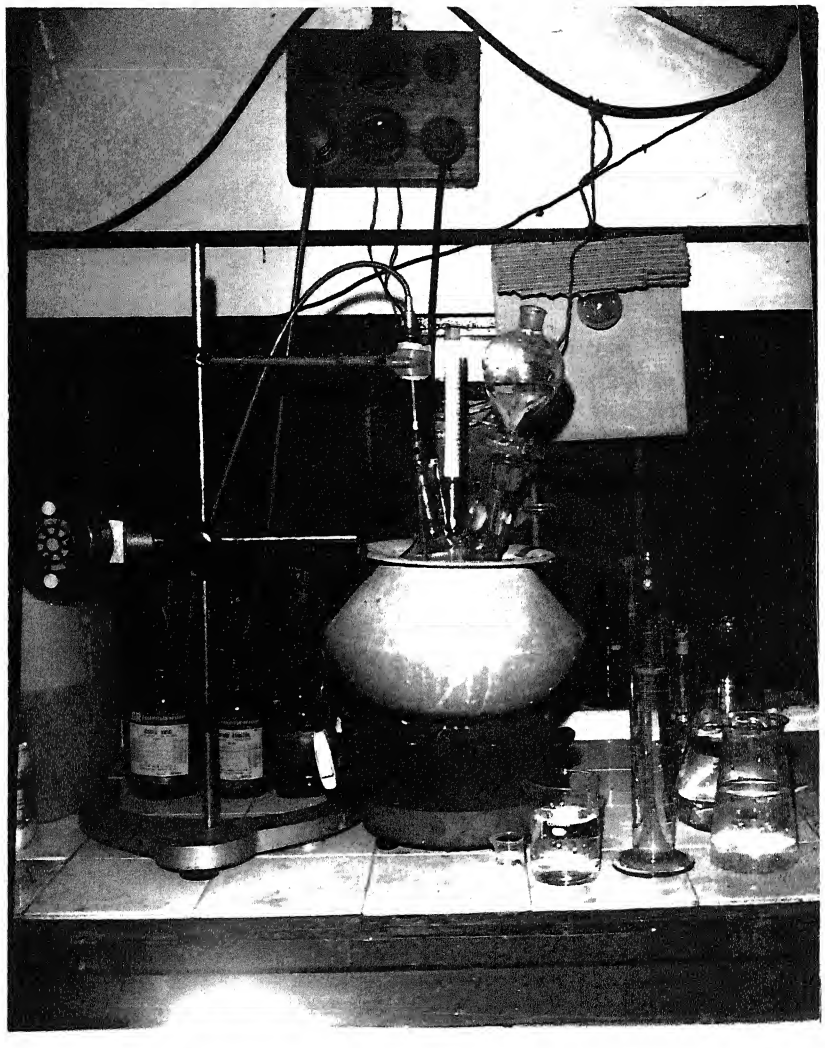

FIG. III.2. Apparatus used for the preparation of BTO.

cooling. The precipitate was washed with distilled water and finally with acetone. The air dried powders were calcined in a muffle furnace at 900°C for 2 hours. To remove the chloride ions which may be coprecipitated along with the compound, the calcined powders were boiled in hot water, filtered and washed with hot water until the filtrate did not show any precipitate with silver nitrate solution. The precipitate was dried at 150°C in an oven. Table III.1 shows the abbreviation of the calcined compositions.

The powder diffraction patterns of the prepared composition were taken by using Philips X-ray diffractometer to confirm the absence of other phases. No other phase except tetragonal $BaTiO_3$ has been identified.

III.1.3. Pelletisation:

The calcined powder was mixed with about 4 wt. percent of 25 percent polyvinyl acetate (PVA) solution and dried. The dried powder was pressed into pellets in a 12.5 mm or 9 mm diameter steel die under a pressure of 5 K bar (75,000 psi) which was applied through a hydraulic press (Carver Laboratory Press, Model B).

III.I.4. Sintering:

During sintering, the pellets of same composition were stacked one over the other in a platinum crucible with sufficient amount of powder of the same composition

Table III.1

Abbreviation of the calcined compositions

Compositions	Concentration of the dopant
$BaTiO_3$(A)	0% Mn
$BaTiO_3$(B)	1.0% Mn
$BaTiO_3$(C)	2.0% Mn
$BaTiO_3$(E)	2.0% Mn
$BaTiO_3$(F) or (G)	2.0% Mn
$BaTiO_3(M_1)$	0.2% Mn
$BaTiO_3(M_2)$	0.6% Mn
$BaTiO_3(M_3)$	1.0% Mn
$BaTiO_3(M_4)$	1.4% Mn
$BaTiO_3(M_5)$	2.0% Mn

in-between them. Sintering was carried out in a platinum tubular furnace. Figure III.3 shows the sketch of the platinum furnace and the sintering unit. The furnace was maintained at 1350°C by the Leeds and Northrup, Electromax controller which controls at the peak temperature, ±1°C. The sintering unit (i.e. Alumina tube which contains the crucible with samples) has been lowered in such a way that the rate of heating is of 200°C/hr upto 1000°C, and 100°C/hr upto the peak temperature. At the peak temperature the samples were soaked for 2 hrs. In the cooling cycle the tube has been raised such that the rate of cooling is 100°C/hr to 800°C and 200°C/hr to the room temperature. Pt/Pt-10 percent Rh thermocouple is used which is placed near the crucible containing the samples through the brass flange. The atmosphere in the furnace is also maintained depending on the requirement (Air, Oxygen and Argon, specified against each sample in Results) with the help of the Brass fittings and Flanges to the Alumina tube. The oxygen gas is passed throughout the sintering schedule at a rate roughly equal to 100 cc per minute. Dried Argon (UHP) gas is passed throughout the sintering schedule at a constant rate by using a calibrated Flow meter such that the partial pressure of oxygen is $P_{O_2} = 10^{-12}$ atm. was maintained. Sintering in H_2 was done in a Globar tubular furnace attached with a programmable controller. Dry H_2 gas was passed throughout the sintering schedule at a rate of 60 cc per minute.

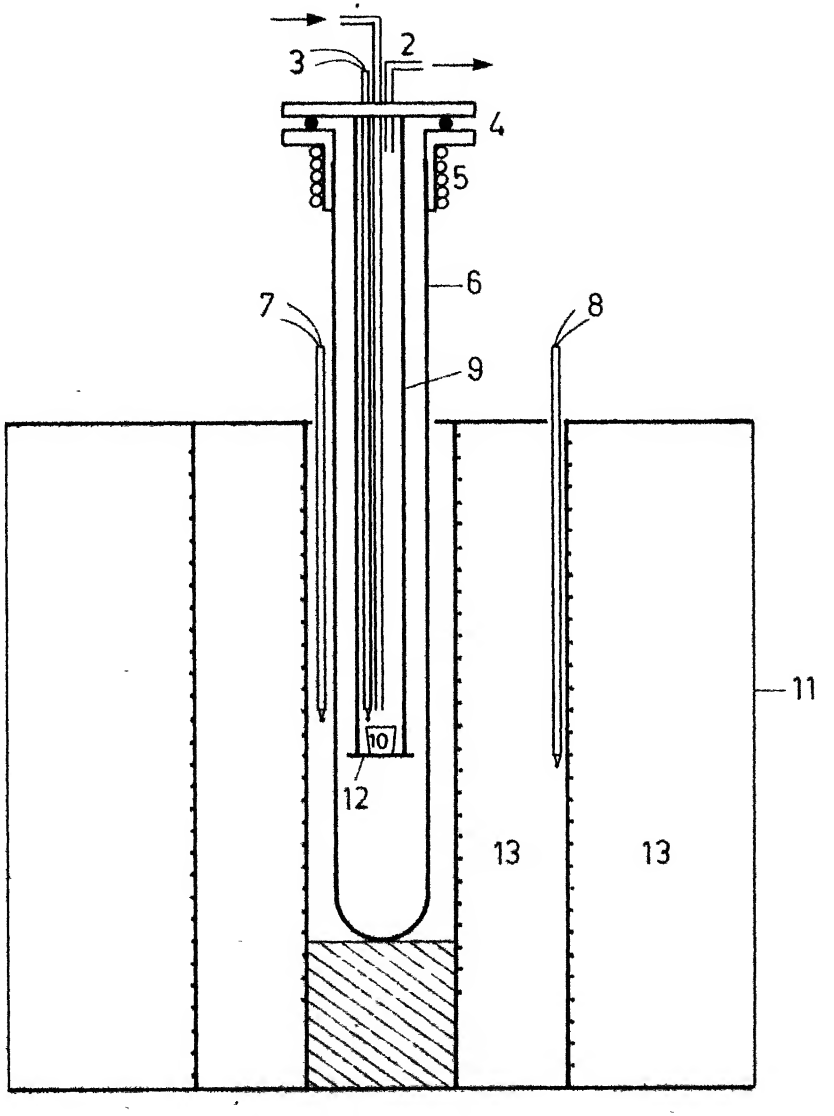

1	Gas inlet
2	Gas outlet
3	Thermocouple to measure the sample temperature
4	Brass coupling
5	Copper cooling coil
6	Alumina tube
7	Thermocouple to control Platinum furnace
8	Thermocouple to control Kanthal furnace
9	Alumina rod
10	Platinum crucible
11	Furnace body
12	Alumina disc
13	Magnesia powder

Fig. III.3. Sketch of the Platinum furnace

In H_2 sintering a alumina boat is used as a sample container.

III.1.5. Electroding:

Different types of electroding was done for different studies. In all cases the sintered samples were ground and polished over different grades of Silicon carbide powder to remove surface contamination as well as to obtain flat and parallel surfaces. Then the surface was cleaned with acetone.

For the capacitance and dissipation factor measurements with temperature, AC amplitude, and for the resistivity at room temperature the electroding of the samples was done with air-dry silver paint (obtained from N.P.L., Delhi). Coaxial identical round patch of electrodes were made on both the surfaces (disc/disc configuration). For the resistivity measurements with temperature, thin coating of unfluxed black platinum paste (Engelhard No. 6926) was applied and baked at 900°C in air for two hours. This was repeated 2 to 3 times to obtain a proper electrode.

Samples which are heat treated in the strong reducing atmosphere at higher temperatures (and hence their resistivity down to 10^4 ohm-cm) were electroded with Indium Amalgam to get good ohmic contact (22). Indium was wetted with Mercury and it was rubbed on the surface.

To study the behaviour of the Nickel electroded samples, finely divided (20 μm) Nickel powder (SISCO Metals, India) dispersed with PVA and made into the paste

form. Then it was coated on the cleaned surfaces of the sample and baked at 900°C for one hour in a reducing atmosphere to obtain a good ohmic contact.

III.2. CHARACTERISATION:

III.2.1. Thermal Analysis:

The DTA, DTG and TGA studies (simultaneously) of the Barium Titanyl Oxalate, pure and doped with Mn were done on MOM Derivatograph. The instrument parameters are given in Table III.2.

Table III.2

Instrument parameters of derivatograph

1.	Heating ratio	10°C/min
2.	Reference sample	Al_2O_3
3.	Sensitivity of DTA	1/10 and 1/5
	DTG	1/10 and 1/5
4.	Maximum temperature upto which it was run	1000°C
5.	Amount of the sample	500 mg and 1000 mg
6.	Weight loss scale	500 mg and 1000 mg.

III.2.2. IR Studies:

The infrared spectras of Barium titanyl oxalates, undoped and doped with different Mn concentrations and calcined powders of these compositions were taken on a Perkin-Elmer-580 spectrometer. The spectras

were run from 4000 cm^{-1} to 400 cm^{-1}. The sample is made into a pellet with KBr.

III.2.3. X-ray Analysis:

X-ray diffraction powder patterns of the calcined compositions were taken with Philips X-ray Diffractometer, fixing the instrument parameters given in Table III.3.

Table III.3

Instrument parameters for X-ray diffraction studies

Radiation	CuK_α
Excitation voltage	30 KV
X-ray current	20 mA
Beam slit	2^o
Scanning speed	2^o/min and 0.2^o/min
Chart speed	2"/min and 1"/min
Time constant	2 - 4 sec.

III.2.4. Estimation of Ba/Ti Ratio - Chemical Analysis:

The essential procedure is similar to that of Clabaugh et al. (21, 23, 6). The preparation of $BaTiO_3$ is from BTO, so in the case of pure $BaTiO_3$, it is necessary to check if the Ti to Ba mole ratio is unity and in the case of Mn-doped $BaTiO_3$, since Mn is expected to occupy the Ti site, to know the respective Ti to Ba ratio that depends upon the dopant concentration. Care has been taken

for the interference of Mn with Ti or Ba values. Appendix I describes the experimental procedure of this method.

III.2.5. Bulk Density Measurements:

Density measurements were done by the water displacement method. The dried pellets were weighed (D) in a Mettler single pan, electric balance (accuracy 0.0001 gm).

The pellets were boiled in distilled water for 5-6 hours and soaked for 24 hours. The water suspended weight (S) and water saturated weight (W) were determined. The bulk density was evaluated using the expression $(\frac{D}{W - S})$.

III.2.6. Temperature Dependence of the Dielectric Properties:

Dielectric properties, capacitance and dissipation factor were measured by using GR-1620-A capacitance bridge assembly. The measuring frequency was 1 KHz at 0.4 V.

A variable temperature sample holder (25) with an access to three samples used for the temperature dependence of the dielectric properties is shown in Figure III.4. The essential parts are the two electrodes, for the sake of simplicity, with associated connections and insulations built in on all metal unit. The low potential electrode is 1/8 in. thick brass plate of diameter. 1.6 in. common to all the three samples. The brass plate is held rigidly by a support rod which is welded into the base plate at one end and the other end passes through the central hole

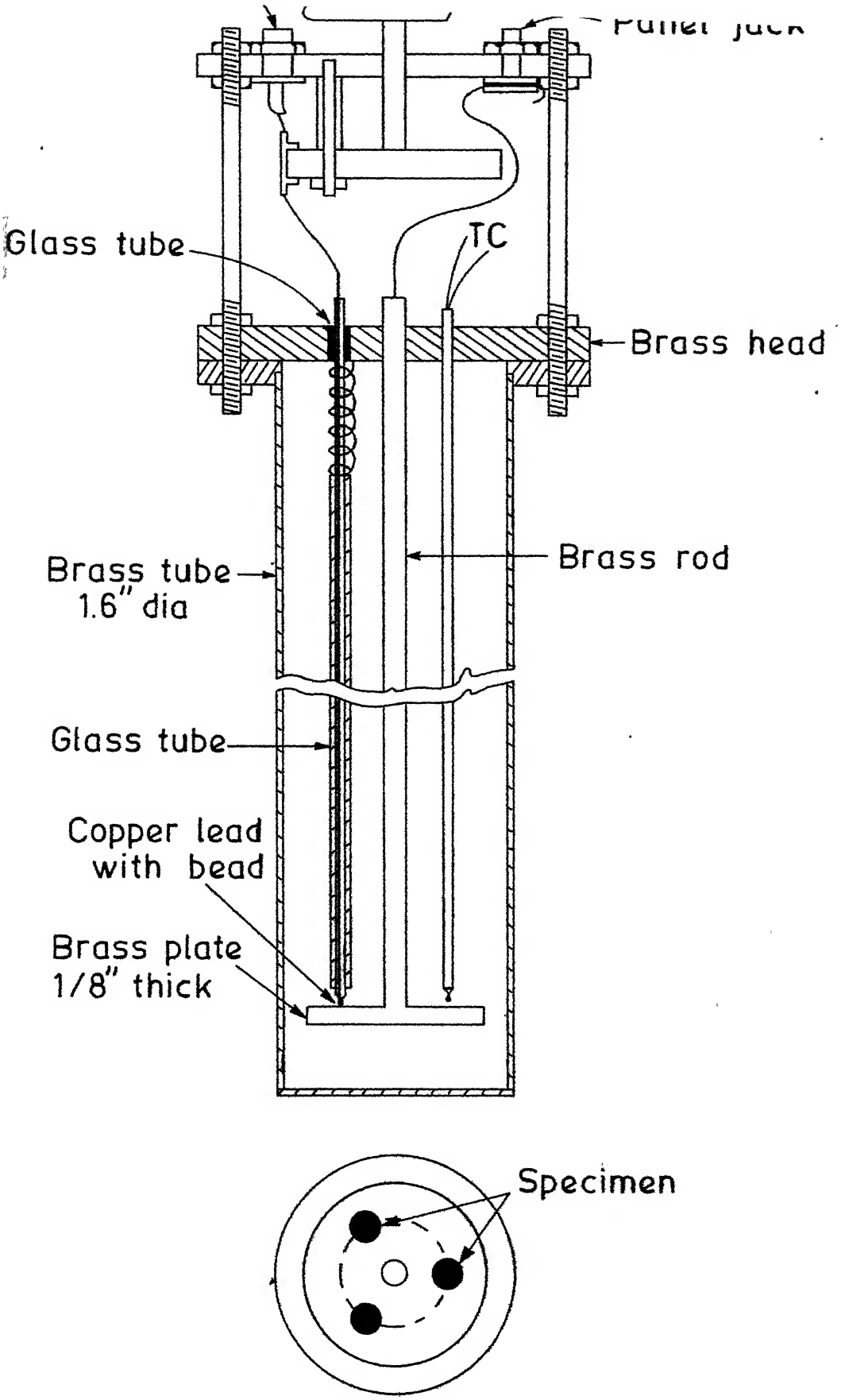

Fig. III.4 Sample holder for high temperature dielectric measurements

with top brass lid and is clamped by means of araldite. The high potential leads are made up of thick copper wire insulated from outside in a glass tube over which a grounded metal sheath is wound. This lead assembly is again insulated in a bigger quartz tube. A spring loaded arrangement presses these leads on the base plate which can be raised a bit to keep the specimens in position. The lower end of the wire is made into a bead to give proper contact on the electrode while the other end soldered to a positional plug of a three position switch. The above assembly is inserted in a thin walled stainless steel tube, 2 in. in diameter and 18 in. in length. The panel carrying the connector, the jack and the switch are firmly attached to the top lid.

The sample holder could be inserted into a small kanthal furnace. The heating rate (1°/min) was regulated manually by a variable autotransformer. The temperature was measured by a chromel-alumel thermocouple with a Rubicon potentiometer ($\pm 0.2^{\circ}$C).

III.2.7. AC Amplitude and Frequency Dependence of the Dielectric Properties:

The ac amplitude dependence of the dielectric measurements were carried out in a sample holder which was described in the Section III.2.6. By using the GR 1620-A, the range of the ac amplitude from 0.1 V to 100 V (open circuit voltage) was covered at constant frequency f = 1 KHz. The frequency dependence of the loss factor

was carried out in the same sample holder and the frequency range from 10^2 Hz to 10^5 Hz was covered by using the GR 1620-A set-up.

III.2.8. Temperature Dependence of the Electrical Resistivity in Air Atmosphere:

For resistivity measurements, the electroded specimens were placed in the sample holder schematically shown in Figure III.5. The sample holder consists of a 5 cm diameter recrystallized alumina tube as its outer envelop, which is fixed to a lower part of a brass flange with silicone adhesive. The specimens were kept at the bottom of the smaller diameter recrystallized alumina tube which was fitted to the upper part of the flange, through removable stainless steel fixtures. At the bottom end of the inner alumina tube, a portion of side wall was cut to facilitate loading and removal of specimens. To keep the specimens in position as well as for better electrical contact, they were pressed through a 1/4 in. diameter recrystallized alumina rod and a spring loading arrangement near the top of the holder. In this specimen holder resistance of three samples can be measured simultaneously. All the platinum lead wires and thermocouples were insulated from each other by taking the wires through recrystallized alumina thermocouple sheaths in hot zone and through teflon insulation in colder zone. Two platinum leads were attached to each surface of the specimen so that two probe as well as four probe measurement could be done with the same

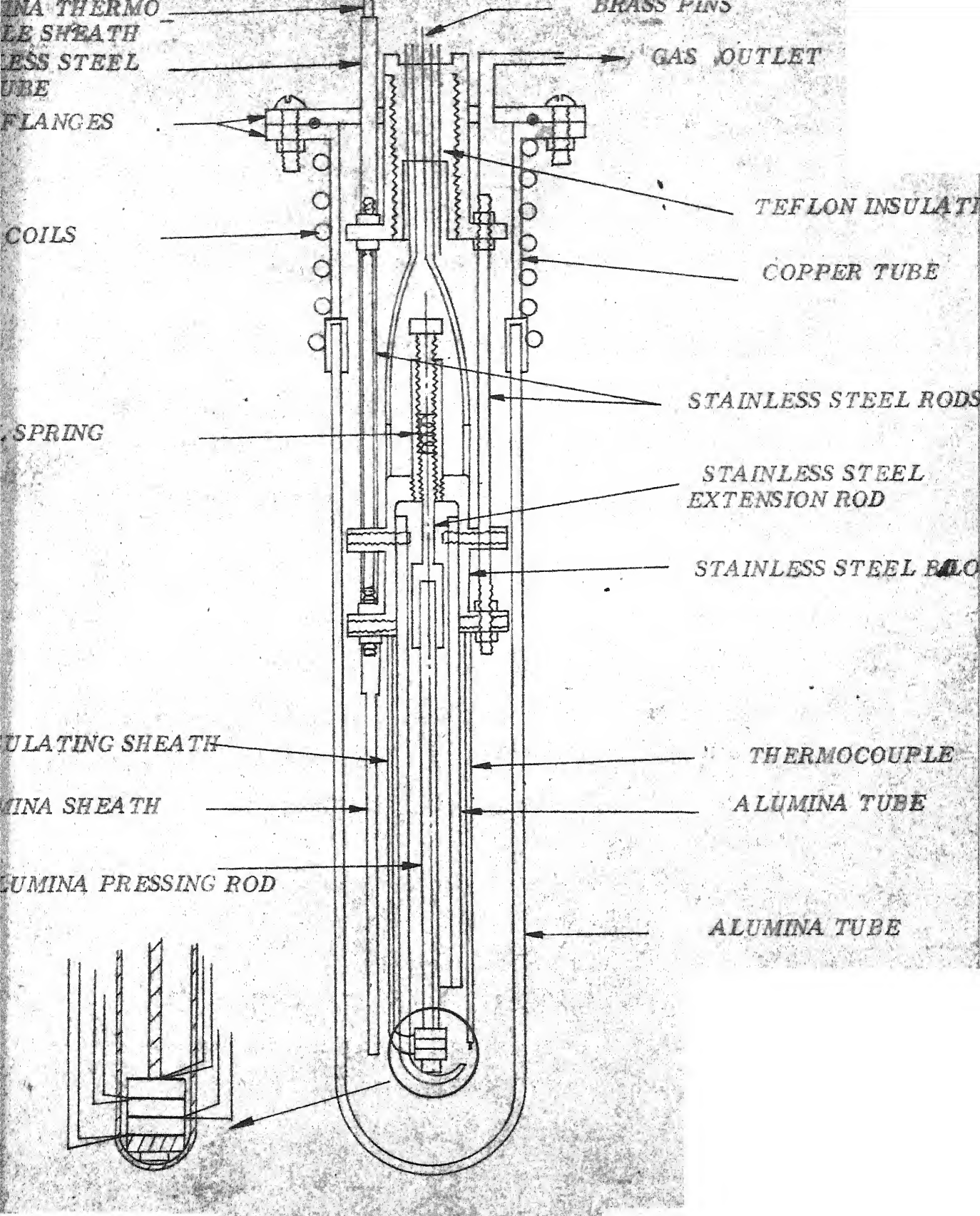

ALUMINA SAMPLE HOLDER
FOR CONDUCTIVITY STUDIES.

FIG. III. 5

set up. In the specimen holder 'O' ring seals were used between the two parts of the brass flanges and the gas inlet (air is the atmosphere in the present study) was through an alumina thermocouple sheath.

The DC conductivity of specimens (by two probe method) was measured with an impedence bridge (General Radio 1650-A) upto 10^6 ohm and at higher ranges (that is upto resistance 10^8 ohm) mega ohm bridge (General Radio) was used.

The specimen holder was heated in a globar furnace and temperature was controlled within $\pm 0.5^{\circ}C$ by a Leeds and Northrup Electromax type temperature controller in circuit with a autotransformer. The exact temperature of the specimen was measured by a Pt/Pt-10 percent Rh thermocouple kept very close to the specimen and EMF was measured by Leeds and Northrup K-3 potentiometer.

III.2.9. Annealing Studies of the Samples:

III.2.9.1. Annealing in H_2:

To get the correct composition of $BaTiO_3$ doped with Mn which can be electroded with Nickel, $BaTiO_3$ doped with different concentrations of Mn were annealed in H_2 for 10 min. at different temperatures in a tubular kanthal furnace. The flow rate of H_2 gas was 60 cc/sec.

III.2.9.2. Annealing in Various Partial Pressures of Oxygen (P_{O_2}) at 1100°C:

With the application for multilayer capacitors in mind, in order to prevent the oxidation of Ni in a given partial pressure P_{O_2} of oxygen at 1100°C, $BaTiO_3$ doped with different concentrations of Mn were annealed and quenched in various P_{O_2} atm. by using Argon-Oxygen mixture. Figure III.6 shows the general outlay of the system used to treat the samples in different P_{O_2} atm. Dry UHP argon was used. The sample holder used for this purpose was described in the Section III.2.8.

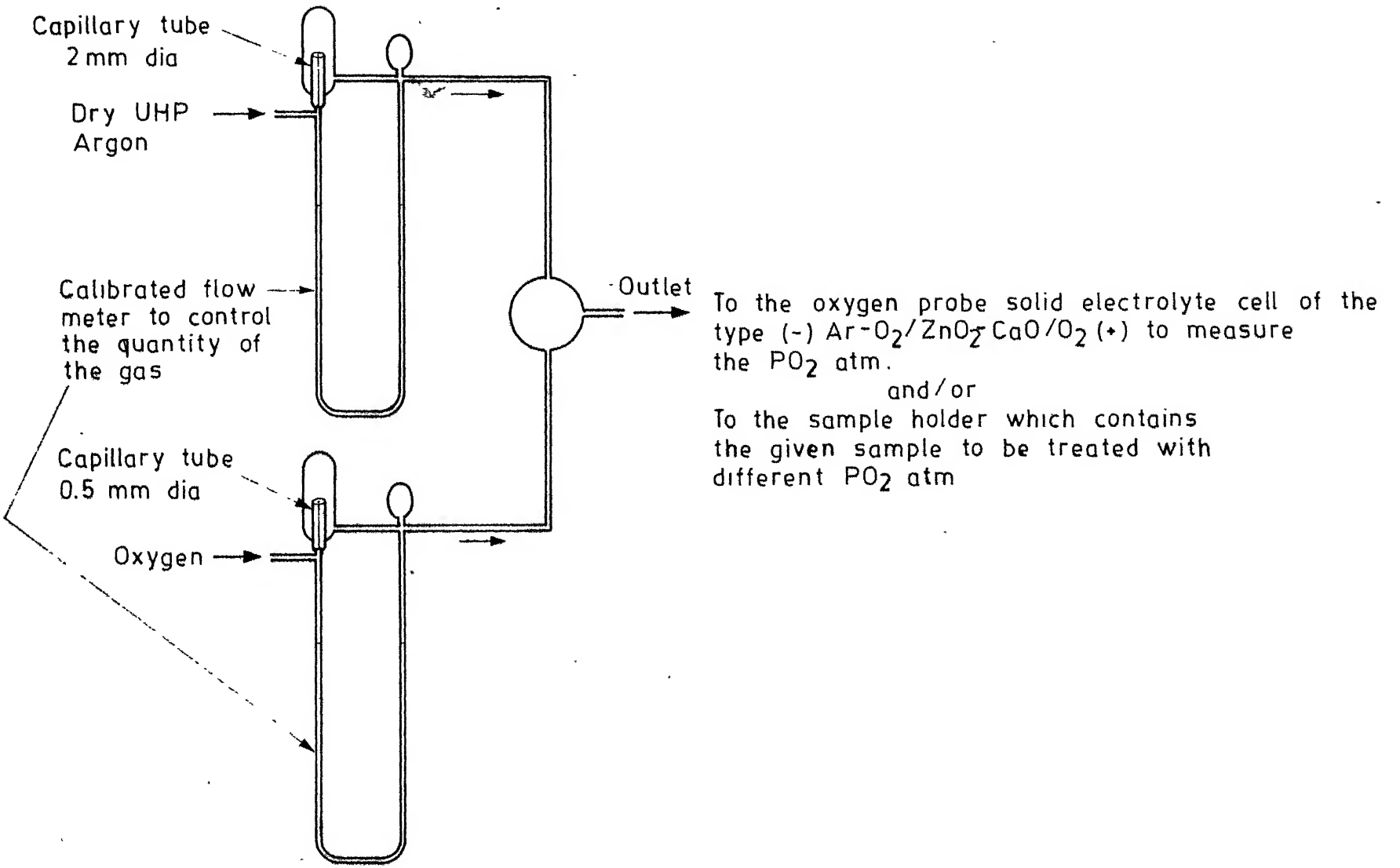

Fig. III.6. General outlay of the system used to treat the samples at

IV. RESULTS AND DISCUSSION

IV.1. Mn-DOPED COMPOSITION OF GROUP I AND UNDOPED $BaTiO_3$ BY OXALATE METHOD:

As discussed in the Introduction, ... the previous work showed that the $BaTiO_3$ doped with Mn by the oxalate method of Group I, does not show any regular behaviour (6). This necessiated the careful study of these materials.

IV.1.1. Thermal Analysis and Infrared Study:

IV.1.1.1. Thermal Analysis:

Table IV.1 shows the peak positions in DTA (Figure IV.1) of undoped and Mn-doped barium titanyl oxalates. The peak around 95°C can be attributed to the initial water losses, and the complete dehydration has been seen around 160°C. The peaks at 245°C and 365°C can be attributed to initial low temperature oxalate and main oxalate decompositions respectively. The final decomposition to $BaTiO_3$ showed up around 790°C as a peak in DTA.

The weight losses observed, in different ranges of temperatures are tabulated in the Table IV.2.

Five major schemes have been proposed for the decomposition of BTO (26-30) most of which are contradictory and inconclusive. It was also argued (31) that the differences may be due to the differences of Ba/Ti ratio of the samples. The schemes are listed below. In all the

Table IV.1

Peak positions in DTA of undoped and Mn-doped barium titanyl oxalates

Composition	Peak positions, °C				
	I	II	III	IV	V
BTO(A)	95	160	245	365	790
BTO(B)	95	165	250	365	785
BTO(C)	80	160	240	*	795

* Because of the low resolution it may not be visible.

Table IV.2

Comparison of weight losses of BTO, observed and calculated

Decomposition	Calculated weight loss (%)	Observed weight loss (%)	Temperature (°C)
Dehydration of BTO and low temperature decomposition of BTO	22.24	20.25	About 250°C
Main oxalate decomposition	18.69	19.50	About 400°C
Final decomposition to $BaTiO_3$	07.11	06.75	About 800°C
Total weight loss in percent	48.09	46.50	-

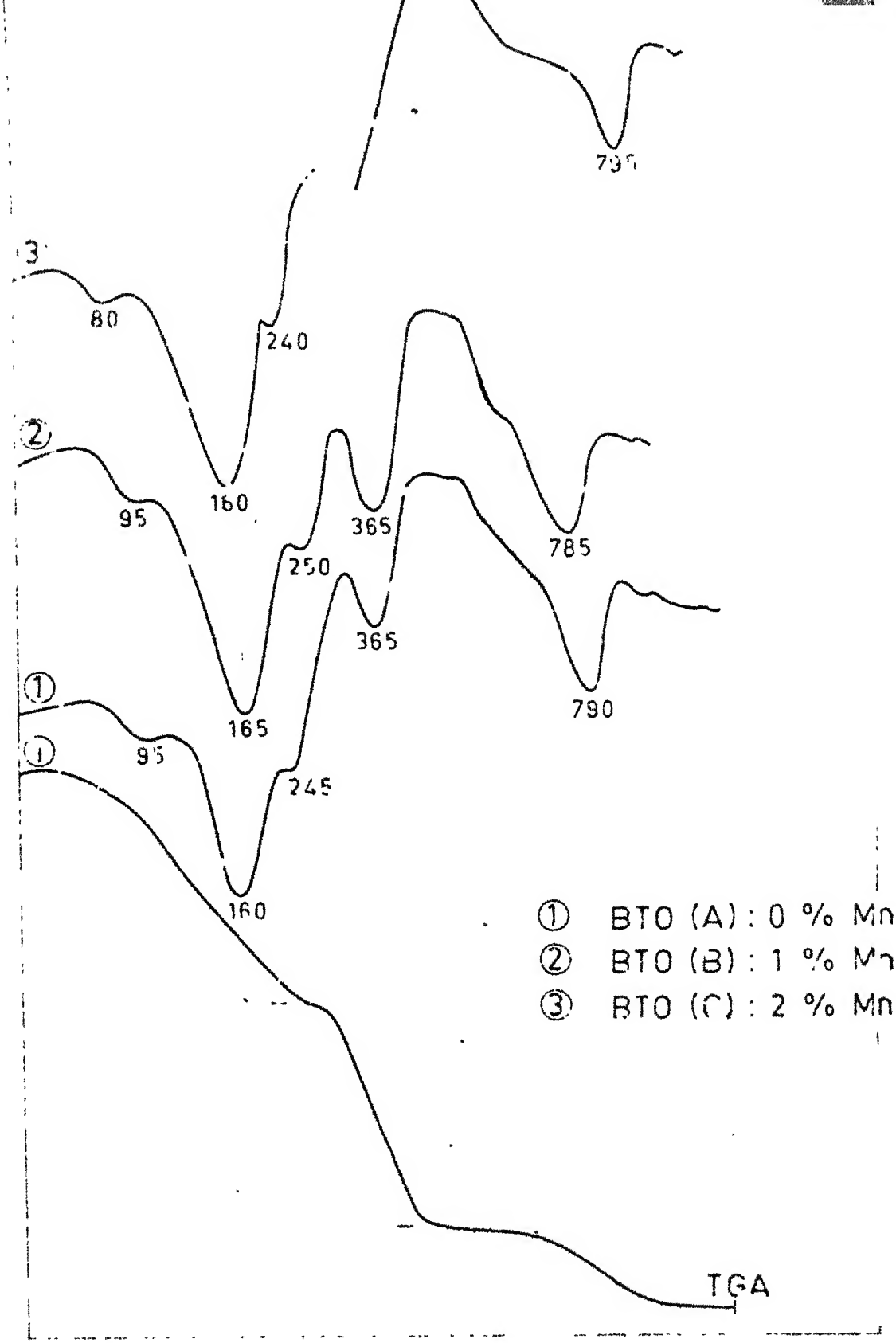

Fig IV 1 DTA and TGA of Barium Titanyl Oxalates..

schemes, dehydration step is common though the temperature varied from 30 to 300°C.

$$BaTiO(C_2O_4)_2 \cdot 4H_2O \longrightarrow BaTiO(C_2O_4)_2 + 4H_2O \qquad (IV.1)$$

1. Scheme A:

$$BaTiO(C_2O_4)_2 \xrightarrow[-2CO_2]{350^\circ C} BaTiO(C_2O_4) \xrightarrow{520^\circ C} BaTiC_3(CO)_2$$

$$\xrightarrow[-2CO]{670^\circ C} BaTiO_{3(1)} \xrightarrow{710^\circ C} BaTiO_{3(2)} \qquad (IV.2)$$

2. Scheme B:

$$BaTiO(C_2O_4)_2 \xrightarrow[-4CO]{300\text{-}600^\circ C} BaTiO_5 \xrightarrow[-O_2]{600\text{-}800^\circ C} BaTiO_3 \qquad (IV.3)$$

3. Scheme C:

$$BaTiO(C_2O_4)_2 \xrightarrow[-2CO_2]{250\text{-}300^\circ C} BaTiO(C_2O_4) \xrightarrow[-CO]{360\text{-}560^\circ C}$$

$$BaTiO_3(CO) \xrightarrow[-CO]{575\text{-}630^\circ C} BaTiO_{3(1)} \longrightarrow BaTiO_{3(2)} \qquad (IV.4)$$

4. Scheme D:

$$BaTiO(C_2O_4)_2 + \tfrac{1}{2} O_2 \xrightarrow[-2CO_2]{225\text{-}465^\circ C} BaCO_3 + TiO_2$$

$$\xrightarrow[-CO_2]{465\text{-}700^\circ C} BaTiO_3 \qquad (IV.5)$$

5. Scheme E:

$$2BaTiO(C_2O_4)_2 \xrightarrow[-CO]{180\text{-}250^\circ C} Ba_2Ti_2O_2(C_2O_4)_3CO_3$$

$$\xrightarrow[-2CO_2]{250\text{-}450^\circ C} Ba_2Ti_2O_5CO_3(CO_2) \xrightarrow[-CO_2]{450\text{-}600^\circ C}$$

$$Ba_2Ti_2O_5CO_3 \xrightarrow[-CO_2]{650\text{-}750^\circ C} 2BaTiO_3 \qquad \text{(IV.6)}$$

The step $BaTiO_{3(1)} \rightarrow BaTiO_{3(2)}$ in Schemes A and C represent the ordering process.

After analysing and observing the nature of the DTA and TGA, the following scheme has been proposed to calculate the weight losses of the present sample:

$$BaTiO(C_2O_4)_2 \cdot 4H_2O \xrightarrow[4H_2O,CO]{\sim 250^\circ C} BaTiO(C_2O_4)\cdot CO_2 \cdot \tfrac{1}{2} O_2$$

$$\xrightarrow[300]{\sim 370^\circ C} BaTiO \cdot 2O_2 \xrightarrow{\sim 800^\circ C} BaTiO_3 \qquad \text{(IV.7)}$$

The weight losses calculated according to the eqn. (IV.7) is summarized in the Table IV.2. The weight losses observed in different ranges of temperatures are nearly comparable to the calculated values. The slight discrepancy in the weight loss involving the dehydration of BTO may be attributed to the slightly less amount of hydrate molecules attached with the compound compared to the actual tetrahydrate taken for the calculation.

There is hardly any variation of the various peak temperatures with Mn concentration at least upto 1 mol

percent, then there is a slight reduction in the peak temperatures at 2 mol percent of Mn. So there is very little effect of Mn on the decomposition of BTO.

IV.1.1.2. IR Studies:

Figure IV.2 shows the IR spectra of the compound, BTO(A) and BTO(C) respectively. The absorption peaks from 4000 cm^{-1} to approximately 1600 cm^{-1} are due to the O-H molecules, from 1600 cm^{-1} to approximately 900 cm^{-1} are due to the C-O molecules and the cation molecule (Ti-O and Ba-O) peaks will be observed below 900 cm^{-1}. Since the positions of the peaks of Ti and Ba in $BaTiO(C_2O_4)_2 \cdot 4H_2O$ depend upon their reduced mass and force constant, so Ti peaks will start to appear first compared to the peaks of Ba. If the Mn expected to form the compound along with Ba, it is natural to expect the disturbance of the Ti peak, but this depends upon the Mn concentration. IR is a powerful technique to identify the impurities in the original compound matrix. From the Figure IV.2, it is clear that there is no shift in any peak due to the Mn doping. This obviously shows that Mn is only coprecipitated along with barium titanyl oxalate and it did not occupy some of the Ti sites in BTO; otherwise one would have observed a shift in the peak at 507 cm^{-1}.

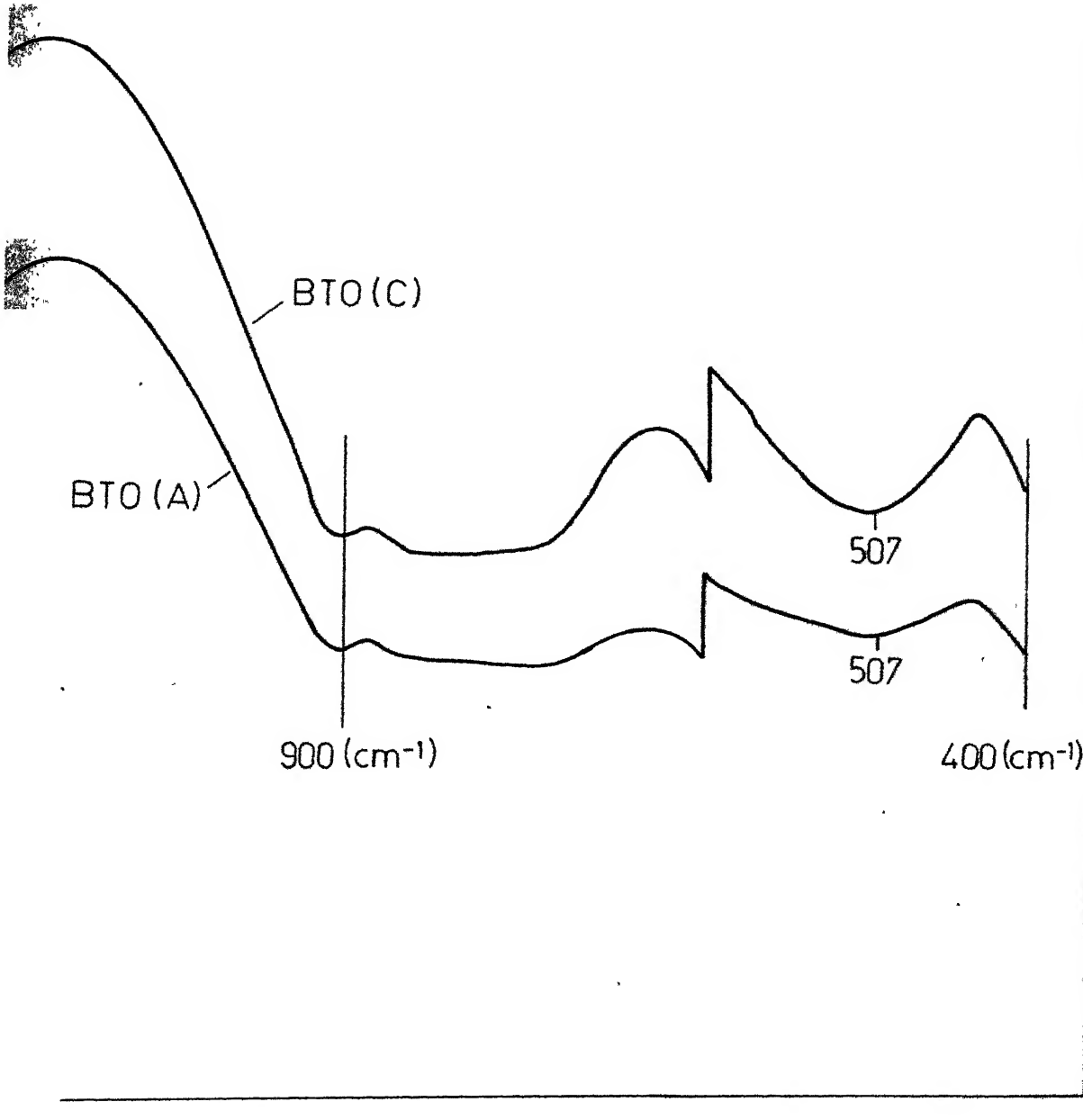
BTO (C)
BTO (A)
507
507
900 (cm⁻¹)
400 (cm⁻¹)

IV.1.2. Chemical and X-ray Studies:

IV.1.2.1. Chemical Analysis:

The Ba/Ti ratio of the undoped and Mn-doped samples are listed below.

Sample	Ba/Ti
$BaTiO_3$(A)	1.00
$BaTiO_3$(B)	0.99
$BaTiO_3$(C)	0.99

IV.1.2.2. X-ray Study:

The X-ray powder pattern of these samples did not show any other phase except the required tetragonal phase. There was no discrepancy between the Mn doped and undoped $BaTiO_3$.

IV.1.3. Temperature and AC Amplitude Dependence of the Dielectric Properties:

Doping of Mn at Ti site in the $BaTiO_3$ lattice mainly (i) inhibits the reduction of $BaTiO_3$ in the reducing atmosphere by Mn acquiring the lower oxidation state and (ii) stabilizes the domain in the applied ac field by TM-V_O alignment preferably parallel to the spontaneous polarisation (14). In addition, increased amount of Mn in the $BaTiO_3$ lattice lowers the permittivity of the material and also affects the Curie point.

IV.1.3.1. Temperature Dependence:

Table IV.3 shows the dielectric properties of undoped and Mn-doped $BaTiO_3$. The dielectric constant value, in the case of conventional method of preparation (6) decreases with increasing Mn addition whereas in the case of oxalate method, the 1 percent Mn added sample shows a slightly higher value compared to 0 and 2 percent. There is no remarkable reduction in Curie temperature of the Mn-doped samples prepared by the oxalate method. Figure IV.3 shows the variation of the dielectric constant with temperature. There is hardly any change in the temperature coefficient of the dielectric constant of the pure and doped samples. But it was shown earlier (32) that the presence of oxygen vacancies will greatly reduce the Curie temperature of undoped $BaTiO_3$ by 40 to 50°C for every 10^{20} oxygen vacancies/cm^3. From this fact one can infer that addition of acceptors to $BaTiO_3$ lattice should decrease the Curie temperature, and the decrease should be proportional to their concentration, because acceptors when present in $BaTiO_3$ lattice will give rise oxygen vacancies for charge compensation (Eq. IV.8) (6).

$$Ba\ Ti^{4+}_{1-x}\ M^{4+}_{x}\ O_3 \longrightarrow Ba\ Ti^{4+}_{1-x}\ M^{2+}_{x}\ O_{3-x} + \frac{x}{2}\ O_2$$

$$\longrightarrow Ba\ Ti^{4+}_{1-x}\ M^{3+}_{x}\ O_{3-\frac{x}{2}} + \frac{x}{4}\ O_2$$

$$\longrightarrow Ba\ Ti^{4+}_{1-x}\ M^{1+}_{x}\ O_{3-\frac{3x}{2}} + \frac{3x}{4}\ O_2 \qquad \text{(IV.8)}$$

Table IV.3

Dielectric properties of Mn-doped and undoped $BaTiO_3$

Composition Mn %	Desu I K	Desu I tanδ	Desu I T_c	Desu II K	Desu II tanδ	Desu II T_c	Present work I K	Present work I tanδ	Present work I T_c	Change in dielectric constant with 500 V/cm ac amplitude ΔK	Change in dielectric constant with 500 V/cm ac amplitude % $\frac{\Delta K}{K}$
0	2500	0.013	120	1980	0.126	123	4000	0.049	122	1500	37.5%
1	6400	0.016	116	1550	0.120	120	6700	0.019	120	1000	14.9 %
2	4800	0.023	115	1300	0.104	118	6000	0.015	119	750	12.5%

I : $BaTiO_3$ and Mn-doped $BaTiO_3$ prepared from oxalate; Mn added to the Ba and Ti solutions and then precipitated as Mn-doped barium titanyl oxalate.

Desu : Sintered at 1300°C for 120 minutes.
Present work: Sintered at 1300°C for 60 minutes.

All the dielectric values are porosity corrected.

II : $BaTiO_3$ and Mn-doped $BaTiO_3$ prepared from $BaCO_3$ + TiO_2, Ba/Ti: 1.0/0.98. Sintered at 1300°C for 60 minutes.

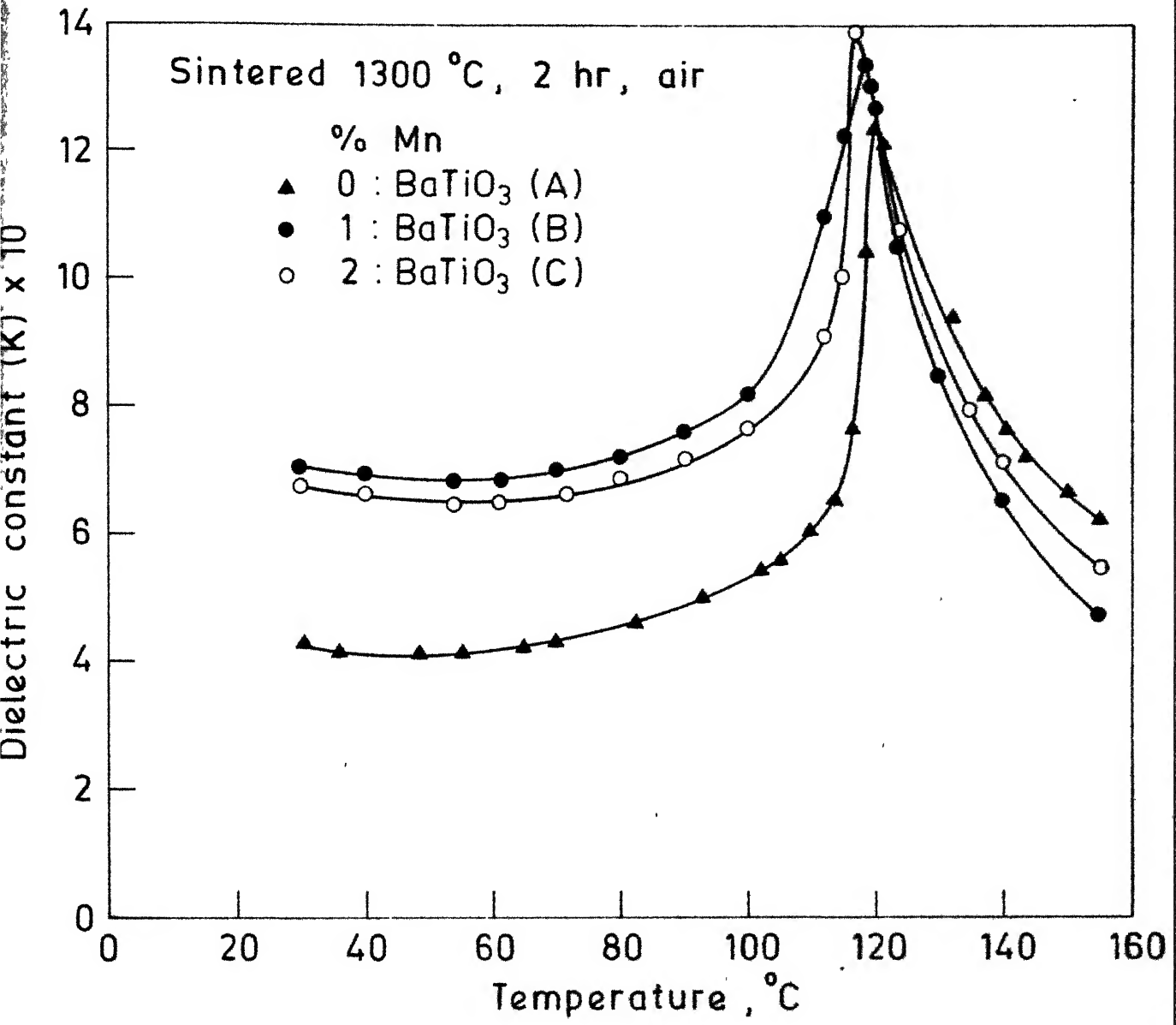

Fig. IV.3. Variation of the dielectric constant with temperature.

One can classify the acceptors into two types depending on their action on Curie point of $BaTiO_3$. (1) The acceptors which cannot change their oxidation state (Mg^{2+}, Ni^{2+} . . . etc.) in which case the Curie point will be a function of only the acceptor concentration. (2) The acceptors which can change their oxidation state (e.g., Mn^{3+}, Co^{3+} . . . etc.). In this case the Curie point of $BaTiO_3$ will be a function of not only the acceptor concentration but also the heat treatment which the sample has undergone. For example, consider the case of Mn^{3+} at Ti^{4+}. It forms oxygen vacancies in $BaTiO_3$ lattice for charge compensation, thus decreasing the Curie point. When this material was treated in reducing atmospheres Mn^{3+} goes to Mn^{2+} accordingly,

$$Ba\ Ti^{4+}\ O_3 \xrightarrow{\text{reduction}} Ba[Ti^{4+}_{1-2x}\ Ti^{3+}_{2x}]O_{3-x} + \frac{x}{2}\ O_2 \qquad \text{(IV.9)}$$

$$Ba(Ti^{4+}_{1-x}\ Mn^{3+}_{x})O_{3-x/2} \xrightarrow{\text{reduction}} Ba(Ti^{4+}_{1-x}\ Mn^{2+}_{x})\ x\ O_{3-x} \qquad \text{(IV.10)}$$

produces a further number of oxygen vacancies and thus decreases the Curie point of $BaTiO_3$ still further. Manganese addition into $BaTiO_3$ in the present investigation, does not affect much either the curie point of the temperature dependence of the permittivity.

IV.1.3.2. AC Amplitude Dependence:

The samples of the present work were studied under ac field (Table IV.3). From the table it is clear that the change in permittivity with increasing field, decreases with increasing Mn concentration.

Figures IV.4 and IV.5 show the ac behaviour of pure and Mn-doped $BaTiO_3$. The measurement has been done on the sintered, well-aged samples. The way the permittivity and the loss factor of the Mn-doped $BaTiO_3$ behaves with the amplitude of the external ac field is almost similar to that of the pure $BaTiO_3$.

IV.1.4. Discussion:

Generally the doping of acceptors (Fe or Mn) into $BaTiO_3$ lattice reduces the room temperature permittivity, decreases the Curie transition point, suppresses the Curie peak, etc. with respect to the pure $BaTiO_3$. These are mainly due to the existing oxygen vacancy concentration and the way O_2 vacancies were distributed within the lattice. The doping of a trivalent ion act Ti^{4+} site should produce the oxygen vacancies, and this will increase with increasing concentration of the trivalent ion at Ti^{4+} site. In general, doping of Mn at Ti site will reduce the permittivity and doping of La at Ba site will increase the permittivity, because the former will increase and the latter will reduce the existing oxygen vacancy concentration in the $BaTiO_3$ lattice.

The result of the present samples indicates, that, doping of Mn in this way into $BaTiO_3$, did not either decrease the Curie point or suppress the Curie peak. Moreover, the permittivity of the doped samples are quite high compared to that of pure $BaTiO_3$. Compared to 1 mol per cent and 2 mol per cent samples, 2 mol per cent Mn doped $BaTiO_3$ showing the decrease in permittivity. The loss factor, in general,

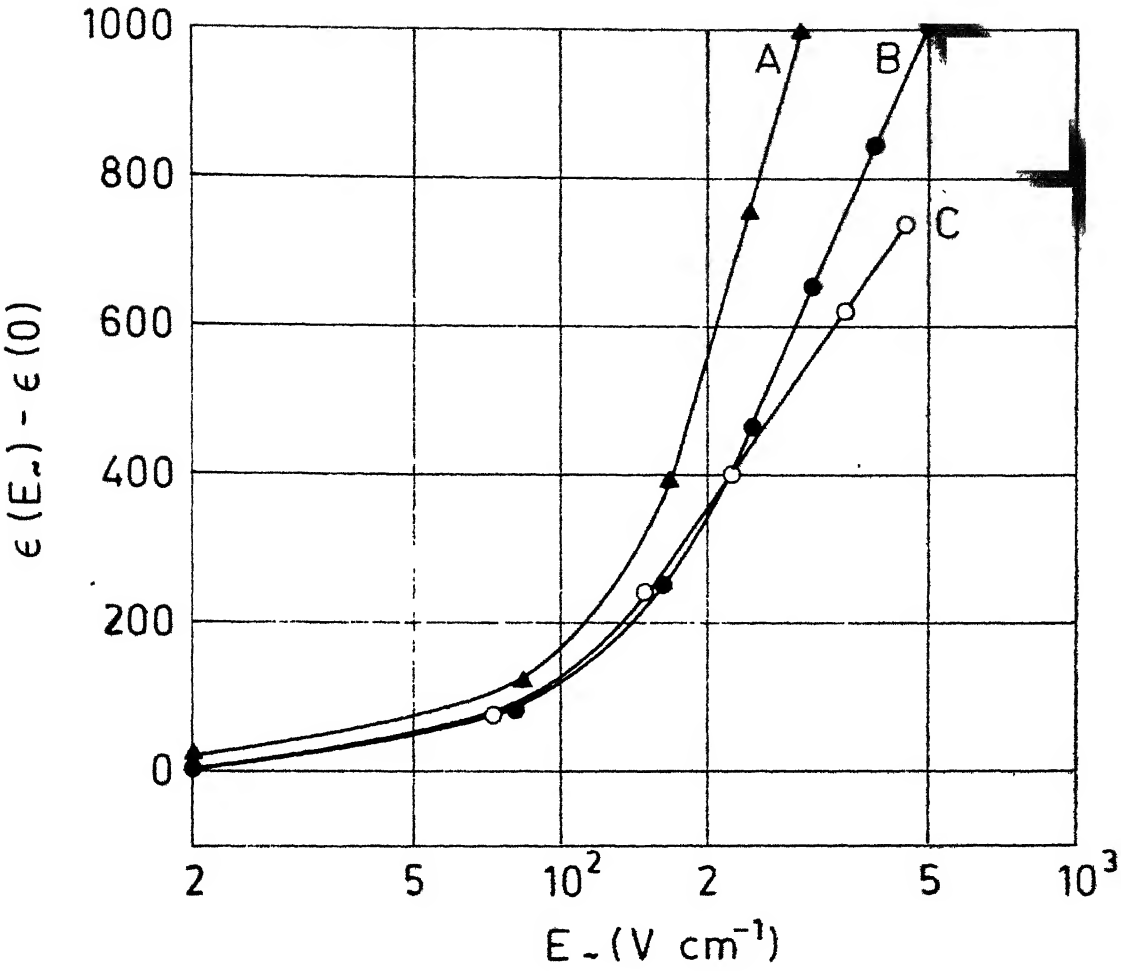

Fig. IV.4 Dependence of ϵ on the amplitude of the external AC field below T_C for different concentrations of Mn doping. Measured at T = 28 °C and f = 1 KHz. Well aged sintered samples.

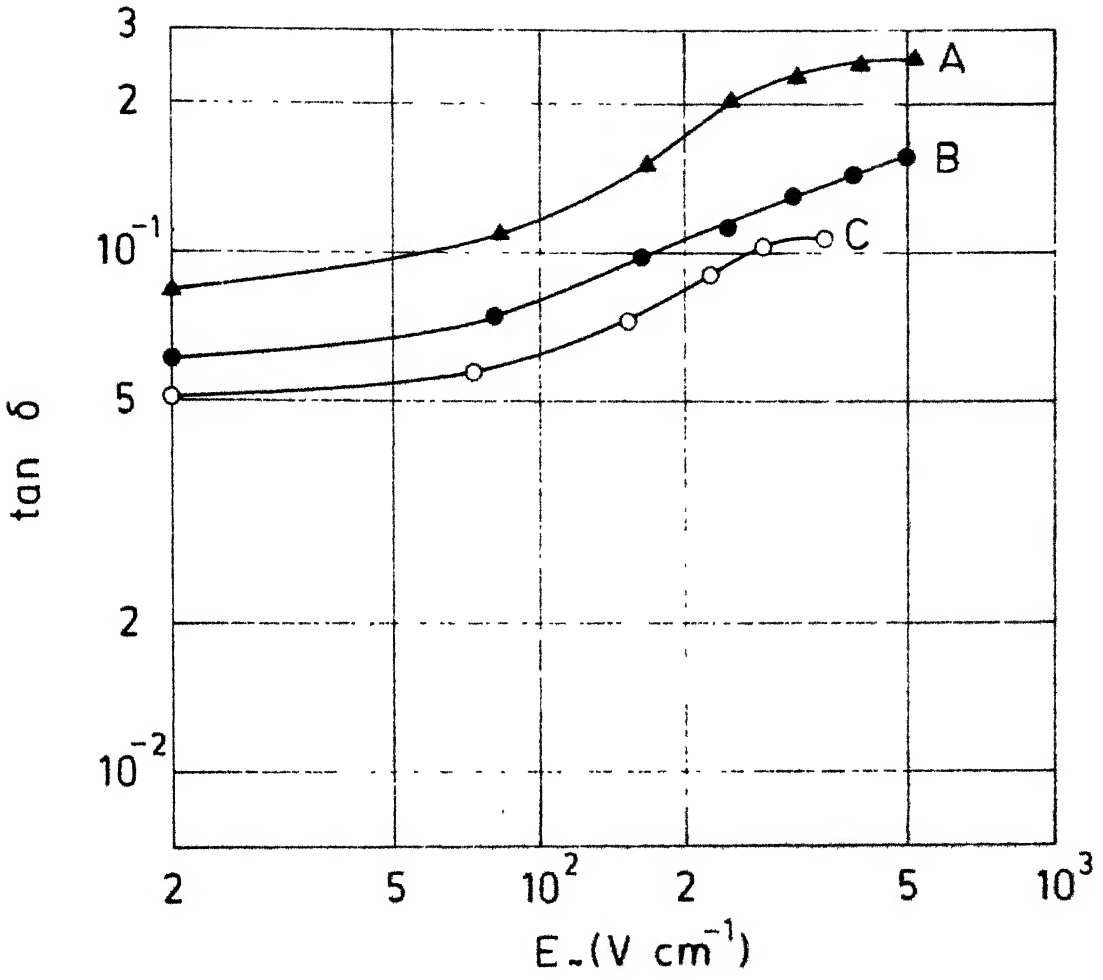

Fig. IV.5. Dependence of the loss factor tan δ on the amplitude of the external AC field below T_C for different concentrations of Mn doping. Measured at T = 28 °C and f = 1 KHz. Well aged sintered samples.

decreases with increasing Mn concentration, in the present investigation. The dependence of the permittivity with the amplitude of the external ac field decreases with increasing concentration of Mn. All these results show that the present Mn-doped $BaTiO_3$ is having a mixed behaviour.

Doping of Mn in the Barium Titanyl Oxalates is having a little or no effect on the decomposition of the BTO. There is a development of slight bending around 600°C on the DTA of doped samples (Figure IV.1). Similarly, doping of Mn in the Barium Titanyl Oxalate does not produce any change in the IR spectra of BTOs. So in the present case, the influence of the dopant Mn on the Barium Titanyl Oxalates is negligibly small.

The large value in permittivity, which comes either due to the occupation of Mn along the grain boundaries and hence it might have inhibited the normal grain growth that occurs during sintering stage, or due to the trivalent Mn occupation at Ba site; but the occupation of the most of the Mn at Ti site is the requirement of the acceptor doped material.

It was decided to have a look on the preparatory doping technique; and simultaneously carry out the investigation on the present samples too. The reason to probe the doping of Mn in the BTO is due to a careful observation of the precipitate formation: in the Mn-doped case the formation of the precipitate was delayed compared to the undoped case. Moreover the careful observation shows that the precipitate

is forming with some difficulty involved in their own system.

Unlike the conventional method, the doping or substituting the foreign element in this oxalate method is rather complex, because it is a precipitating technique. This will be much more complicated when (i) the dopant concentration is small and (ii) the dopant cation is unstable in the presence of barium and titanyl oxalates. This necessiated a careful study of the role of Mn while it is precipitated with BTO.

To proceed further, a working hypothesis has been assumed, in the following way: when Mn added to the barium titanyl solution and hence formed the Mn-doped BTO the chance for Mn to form its oxalate along with barium titanyl oxalate is small; and mostly it settles down on the BTO precipitate. It is only the assumption based on the observation, to "zeroed in" in the development of the doping technique.

IV.2. DEVELOPMENT OF THE Mn-DOPED COMPOSITION:

IV.2.1. Developmental Ideas and Their Influence on the Mn-doped Compositions:

The points involved in the development process (23,33) are, compared to the undoped case, when Mn-added barium titanyl solution was tried to be precipitated, the careful observation of the experiment showed that although the experiment running similar to that of undoped case but in the doped case, the formation of the precipitate was slightly delayed. This indirectly tells that the presence of Mn is disturbing the other cation oxalates or vice versa.

So to evolve a reasonably doped composition, three different pilot experiments were done.

Neither the concentrations of barium and titanium was changed nor any external catalyst was used. The temperature of the formation was maintained similar to that of undoped case.

IV.2.1.1. Basis, Result and the Discussion of the Pilot Experiments:

In the first pilot experiment, since the amount of Mn is negligible and Mn is not very stable in the presence of other oxalates, instead of adding to barium and titanium solutions, Mn was added to the oxalic acid solution and Mn-doped compound was precipitated. The idea which was used in this experiment: After forming barium oxalate in the presense of excess of oxalic acid, Mn was added in drops to see the possibility of barium manganese oxalate formation. It was observed that the barium oxalate started to disappear. This means there exists a reaction between Mn and the oxalate ion. This explains why the delay was observed in the precipitation of Mn-doped BTO of earlier experiments. To proceed further one may advance a hypothesis: From the above experiment we will assume that there exists a reaction between Mn and oxalate ion and probably Mn is getting reduced, the question is how is it possible for Mn to form its oxalate if it is present in this reduced condition. If we go back to the earlier Mn-doped BTO experiments one can see that Mn was accepted to some extent by the compound. This means, is there any more reaction occurring in the solution in order to oxidise the Mn to form its oxalate.

To gain further understanding, the oxalic acid solution which contains barium ion and reduced Mn ion was taken back, and $TiCl_4$ solution was added drop by drop into this solution. It was observed, immediately after $TiCl_4$

drop touches the solution, there forms a intense change in the colour of the solution from clear to reddish brown and a precipitate settles down. The precipitate was reddish brown against a background of a white matrix. It is clear that there exists a reaction between $TiCl_4$ solution and the Mn ion, preferably reduced Mn ion. This was the basis for the first pilot experiment. Differential thermal analysis was done on this sample (Figure IV.6) and Table IV.4 shows its peak temperature. In this case also there is hardly any effect of Mn on the decomposition of BTO.

The IR spectra of the compound was taken to see the influence of Mn in this compound with respect to the pure barium titanyl oxalate. Figure IV.7 shows the IR spectra of BTO(A) and BTO(E).

If we refer the Figure IV.7, the band which is due to the titanium molecule has been shifted to higher frequency, 520 cm^{-1}, compared to the undoped case, 507 cm^{-1}. Firstly it shows that the manganese has been accepted within the compound, as required in the titanium site, and secondly, the higher frequency shift of the peak tells that Mn which get into the BTO compound is having the oxidation state higher than the +2 state in which it was doped, since Mn is heavier than Ti, so one has to expect the shift to lower frequency.

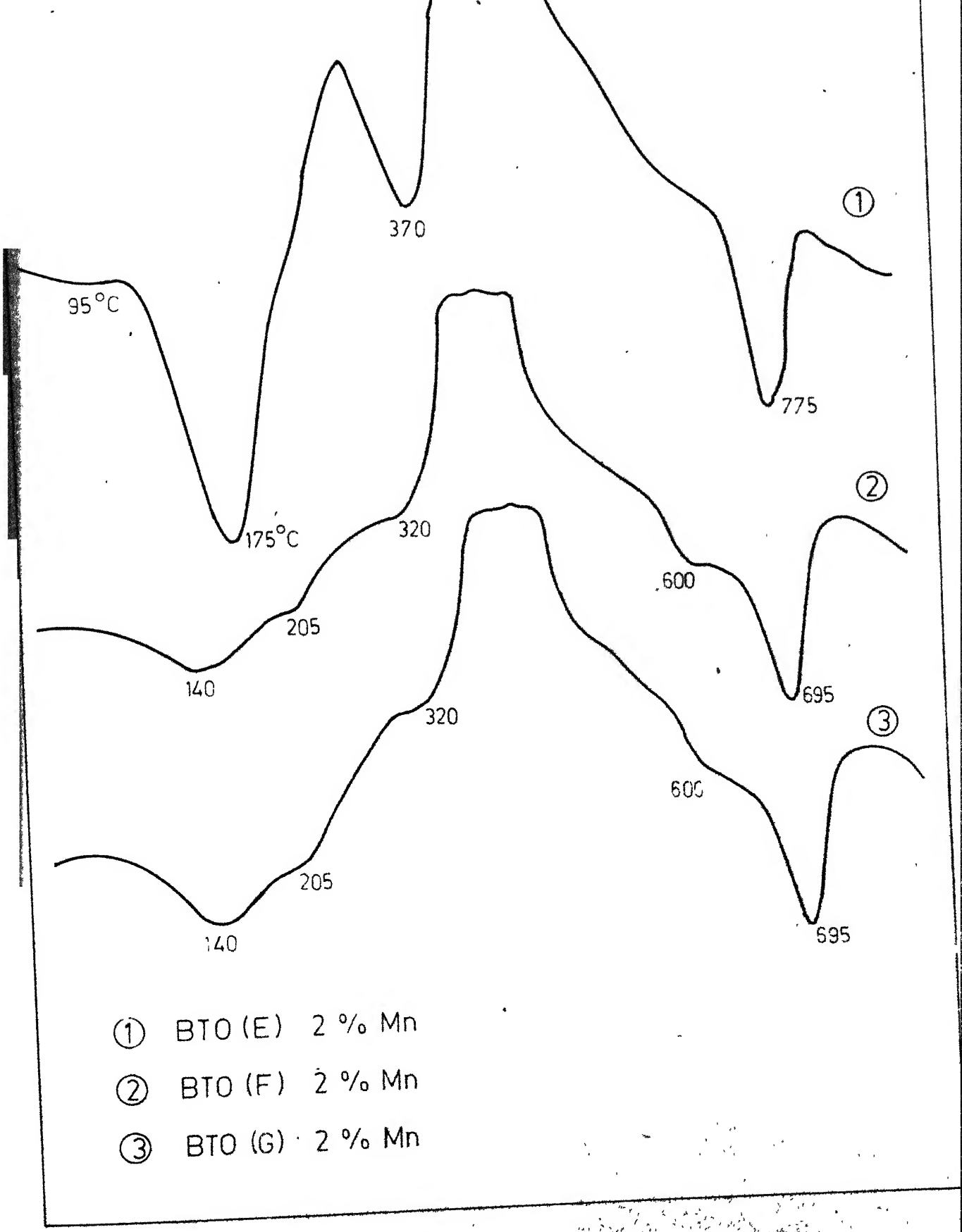

Fig. IV.6. DTA of Mn - Doped Barium Titanyl Oxalates.

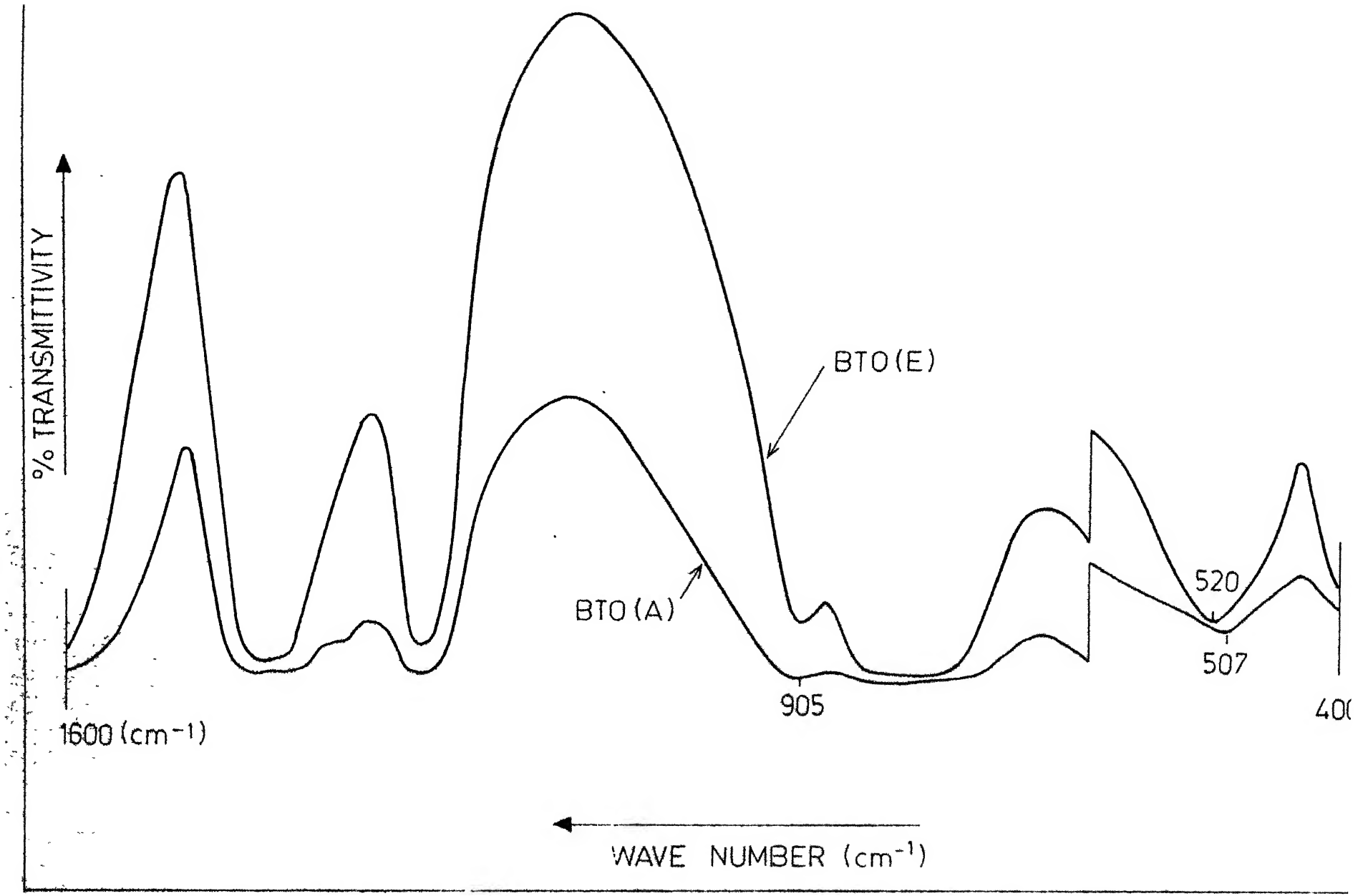
% TRANSMITTIVITY
BTO (E)
BTO (A)
520
507
905
1600 (cm⁻¹)
WAVE NUMBER (cm⁻¹)

Table IV.4

Peak position in DTA of undoped and Mn-doped barium titanyl oxalates

Compositions	Peak positions, °C					Additional peak, °C
	I	II	III	IV	V	
BTO(A): 0% Mn	95	160	245	365	790	-
BTO(C): 2% Mn	80	160	240	x	795	-
BTO(E): 2% Mn	95	175	x	370	775	-
BTO(F): 2% Mn	x	140	205	320	695	600
BTO(G): 2% Mn	x	140	205	320	695	600

Table IV.5

Chemical analysis - Ti/Ba ratio

Sample	Ratio of Ti to Ba
$BaTiO_3$(E)	0.95
$BaTiO_3$(F)	0.98
$BaTiO_3$(G)	0.97

By using X-ray diffraction pattern, the tetragonality of the $BaTiO_3$ was checked. In this, the tetragonal splitting was not satisfactory and the chemical analysis, Table IV.5, shows that more than 2 percent of Mn was accepted by the compound, since we took only 2 percent of Mn to dope. In the preparation of this compound, Ba was taken only stoichiometric requirement and Ti moles was removed by 2 percent in order to facilitate Mn doping. In analysing these facts, if there exists the reaction between Mn and the oxalate ion, then, when Ba and Ti solution touches the oxalic acid, Mn will spoil the titanium oxalate also, since we already removed the 2 percent of titanium.

The second pilot experiment was done to tackle this problem. The principle of this experiment is similar to that of the first pilot experiment, and Ba was added to the oxalic acid, the amount which is equal to the amount of Mn addition and then Ti was kept the same as required for stoichiometric requirement. Figure IV.8 shows, its IR spectra and Figure IV.6 shows its DTA. Table IV.5 shows its chemical analysis.

X-ray pattern was taken. The tetragonal splitting was clear, and only the tetragonal phase was detected. The chemical analysis was satisfactory and IR spectra shows Mn did get accepted by the compound. The third pilot experiment was the same as the second pilot experiment, but only the different form of Mn ($MnCl_2$) was added to the

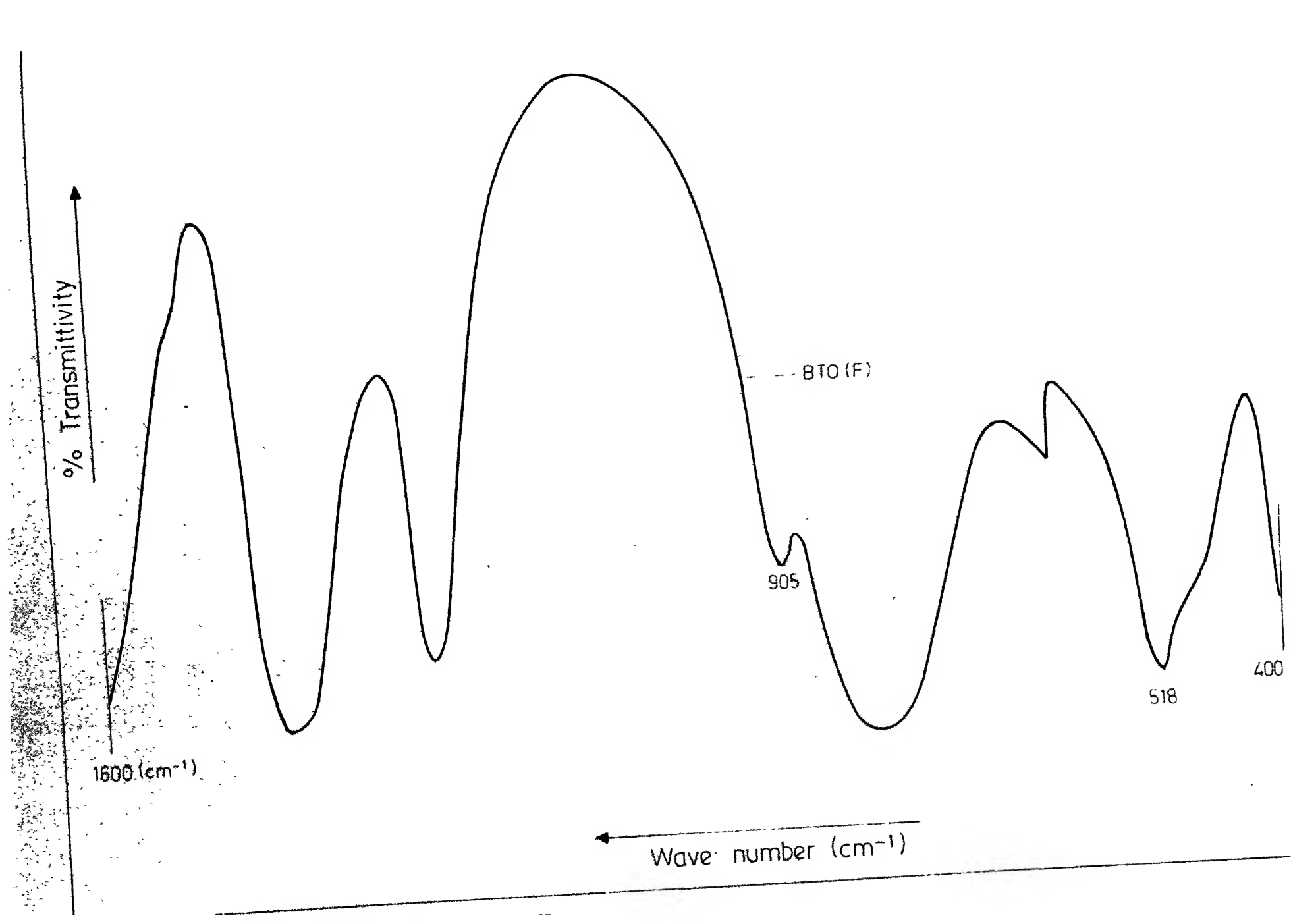
% Transmittivity
BTO (F)
905
518
400
1600 (cm⁻¹)
Wave number (cm⁻¹)

oxalic acid solution. Its chemical analysis showed expected result and in the X-ray pattern only tetragonal phase was observed.

In the case of BTO(F) and BTO(G), the peak position has got decreased to lower temperatures compared to the BTO(A). There was also an additional peak at 600°C. This can be attributed to the transformation of Mn oxalate group to the Mn_2O_3 (generally Mn_2O_3 phase will appear above 500°C). Also the enthalpy change of the peaks, particularly the one which is due to the main oxalate decomposition (around 320°C) has got decreased.

Figure IV.9 shows the IR spectra of $BaTiO_3$(A), $BaTiO_3$(C) and $BaTiO_3$(F). In this, there is no change in the peak positions. In the case of the IR spectra of BTO(E) and BTO(F), as discussed earlier, the shift of the Ti peak is to the higher frequency compared to the BTO(A) spectra. This indirectly tells that the complex in which Mn precipitated with BTO is having higher force constant, since the concentration of Mn is only 2 mol percent. This proves the successful use of IR spectra as a tool to detect the Mn in the BTO.

Figure IV.10 shows the variation of the permittivity with temperature and Table IV.6 summarizes their dielectric properties. The things to be noted are: (i) compared to the $BaTiO_3$(A) in the well doped case the Curie temperature has been lowered by 5°C, (ii) the peak position at T_c has been lowered considerably, (iii) the room

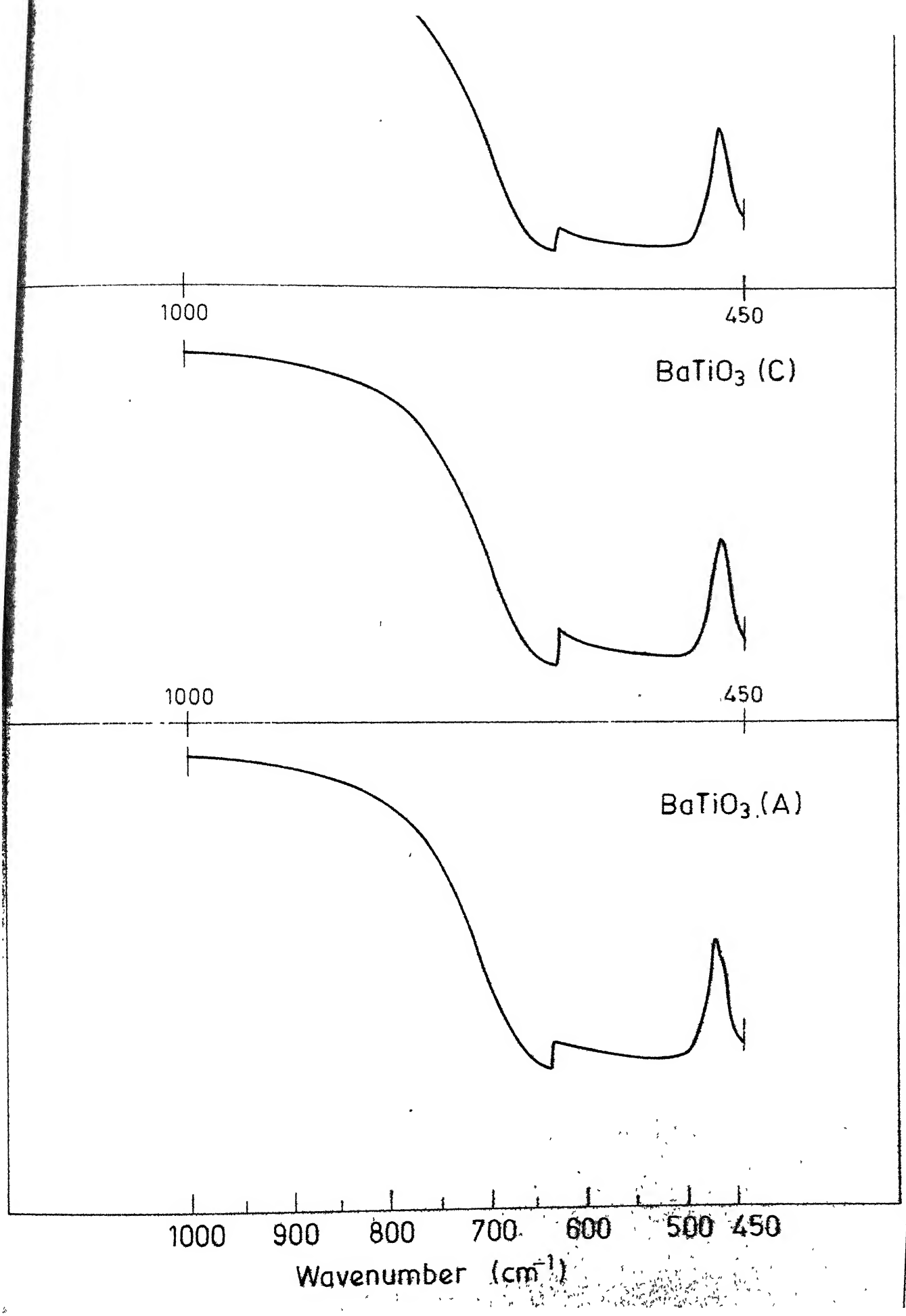
1000
450
BaTiO3 (C)
1000
450
BaTiO3 (A)
1000 900 800 700 600 500 450
Wavenumber (cm-1)

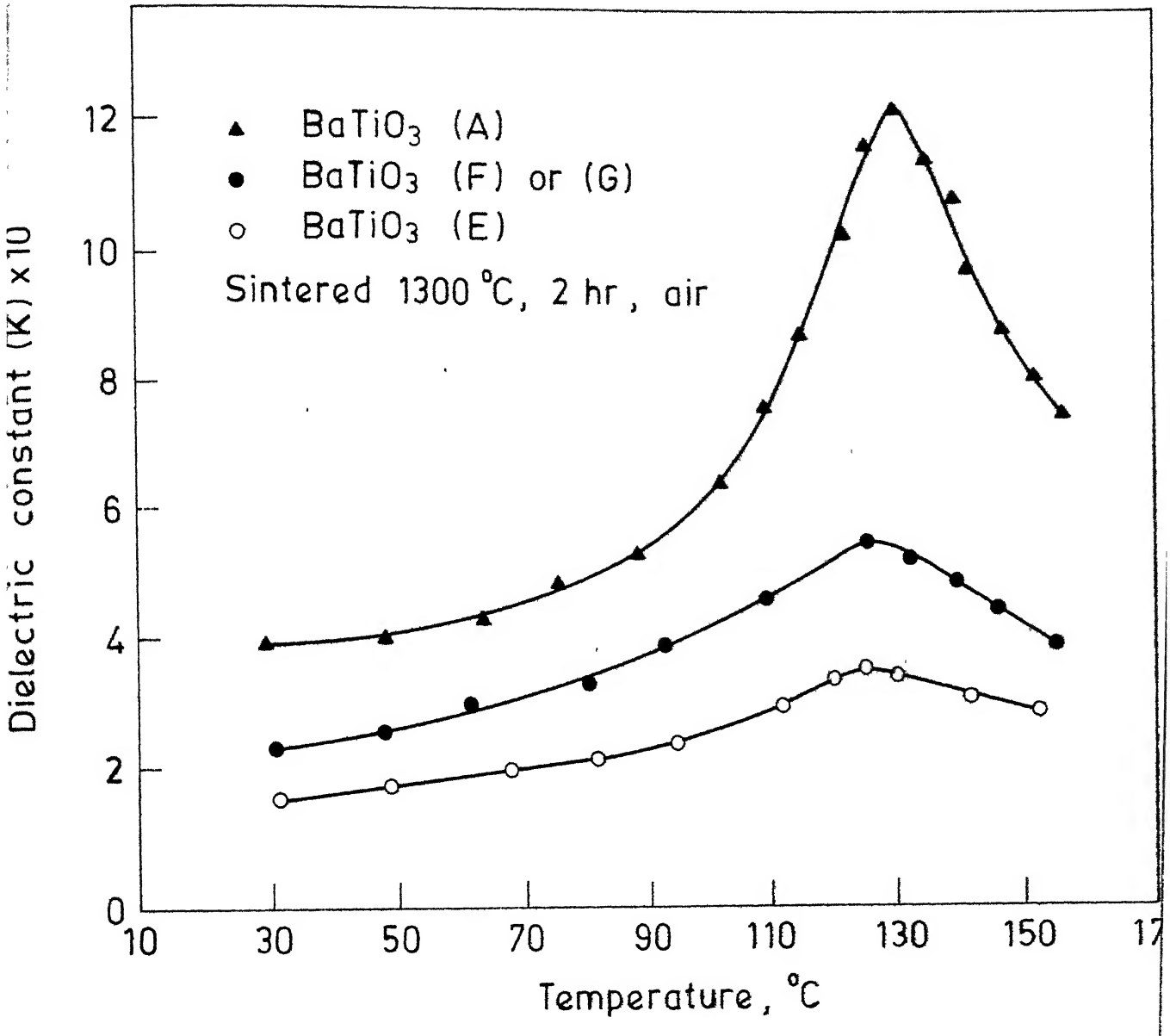

Fig. IV.10. Variation of the dielectric constant with temper

Table IV.6

Dielectric properties of Mn-doped and undoped samples

Composition	Dielectric constant*		T_c	tanδ R.T.	Change in permittivity with 500 V/cm, ac amplitude	
	at R.T.	at T_c			ΔK	% $\frac{\Delta K}{K}$
$BaTiO_3$(A)	3600	12000	130[X]	0.045	1400	39.9%
$BaTiO_3$(E)	1600	2800	124	0.040	190	11.9%
$BaTiO_3$(F)	2400	4800	125	0.020	220	9.2%
$BaTiO_3$(G)	2200	4700	125	0.019	220	10%

*All the values are porosity corrected datas.

X Most of the 0% samples in this batch showed Curie point at 130°C.

temperature dielectric constant is decreased to around 2000 compared to the 3600 of the pure $BaTiO_3$.

Figures IV.11 and IV.12 show the ac behaviour of these samples. It is clear from the figures and also from the Table IV.6 that the samples $BaTiO_3$(F) and $BaTiO_3$(G) show less change in permittivity and tanδ values compared to the other samples. All these effects are due to the effective role of oxygen vacancy donors with the Manganese ion acceptors.

IV.2.1.2. Electrochemical Experiment to Support the Redox Hypothesis:

Two electrochemical cells were formed to check the hypothesis as described in the Section IV.2.1.1. The procedure of the experiment is briefly described in the Appendix III. The gain in weight (in mg) of the manganese electrode when it was in the oxalate electrochemical cell and loss in weight (in mg) when it was in the $TiCl_4$ electrochemical cell and the developed voltage of 900 mV and 600 mV respectively in the former and latter positions of Mn supports the hypothesis.

IV.2.2. Domain Stabilization and Resistivity Studies:

Hagemann (14) studied the domain stabilisation in doped $BaTiO_3$. The dependence of dielectric constant and tanδ with ac amplitude becomes larger with La doping and appreciably decrease with growing Fe and Mn concentrations upto 1 mol percent. To understand the stabilisation

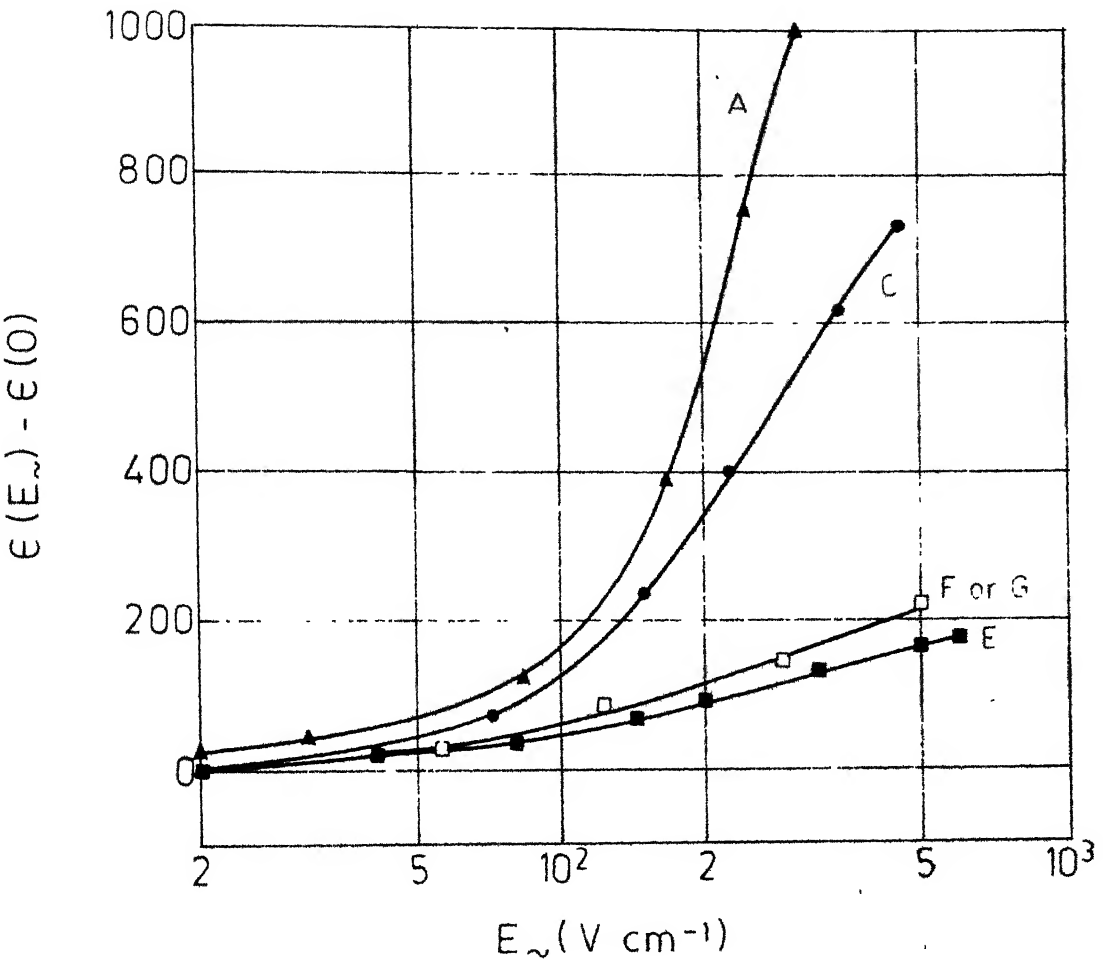

Fig IV 11. Dependence of ϵ on the amplitude of the external AC field. Measured at T=28°C and f=1KHz, well aged sintered samples.

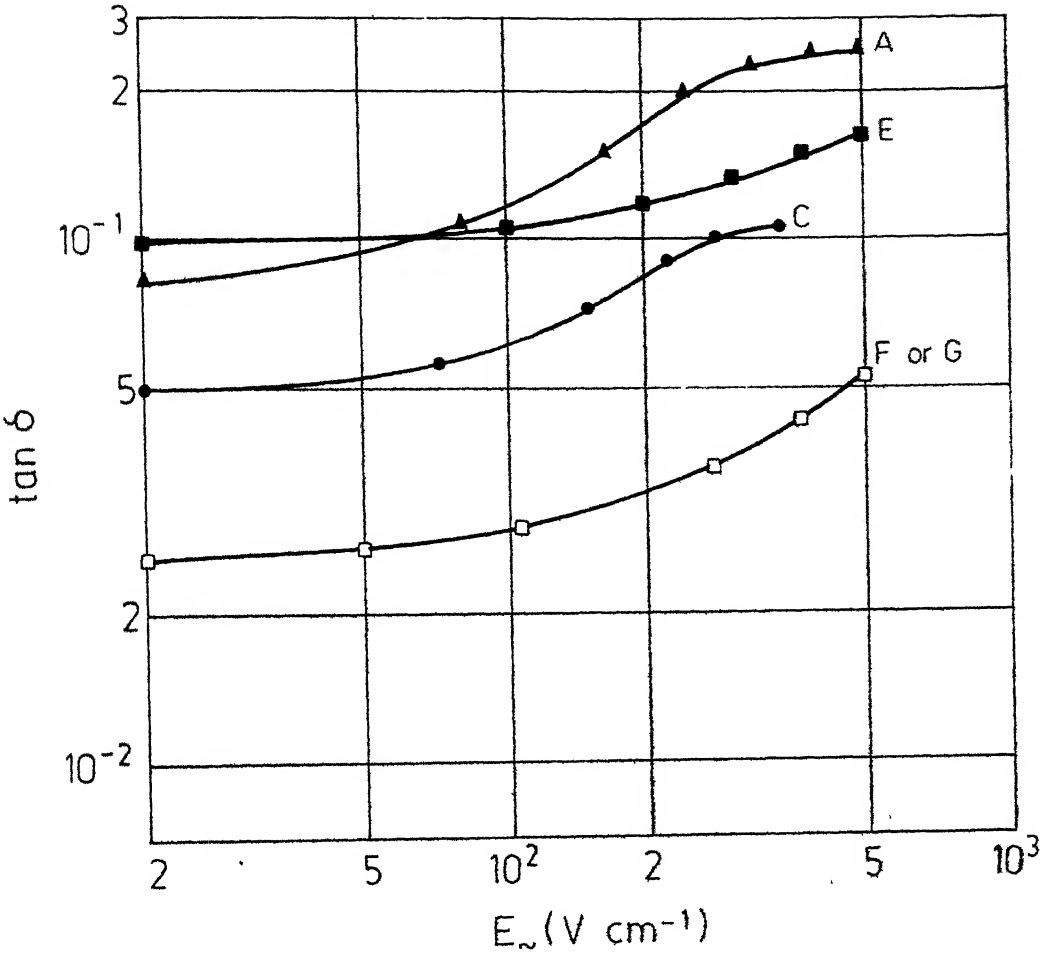

Fig IV.12. Dependence of the loss factor tan δ on the amplitude of the external AC field. Measured at T=28°C and f=1KHz, well aged sintered samples.

of domains three different mechanisms have been proposed (34,35,36): (i) anisotropic defect centres are oriented by the local spontaneous electrical moments which, in turn, favour an existing direction of P_s within each domain (bulk effect); (ii) lattice defects diffuse to regions near domain walls and reduce the mobility of the walls (wall effect); and (iii) to compensate the electric fields that arise from jumps in P_s at the grain boundaries charged defects move towards or along grain boundaries and fix the overall domain structure (grain boundary effect).

The bulk and the wall effects are controlled by defects in the $BaTiO_3$ lattice which can be altered by doping. If $BaTiO_3$ is doped with Ca, Sr, or Zn no additional defects are formed because no charge compensation is necessary. If it is doped with Mn or Fe the concentration of oxygen vacancies is increased, and if $BaTiO_3$ is doped with La the concentration of oxygen vacancies is lowered.

The ESR measurements of Fe-doped $SmTiO_3$ (37), Mn-doped $SrTiO_3$ (38), and Mn doped $BaTiO_3$ (39) shows that the transition metal (TM) dopes are associated with charged oxygen vacancies in the same Perovskite cell. In this way 'axial' defect centres are formed. It was proved recently that Mn-oxygen vacancy centres are preferentially oriented parallel to the spontaneous polarisation P_s in the tetragonal ferroelectric phase of $BaTiO_3$ single crystals. The stabilisation in Mn doped single crystals was attributed to the bulk effect.

Hagemann (14) hypothesised, that in $BaTiO_3$ ceramic, too, the stabilisation of the domains upon the Fe or Mn addition, is by a gradual orientation of axial TM-V_o associates. The degree of stabilisation is controlled by the V_o concentration. This demands the annealing of the samples at higher temperature and then subsequent cooling to room temperature very rapidly in order to achieve a defect structure defined by unequivocal thermodynamic conditions. During quenching, the high temperature concentrations of the atomic defects are frogen: the electric equilibria, on the other hand, will readjust. This means that the total concentration of vacancies remains constant but the charge of the individual defects can be redistributed. Sintered pellets of A, B, C, E, F and G were annealed at 1100°C for 10 minutes and then cooled rapidly to room temperature to achieve the defect structure. These samples were studied under ac field. Figures IV.13 and IV.14 shows the dependence of ε and $\tan\delta$ with ac amplitude. In the case of F or G there is hardly any change in permittivity and dissipation factor with ac field upto the possible amplitude limit. There is a slight change in permittivity of the sample after 500 V/cm. Samples B and C show the donor and acceptor doped behaviour.

This experiment indirectly tells that in the samples B and C, Mn might have occupied the Ba site strongly, apart from the grain boundary and Ti positions, because the change in permittivity with field is higher

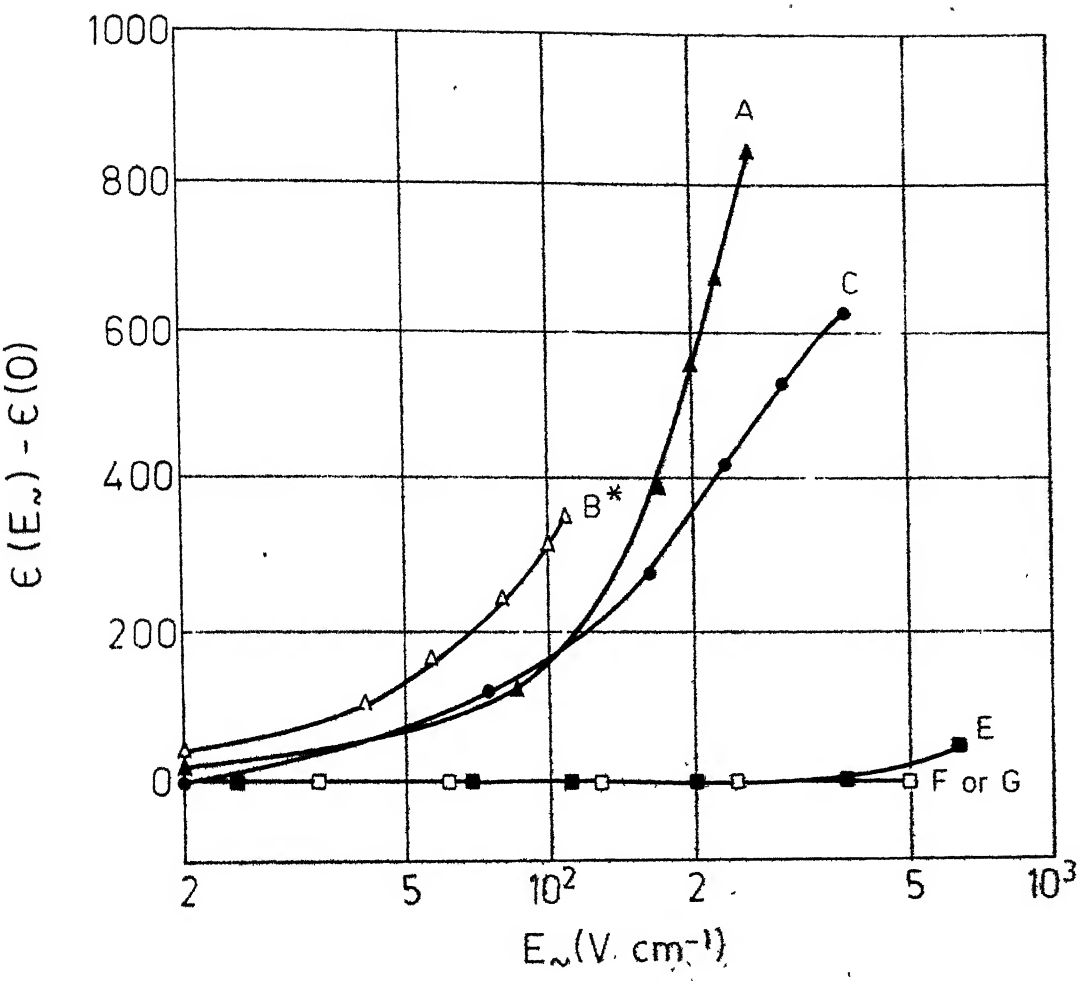

Fig. IV.13 Dependence of ϵ on the amplitude of the external AC field. Measured at T = 28°C and f = 1KHz. Samples were annealed at 1100°C for 10 min. and quenched to R.T. in air atmosphere.

* Sample B: 1 mole % Mn addition to the Ba and Ti solutions. B and C belong to one set of system.

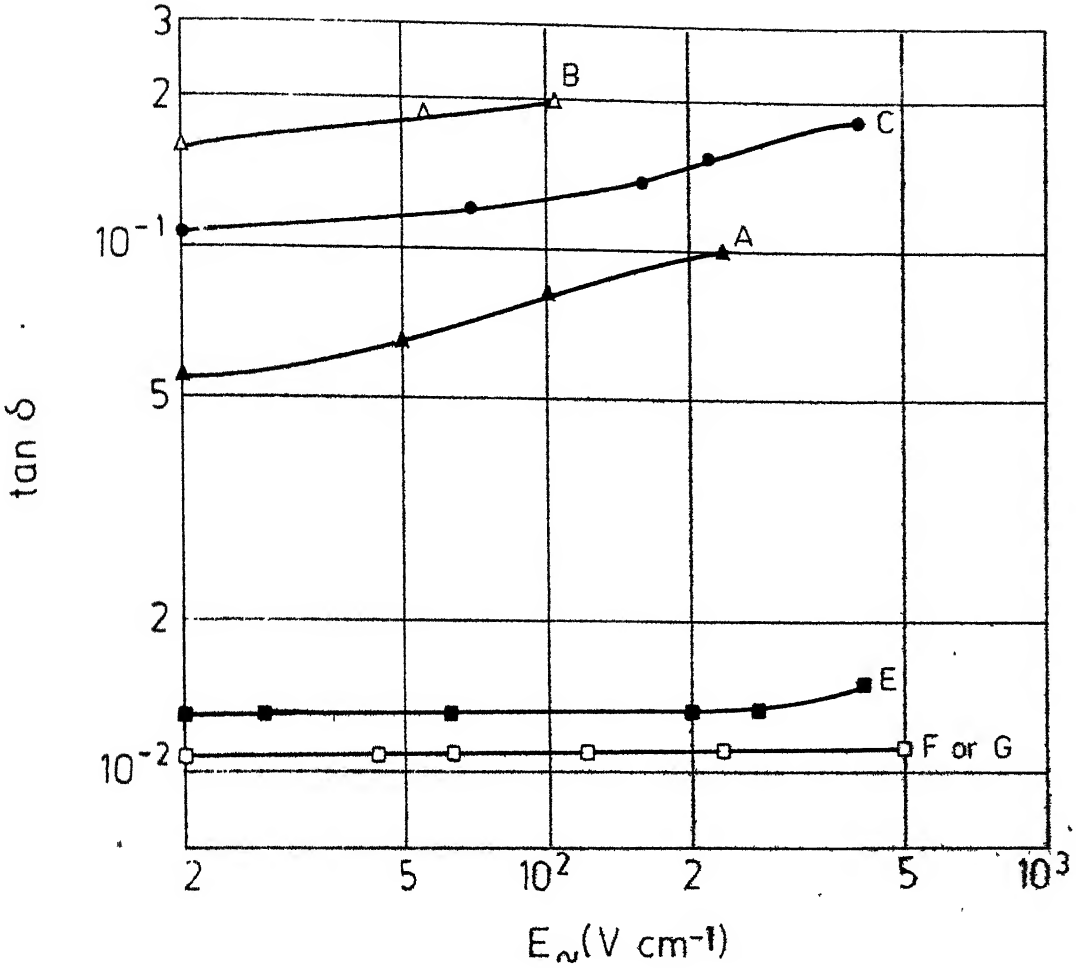

Fig IV·13. Dependence of the loss factor tan δ on the amplitude of the external AC field. Measured at T = 28°C and f = 1KHz. Samples were annealed at 1100°C for 10 min. and quenched to R.T. in air atmosphere.

than that of the undoped sample and the degree of stabilisation is poor, which is controlled by the oxygen vacancy concentration.

In order to see the grain boundary effect, identical sintering (1300°C/2 hrs) and annealing (1100°C/4 hrs) treatments were given to the samples A, B, C, E, F and G. Figures IV.15 and IV.16 shows the dependence of the dielectric constant and the loss factor with ac amplitude. There is no change in the case of F and G as compared with their sintered condition (Figures IV.11 and IV.12). But B and C started to show the domain stabilisation to some extent. This shows these samples are having some amount of grain boundary effect too.

To see the behaviour of these samples in the low partial pressure of oxygen, the freshly sintered samples of A, B, C, E, F and G were annealed at 800°C for 30 minutes in the partial pressure of oxygen, $P_{O_2} = 10^{-12}$ atm.

Figures IV.17 and IV.18 shows the permittivity and the loss factor dependence with ac amplitude. Samples B and C shows good stabilisation behaviour compared to other samples. These studies shows that the presence of Mn in the grain boundaries, and at Ba sites apart from its favourable Ti site.

The resistivity of these samples were measured at room temperature and at 150°C. Table IV.7 shows their resistivity values.

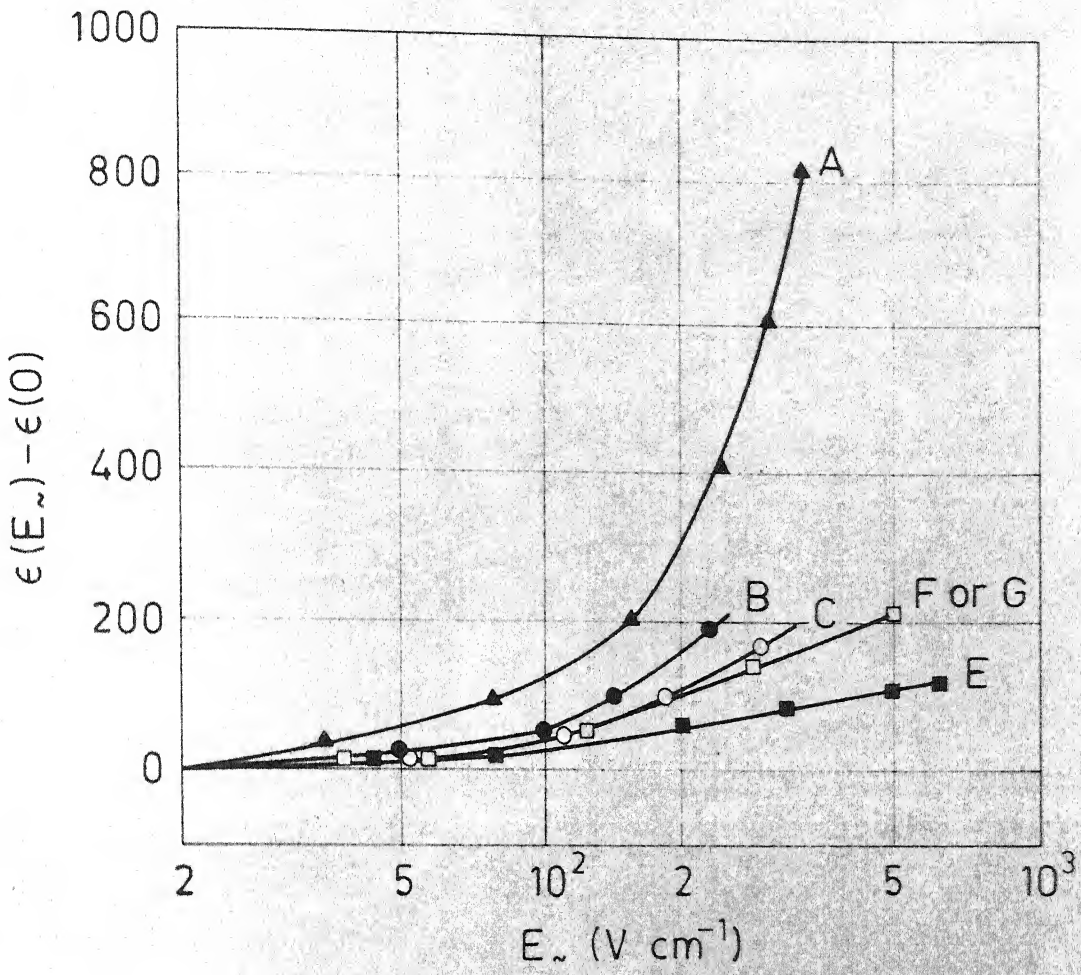

Fig. IV.15. Dependence of ϵ on the amplitude of the external AC field below T_c for different concentrations of Mn doping. Measured at T = 28 °C and f = 1 KHz. Identical sintering (1300 °C/2 hrs) and annealing (1100 °C/4 hrs) treatments were given to check the grain boundary effect. Well aged samples.

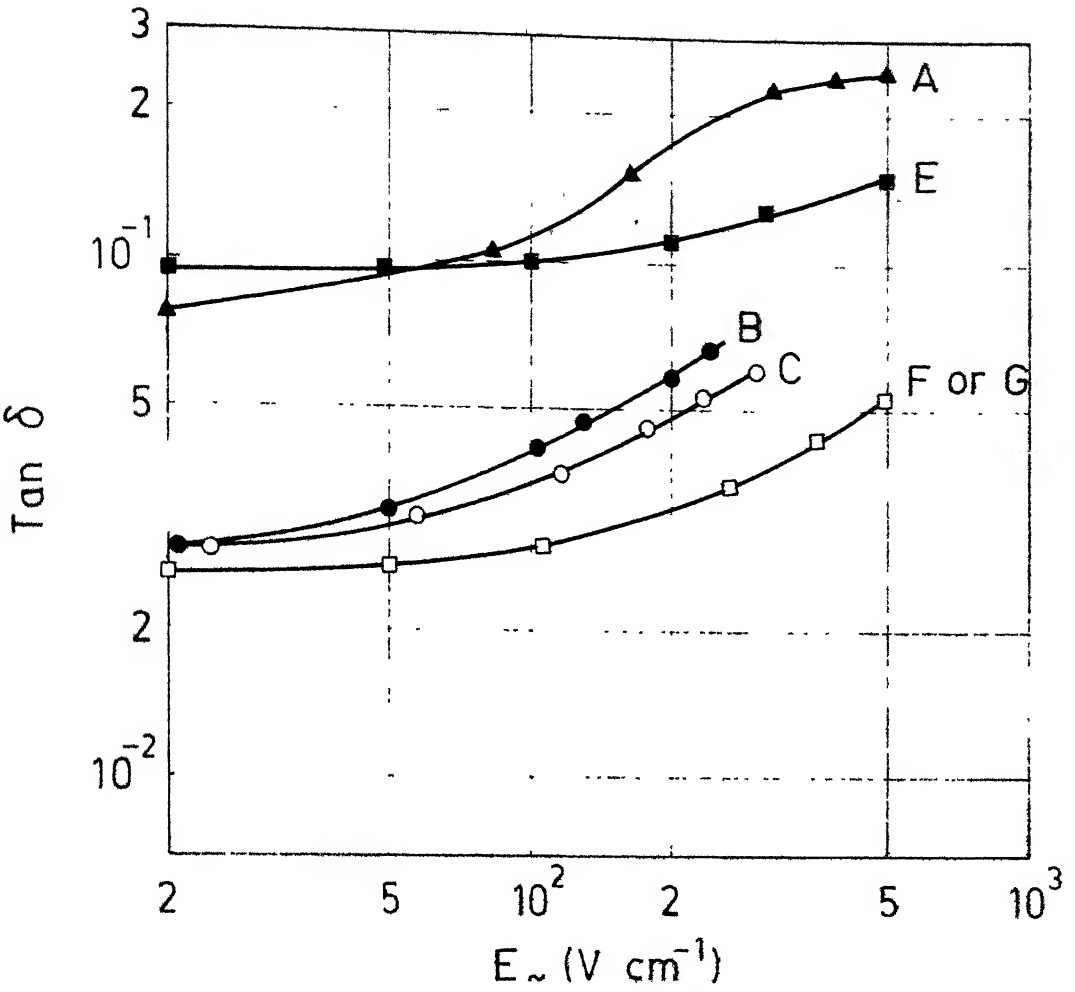

Fig. IV.16. Dependence of the loss factor tan δ on the amplitude of the external AC field below T_c for different concentrations of Mn doping measured at T = 28 °C and f = 1 KHz. Identical sintering (1300 °C/2 hrs) and annealing (1100 °C/4 hrs) treatments were given to check the grain boundary effect. Well aged samples.

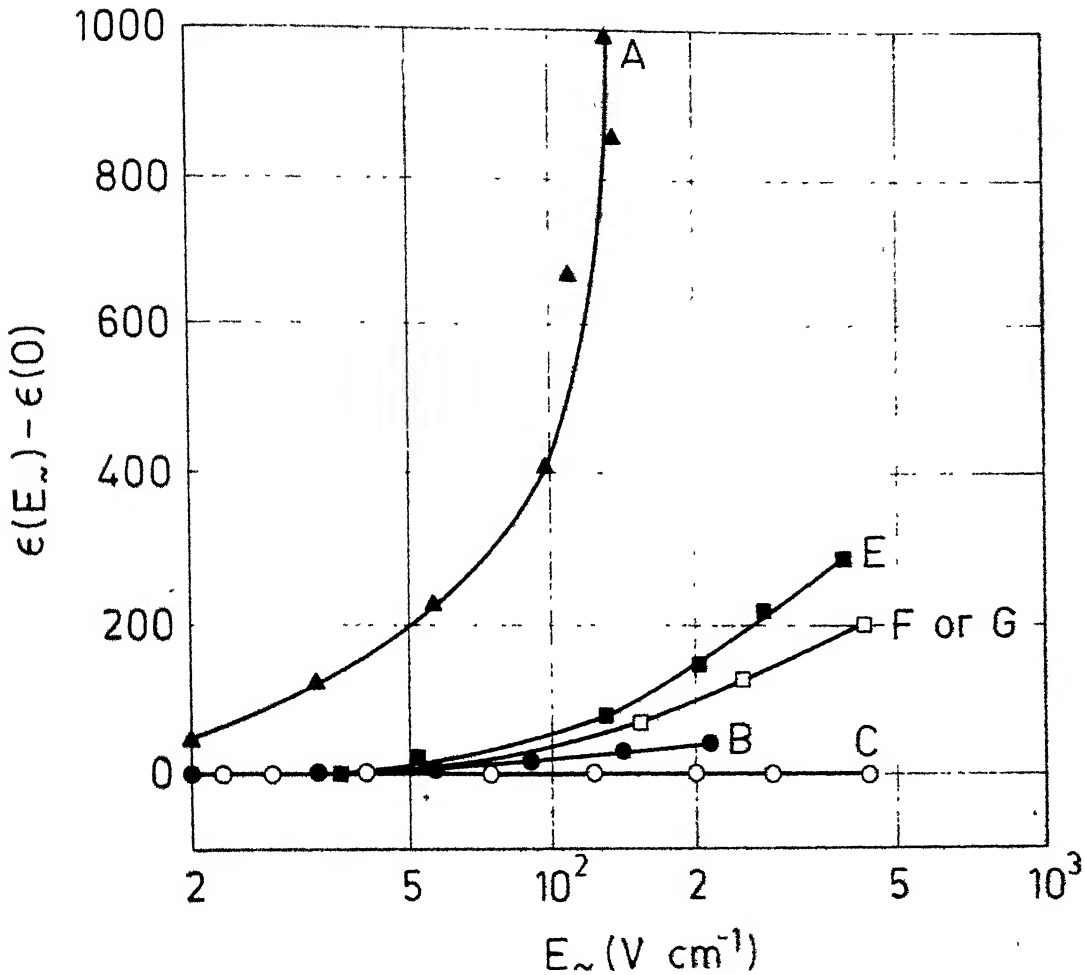

Fig. IV.17. Dependence of ϵ on the amplitude of the external AC field below T_c for different concentrations of Mn doping. Measured at T = 28 °C and f = 1 KHz. Samples were annealed in UHP Argon at 800 °C with $PO_2 = 10^{-12}$ atm for 30 min. Well aged samples.

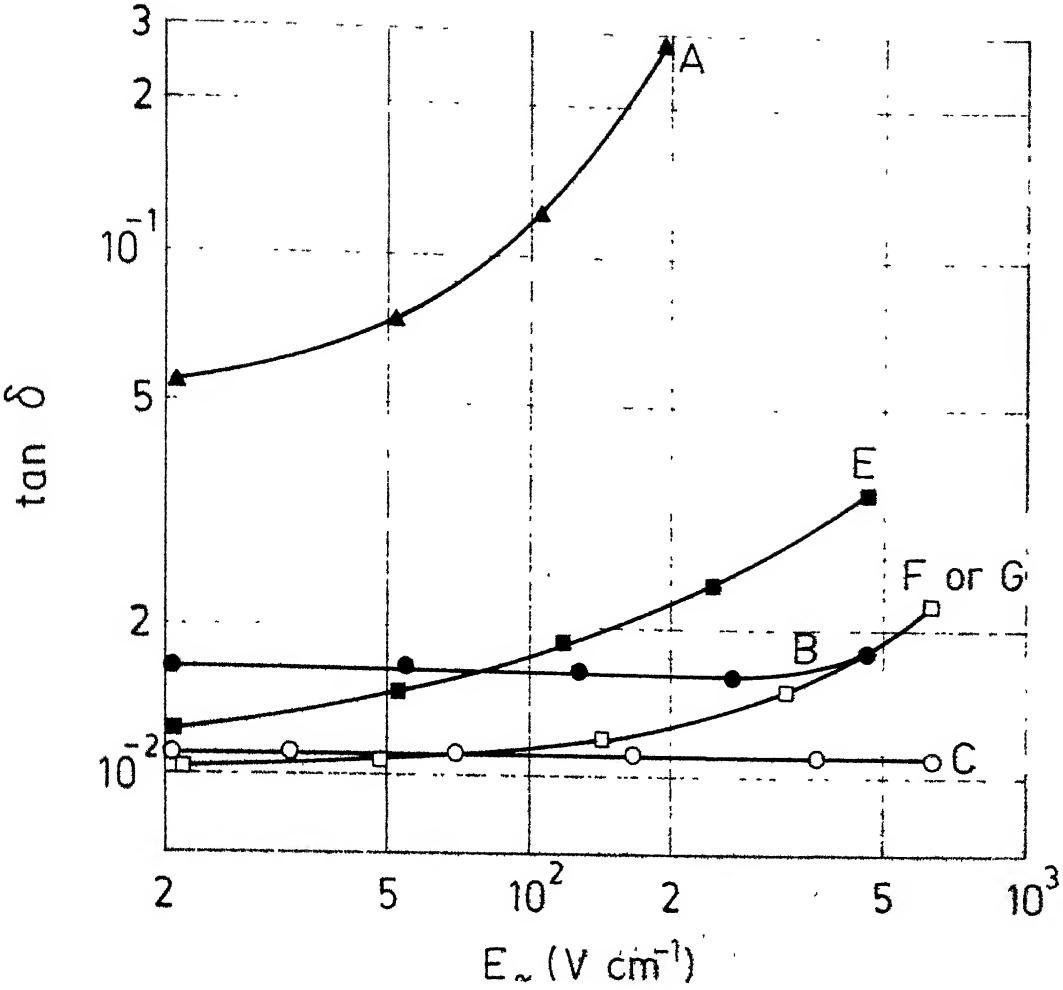

Fig. IV.18. Dependence of the loss factor tan δ on the amplitude of the external AC field below T_c for different concentrations of Mn doping. Measured at T = 28 °C and f = 1 KHz. Samples were annealed at 800 °C with $PO_2 = 10^{-12}$ atm for 30 min. Well aged samples.

Table IV.7

Resistivity of undoped and Mn-doped samples after annealed at 800°C for 30 minutes; $P_{O_2} = 10^{-12}$ atm.

Composition	Resistivity at room temperature ohm-cm	Resistivity at 150°C ohm-cm
A	7.1×10^{8}	5.6×10^{8}
B	1.1×10^{9}	2.9×10^{9}
C	1.6×10^{9}	4.5×10^{9}
E	6.9×10^{10}	5.1×10^{10}
F or G	2.7×10^{10}	1.9×10^{10}

Compared to all other samples E, F or G retains their high resistivity. All the pellets had the resistivity of 10^{12} ohm-cm, before the low partial pressure annealing. There was no change in colour of the pellets except in the case of pure $BaTiO_3$, there induces a slight blueish colour with white background. Referring the resistivity values at room temperature and at 150°C the samples A, E, F or G show the descending nature whereas the samples B and C show the slight increase in their values. Actually the acceptor doped $BaTiO_3$ does not have any positive temperature coefficient of resistance. This shows that the samples B and C have, to some extent, the defective grain surfaces. It is clear that the doping procedure has a marked influence in the properties of Mn-doped $BaTiO_3$. This is due to the

fact that Mn has three important oxidation states (+2, +3 and +4) and in different oxidation states it may occupy different sites, thus the doping procedure may influence the doping site and the properties.

IV.3. STUDY OF THE Mn-DOPED COMPOSITIONS: GROUP I AND GROUP III:

Based on the pilot experiments $BaTiO_3$ doped with Mn concentration 0.2, 0.6, 1.0, 1.4 and 2.0 mole percent prepared. Their behaviour is discussed below.

IV.3.1. Thermal Analysis Study:

Figure IV.19 shows the DTA of Mn doped barium titanyl oxalates. Table IV.8 summarising the peak positions and Table IV.9 comparing the weight losses of the BTO(M_5) and BTO(A). There is a gradual decrease of the peak temperatures with increasing concentration of Mn. There is no separate water peak at 95°C in the case of BTO(M_4) and BTO(M_5). There is a additional peak at 600°C in the case of BTO(M_4) and BTO(M_5) indicates the conversion of the Mn oxalates into the oxide of Mn. The enthalpy change of the endothermic peak that corresponds to the main oxalate decomposition ($\sim$350°C), in the case of BTO(M_5) is nearly 2/5 of the BTO(A) peak. From the Table IV.9, it is clear, that in the weight loss corresponds to the dehydration and initial decomposition of the oxalate, the weight loss involved in BTO(M_5) is nearly 14.5 mg lesser compared to the BTO(A). These things show that the water molecules

Table IV.8

Peak positions in DTA of undoped and Mn-doped barium titanyl oxalates

Compositions	Peak positions, °C					Additional peak
BTO(A) : 0 Mn	95	160	245	365	790	-
BTO(M_1): 0.2 Mn	95	165		345	742	-
BTO(M_2): 0.6 Mn	95	162		340	740	-
BTO(M_3): 1.0 Mn	95	162		340	720	-
BTO(M_4): 1.4 Mn		162		340	710	600
BTO(M_5): 2.0 Mn		156		320	697	600

attached with the doped case is smaller compared to the undoped one. The weight loss which corresponds to the main oxalate decomposition of the BTO(M_5) is nearly 20.5 mg higher compared to the BTO(A). This shows that the oxalate

Table IV.9

Comparison of the weight losses of the BTO(M_5) and BTO(A) per gram of the sample

Compositions	(i) mg	(ii) mg	(iii) mg	Total mg
BTO(A)	202.5	195.0	67.5	465.0
BTO(M_5)	188.0	215.5	47.0	450.5

(i) Dehydration and initial decomposition of the oxalate (~200°C)
(ii) Main oxalate decomposition (~350°C)
(iii) Final decomposition to $BaTiO_3$ (~750°C).

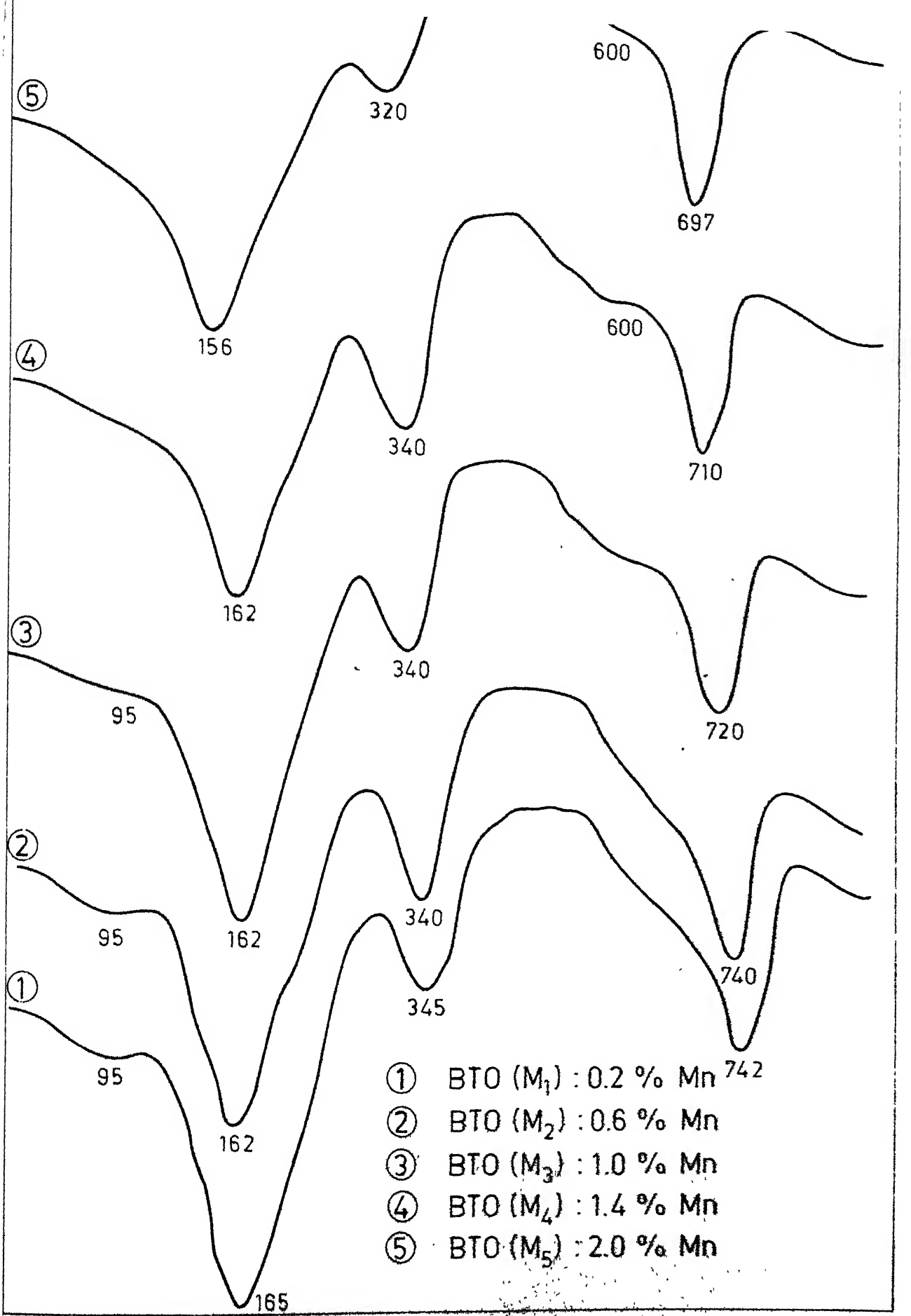
⑤
320
600
697
156
④
600
340
710
162
③
340
95
720
②
95
162
340
740
①
95
345
742
162
165
① BTO (M_1) : 0.2 % Mn
② BTO (M_2) : 0.6 % Mn
③ BTO (M_3) : 1.0 % Mn
④ BTO (M_4) : 1.4 % Mn
⑤ BTO (M_5) : 2.0 % Mn

which formed by Mn is in its higher oxalate form. In the final decomposition BTO(M_5) is having 20.5 mg lesser weight loss compared to BTO(A). This is because, the amount of O_2 evolved in the final decomposition is less in the case of Mn doped BTO since the dopant turns to its oxide form at 600^{o}K itself. There is a difference of 14.5 mg in the total weight loss.

When the precipitate of Mn doped BTO was make, as described earlier, as soon as the $TiCl_4$ touches the reduced Mn the colour of the solution becomes intense reddish brown. This is confirmed, mostly, as Mn^{3+} oxalate, $[Mn^{3+}(C_2O_4)_3]^{3-}$ (40). This is one of the reasons, why IR spectra shows the shift of Ti-O peak towards the higher frequency.

IV.3.2. X-ray Analysis:

The X-ray diffraction pattern of the calcined powders of undoped and Mn doped $BaTiO_3$ with different concentrations showed the presence of tetragonal phase. There is no change in the c/a ratio of the pure and Mn-doped samples upto the second decimal.

IV.3.3. Chemical Analysis:

Table IV.10 shows the Ti/Ba ratio of the pure and Mn doped samples. As expected Ti/Ba ratio decreases with increasing concentration of Mn.

Table IV.10

Chemical analysis: Ti/Ba ratio

Compositions	Ti/Ba
$BaTiO_3(M_1)$	0.99
$BaTiO_3(M_2)$	0.99
$BaTiO_3(M_3)$	0.99
$BaTiO_3(M_4)$	0.98
$BaTiO_3(M_5)$	0.98

IV.3.4. Temperature Dependence of Dielectric Properties:

Table IV.11 shows the dielectric properties of the undoped and Mn-doped $BaTiO_3$. Figure IV.20 shows the variation of the dielectric constant with temperature. The dielectric constant and the loss factor values decreases with increasing Mn concentration. There is a reduction of $5^{o}C$ of the Curie point in the 2 percent Mn sample compared to that of 0 percent sample. The peak height also has got suppressed. This means that the temperature coefficient of dielectric constant of the doped samples is small compared to the undoped one.

When the trivalent ions with similar radius of Ti^{4+}, replace the Ti ions in $BaTiO_3$ with one or more of the following three effects (10)

(1) The structure remains perovskite, with random replacement throughout the lattice; the distribution

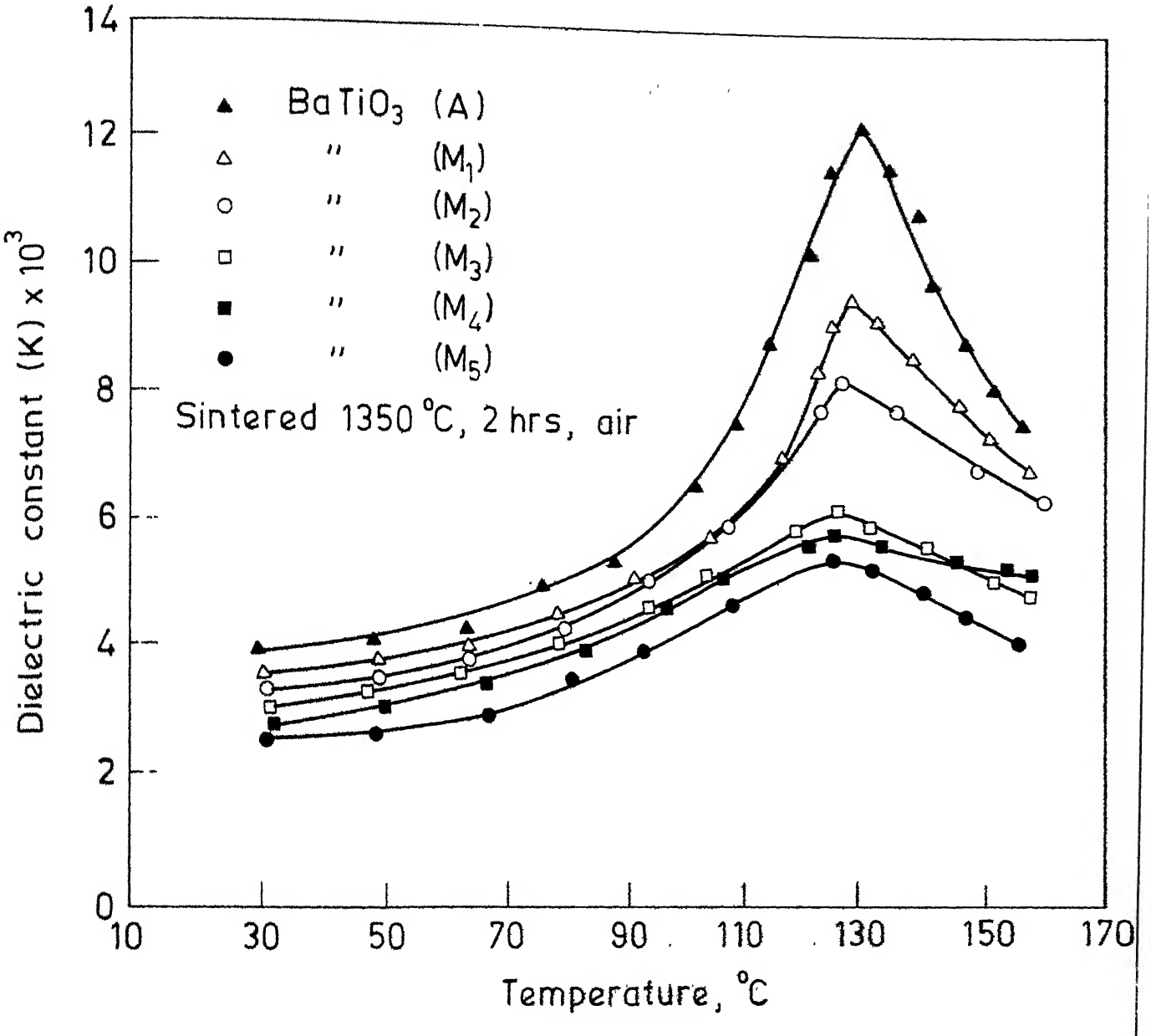

Fig. IV.20. Variation of the dielectric constant with temperatur

of the vacant O sites required to balance the reduced charge on the Ti sites is also random; the Curie point is lowered.

(2) The structure remains perovskite for the greater part and replacement is confined to certain laminae which also contain a high concentration of vacant O sites; the structure in these planes is similar to that in hexagonal $BaTiO_3$; the planes have a clamping effect which largely inhibits the ferroelectric behaviour of the material.

(3) The structure becomes hexagonal with random distribution of both trivalent ions and vacant O sites; the material is entirely paraelectric.

A structure similar to that described under (2) may also be assumed to occur in the absence of trivalent ions when high-purity barium titanyl oxalate is calcined at temperatures upto 1250°C.

This can only be given the status of a observed trend in the present study.

Table IV.12 shows the variation of the Curie point of the Mn doped samples which were subjected to different heat treatment. There is a decrease of T_c in the case of the low P_{O_2} treated samples and this decrease is large in the case of higher concentration of Mn doping. It is clear that the acceptor changes its oxidation state and thereby produces the oxygen vacancy for compensation. There is hardly any change in the T_c of the O_2 treated samples with the higher concentration of Mn but with lower concentration of Mn there is a increase of 1°C.

Table IV.11

Dielectric properties of Mn-doped $BaTiO_3$

Compositions	Sintered in air, 1350°C/2 hrs.				
	Bulk density (percent)	K at R.T.	tanδ	T_c	K at T_c
$BaTiO_3$(A)	97	4000	0.08	130	12000
$BaTiO_3$(M_1)	95	3700	0.076	129	9600
$BaTiO_3$(M_2)	96.5	3100	0.043	127	8000
$BaTiO_3$(M_3)	98	3800	0.023	127	5600
$BaTiO_3$(M_4)	98	2650	0.020	125	5400
$BaTiO_3$(M_5)	97.5	2500	0.020	125	5000

Table IV.12

Variation of the Curie point of Mn-doped samples with respect to the heat treatment

Composition	Sintered in air °C	Sintered in air and annealed and quenched in air °C	Sintered in argon (10^{-12} atm) and annealed and quenched in argon °C	Sintered in oxygen and annealed and quenched in oxygen °C
$BaTiO_3$(A)	130	129	128	130
$BaTiO_3$(M_1)	129	129	125	130
$BaTiO_3$(M_2)	127	126	122	129.5
$BaTiO_3$(M_3)	127	127	120	127
$BaTiO_3$(M_4)	125	124.5	117	125

IV.3.5. Domain Stabilisation and Loss Mechanism:

Figures IV.21 and IV.22 show the behaviour of permittivity and the loss factor with the ac amplitude of the Mn doped and undoped $BaTiO_3$. Figures IV.23 and IV.24 shows their behaviour after annealing and quenching treatments in air. At any change of unit field the change in permittivity and loss factor decreases with increasing Mn concentration. The quenched samples of higher Mn concentration showed the domain stabilisation. Figures IV.25 and IV.26 show their variation with ac amplitude, after quenched in the low partial pressure of oxygen. The stabilization strengthened still further because of the increase in the V_o concentration and therefore more TM-V_o alignment depends upon Mn concentration. Figures IV.27 and IV.28 show the permittivity and loss factor dependence with the ac field; these samples are quenched in the oxygen atmosphere. The behaviour is similar to the air sintered samples one and no stabilization is found out. Compared to the low partial pressure of oxygen treatment the loss involved here is quiet high because of the reduction of the V_o concentration and so the absence of effective TM-V_o alignment. Figure IV.29 shows the calculated oxygen vacancy (14,19) with various Mn concentration and with various P_{O_2}. Oxygen vacancy concentration increases with increasing Mn concentration and also with decreasing the partial pressure of oxygen. It is clear that the samples with proper TM-V_o alignment show the less loss current compared to the other

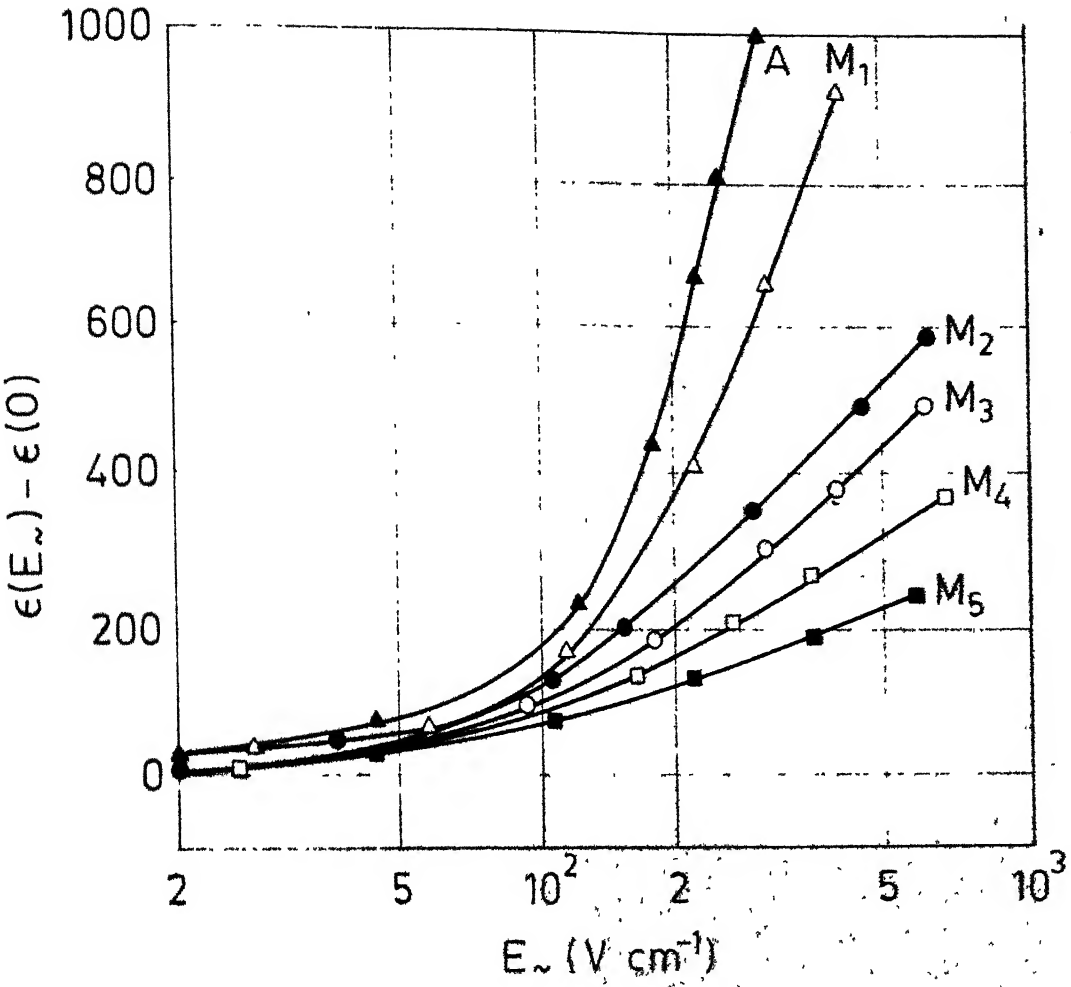

Fig. IV.21. Dependence of ϵ on the amplitude of the external AC field measured at T = 28 °C and f = 1 KHz. Well aged sintered samples (1350 °C/2 hrs) air atmosphere.

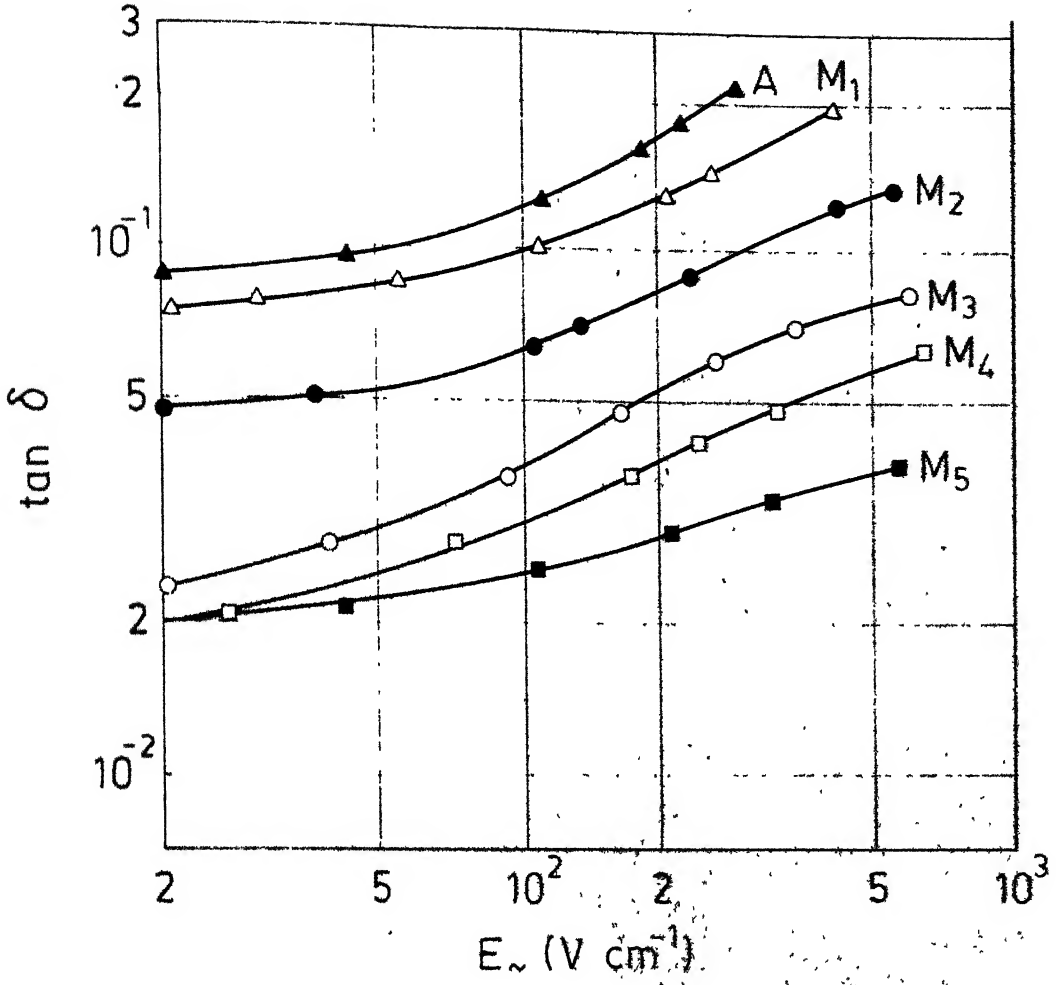

Fig. IV.22. Dependence of the loss factor tan δ on the amplitude of the external AC field. Measured at T = 28 °C and f = 1 KHz. Well aged sintered samples. [Sintered at 1350 °C/ 2 hrs in air atmosphere]

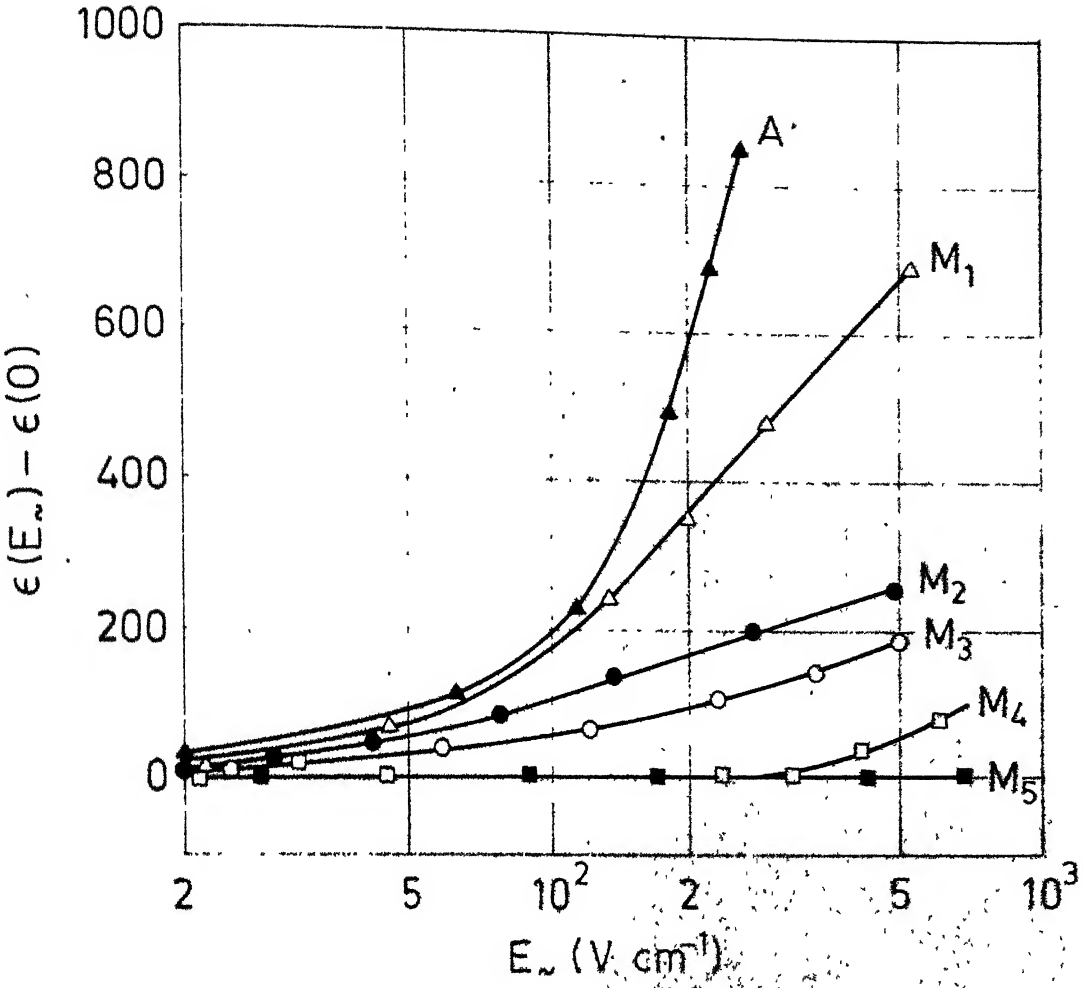

Fig. IV.23. Dependence of ϵ on the amplitude of the external AC field. Measured at 28 °C and f = 1 KHz. Samples were annealed at 1100 °C for 10 min and quenched to room temp. in air atmosphere at 1350 °C/2 hrs.

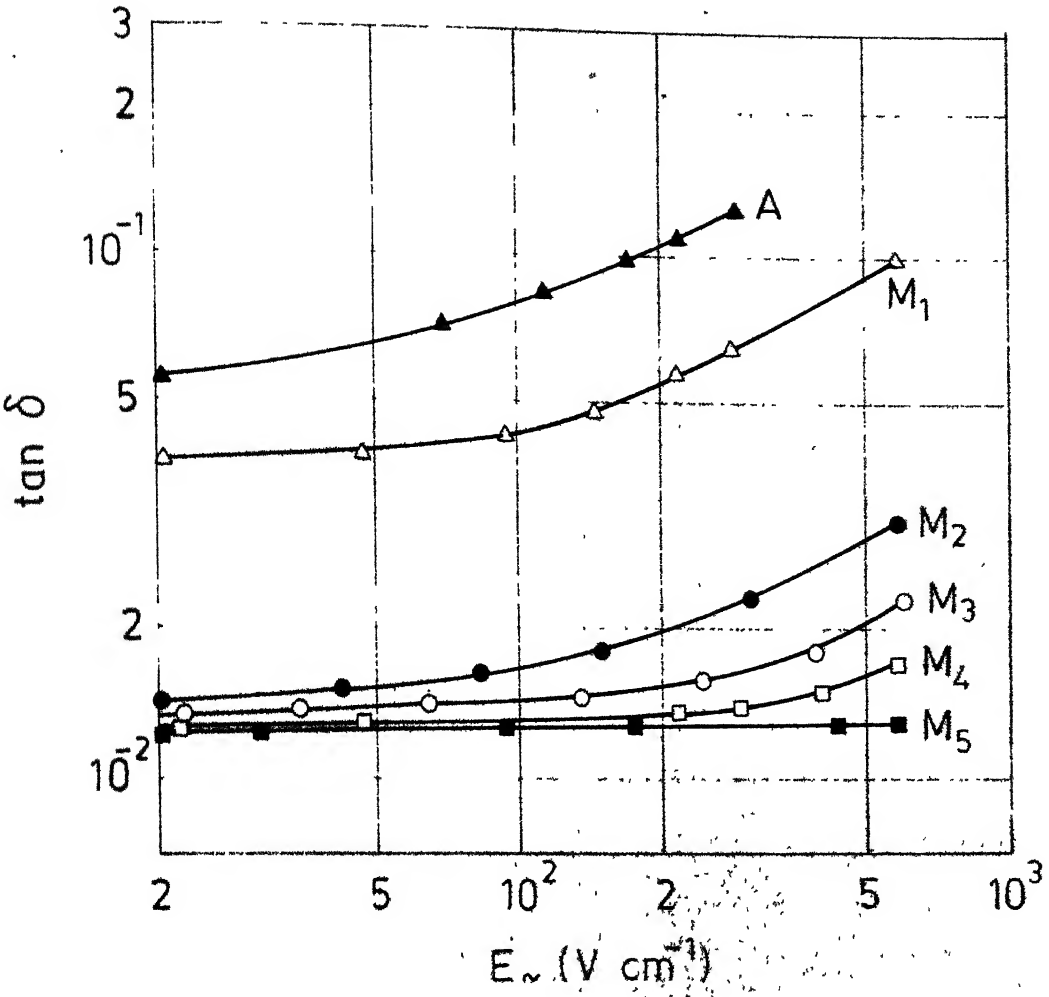

Fig. IV.24. Dependence of the loss factor tan δ on the amplitude of the external AC field. Measured at T = 28 °C and f = 1 KHz. Samples were annealed at 1300 °C for 10 min and quenched to room temp. in air atmosphere. [Sintered in air atm. at 1350 °C/2 hrs]

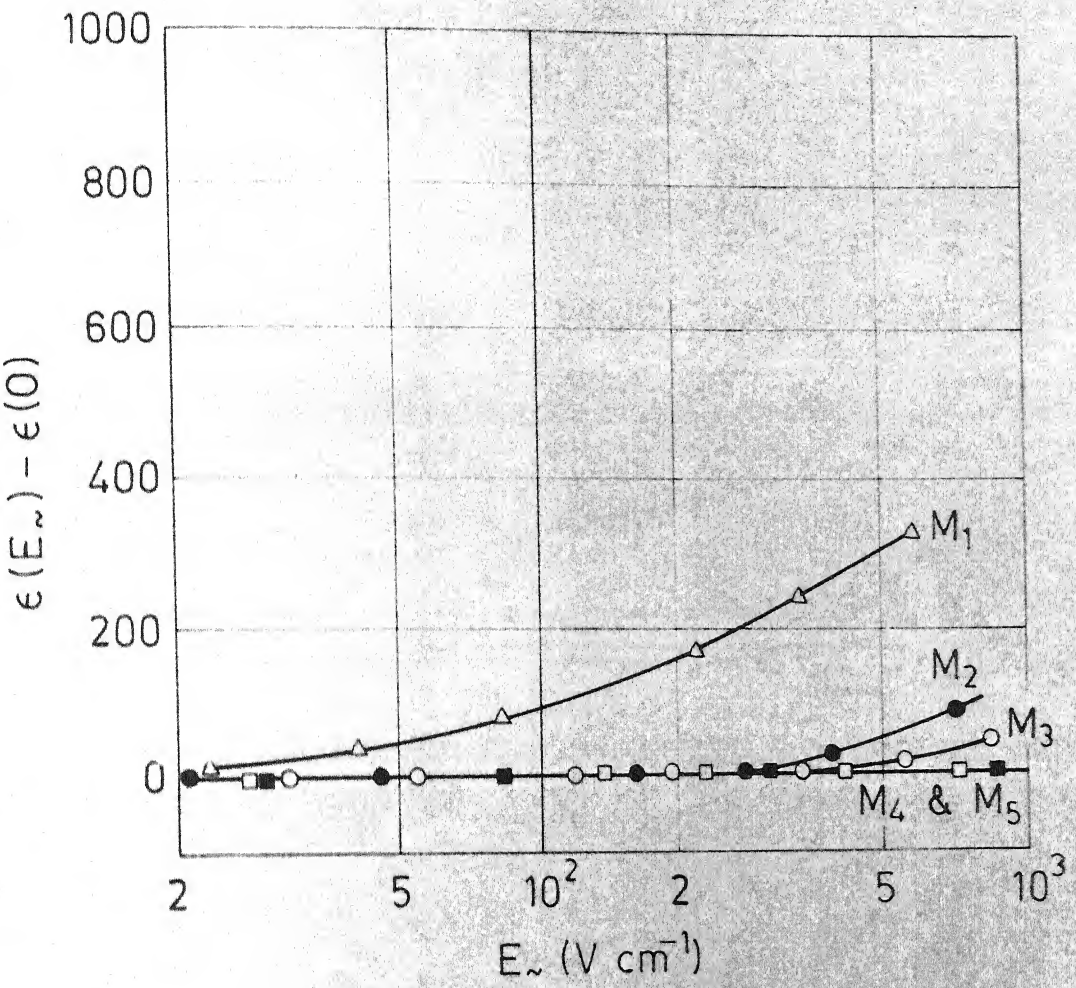

Fig. IV.25. Dependence of ϵ on the amplitude of the external AC field. Measured at T = 28 °C and f = 1 KHz. Samples were annealed at 1300 °C for 10 min and quenched to room temp. in the low partial pressure of oxygen ($PO_2 = 10^{-12}$ atm [Sintered in the purified argon with $PO_2 = 10^{-12}$ atm at 1350 °C/2 hrs].

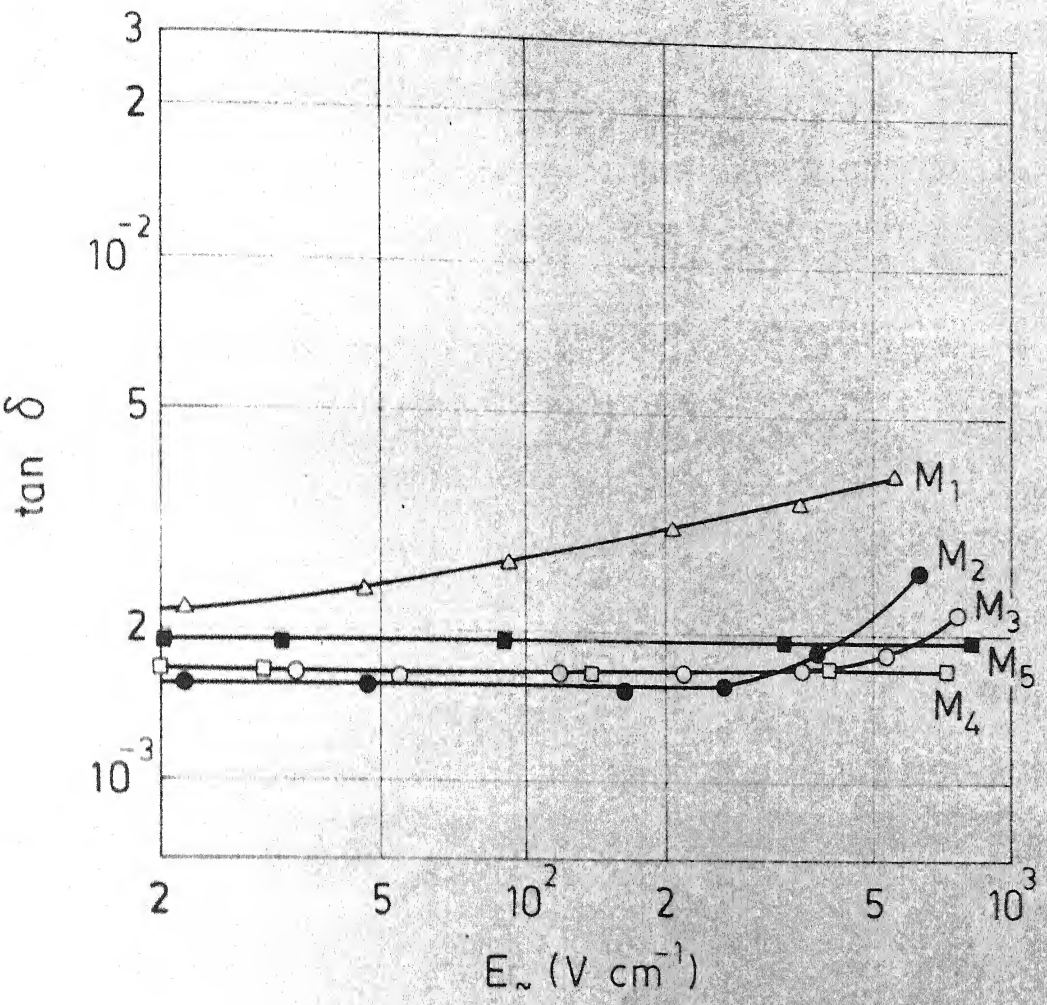

Fig. IV.26. Dependence of the loss factor tan δ on the amplitude of the external AC field. Measured at T = 28 °C and f = 1 KHz. Samples were annealed at 1300 °C for 10 min and quenched to room temp. in the low partial pressure of oxygen ($PO_2 = 10^{-12}$ atm). [Sintered in the purified argon with $PO_2 = 10^{-12}$ atm. at 1350 °C/2 hrs]

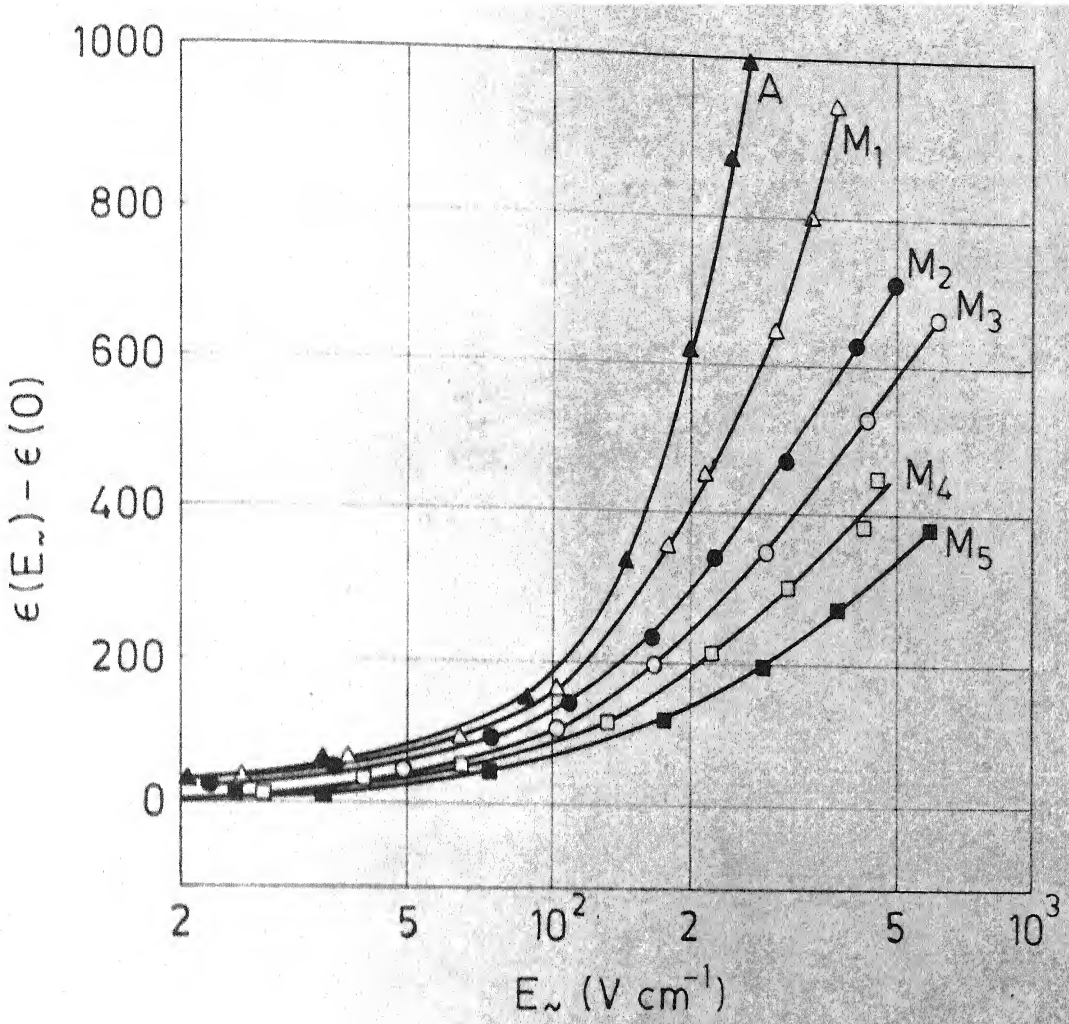

Fig. IV.27. Dependence of ϵ on the amplitude of the external AC field. Measured at T = 28 °C and f = 1 KHz. Samples were annealed at 1300 °C for 10 min and quenched to room temp. in the oxygen atmosphere. [Sintered in the oxygen atm. at 1350 °C / 2 hrs]

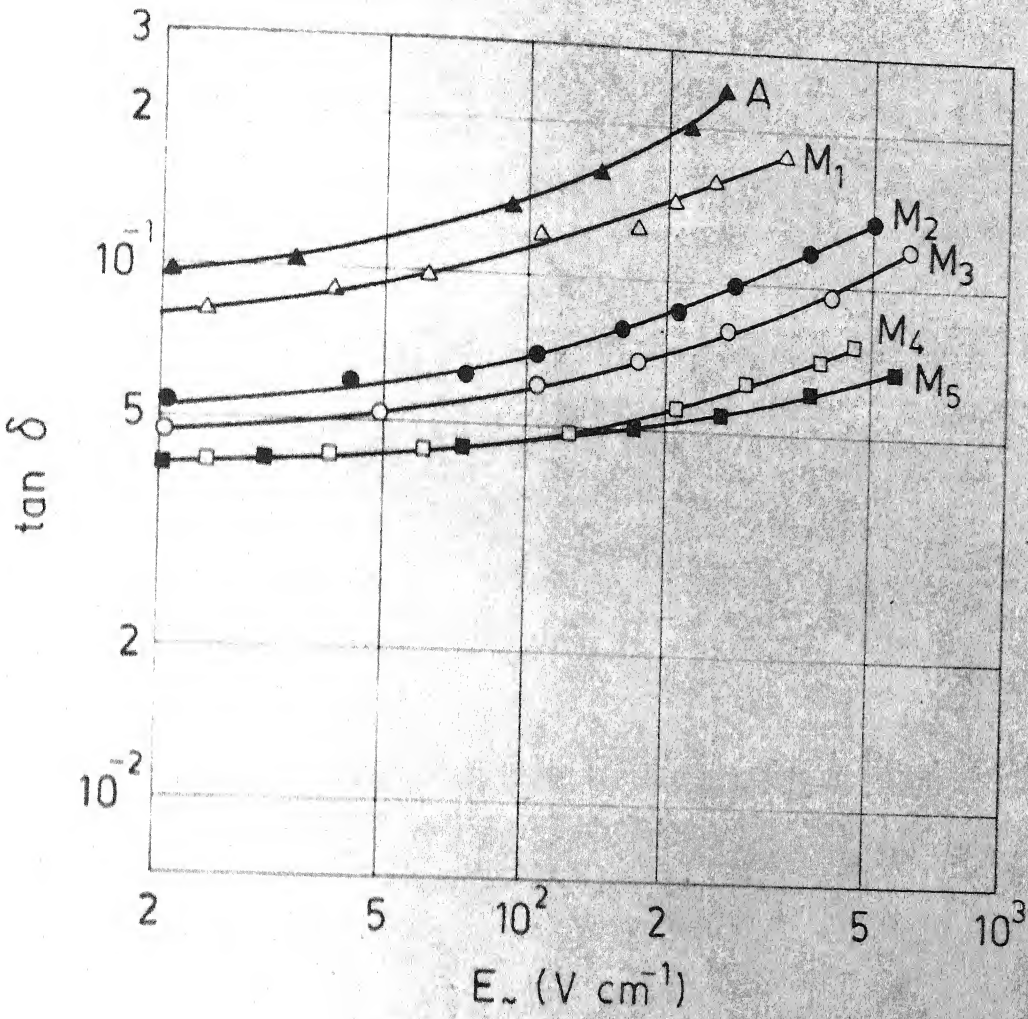

Fig. IV.28. Dependence of the loss factor tan δ on the amplitude of the external AC field. Measured at $T = 28\,^{\circ}C$ and $f = 1$ KHz. Samples were annealed at 1300 °C for 10 min and quenched to room temp. in the oxygen atm. [Sintered in the oxygen atm at 1350 °C/2 hrs]

(i)

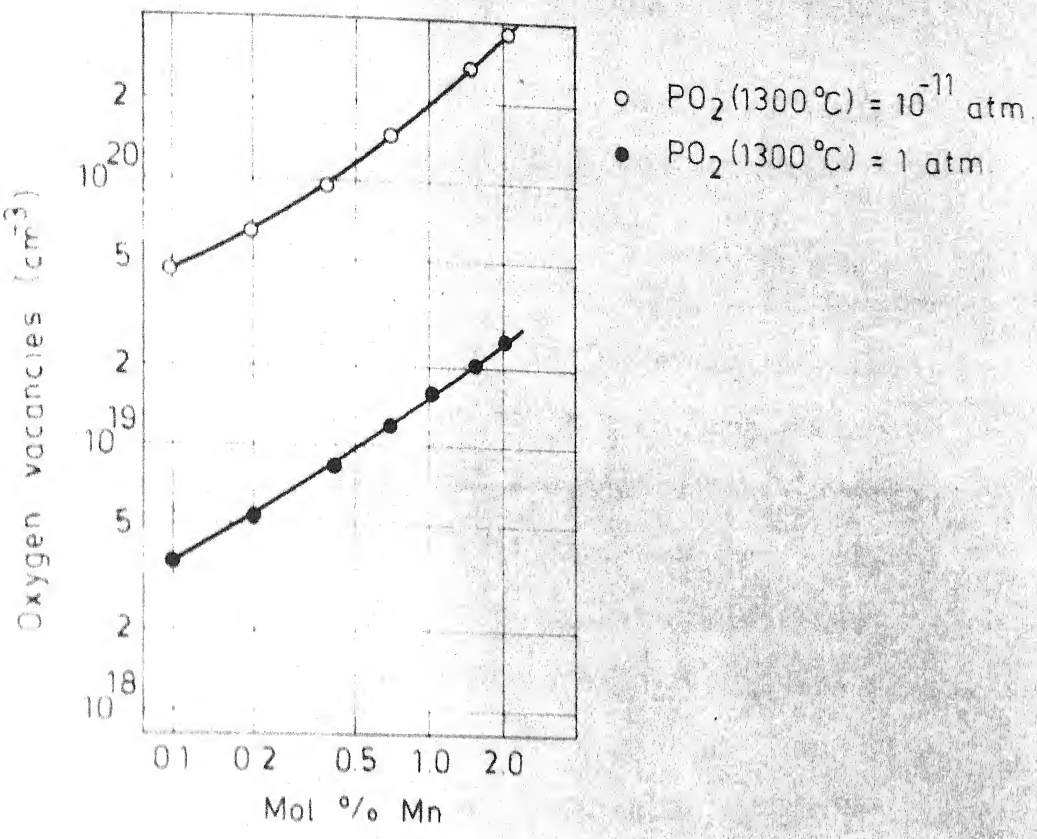

(ii)

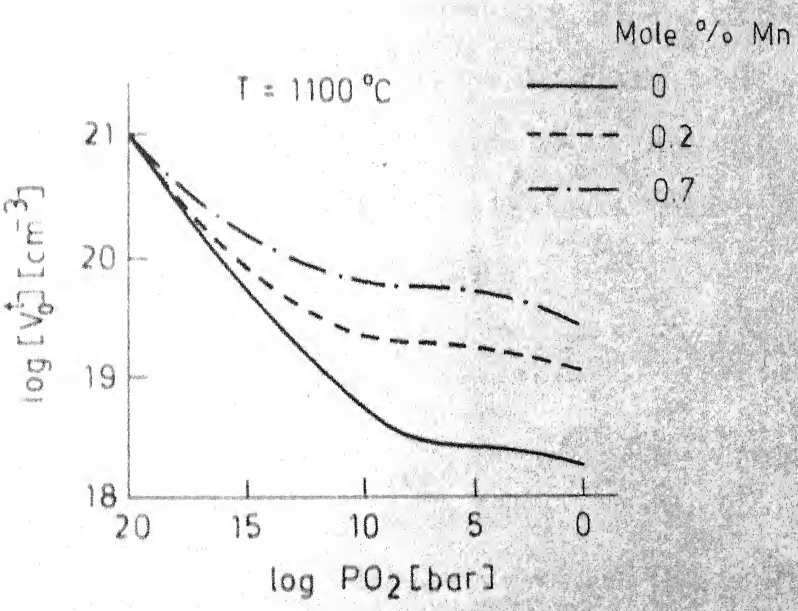

IV.29. Calculated total oxygen vacancy concentration $[V_O^t] = [V_O] + [V_O^{\cdot}] + [V_O^{\cdot\cdot}]$ in the Mn-doped $BaTiO_3$. (i) as a function of Mn concentration and (ii) as a function of the oxygen partial pressure.

ones. In all the cases the samples are having a regular trend of behaviour and showing the expected nature of the acceptor doped sample.

Hagemann (14) reported that the effect of acceptor doping on the small-signal dielectric losses is not likely to originate from domain effects but rather from a change of the low frequency relaxational response of the material. This is because, the change of loss with frequency, of the doped samples, is greater compared to that of the pure ceramic. Figure IV.30 shows the frequency dependence of the loss factor for pure and acceptor doped $BaTiO_3$. Here fine grained pure $BaTiO_3$ also exhibits the greater change of loss with frequency whereas the $BaTiO_3$ prepared from $BaCO_3$ and TiO_2 does not have this behaviour. At any frequency, the Mn doped sample show the less loss current value compared to the undoped one. It seems that apart from the acceptor doping, the fine grains also have this effect of low frequency relaxational response.

IV.3.6. Annealing in H_2:

These studies have been carried out to get the optimum concentration of Mn which will give high resistivity bodies of $BaTiO_3$ even if they are treated in reducing atmospheres. From the Table IV.13 one can see that all the Mn doped compositions are showing higher resistivity in H_2 annealing at high temperature compared to the undoped one. Compositions B and C are retaining their resistivity

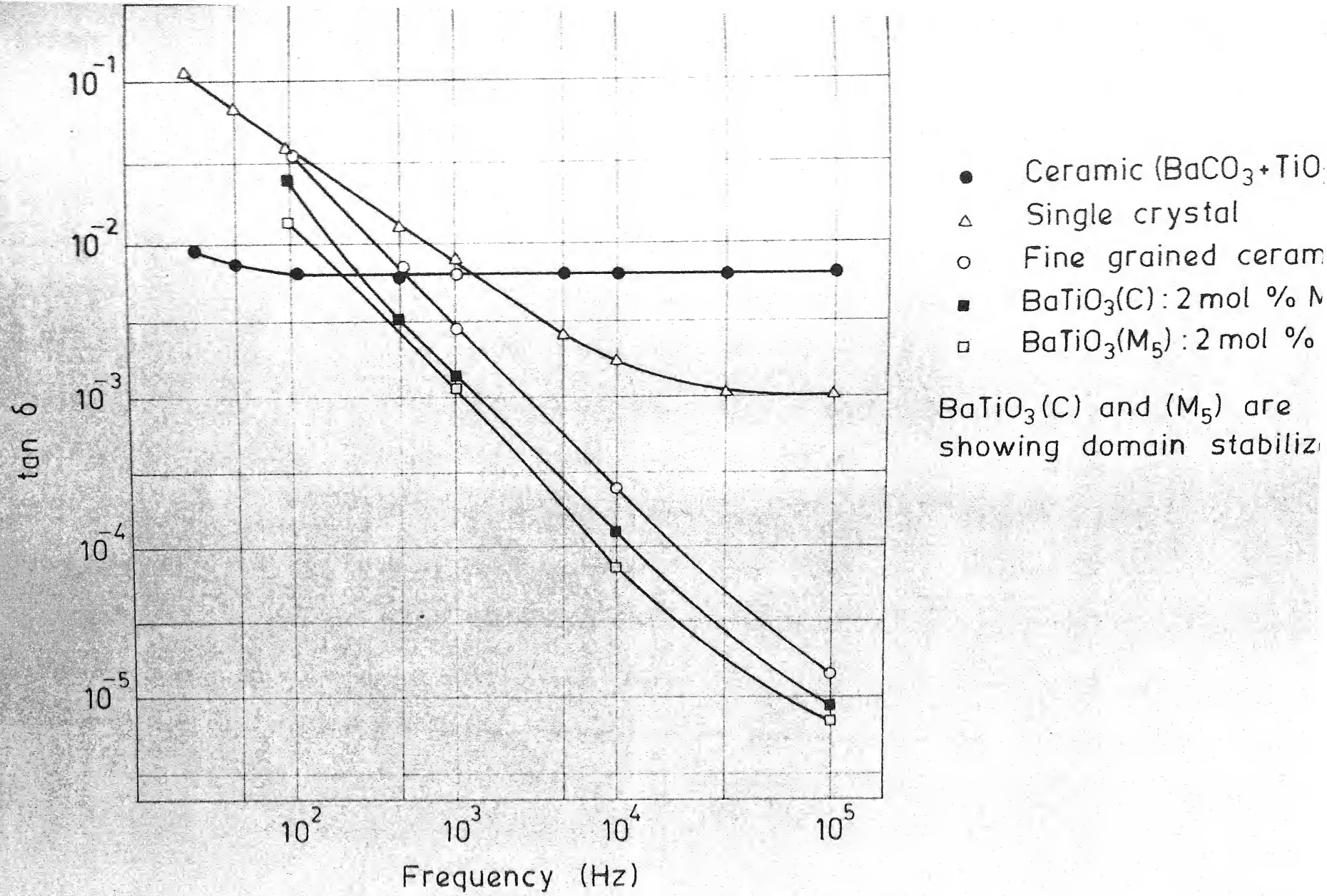

Fig. IV.30. Frequency dependence of tan δ for pure and doped $BaTiO_3$. Well aged samples.

Effect of annealing, in H_2 on the different properties of the Mn-$BaTiO_3$, at various temperatu

Compositions	Annealing temperature in H_2	500°C			700°C			900°C			1100°C		
		log ρ	K	tanδ	log ρ	K	tanδ	log ρ	K	tanδ	log ρ	K	
$BaTiO_3$(A)		10.0	2500	0.07	8.5	2800	0.08	5.0	2900	0.15	2.0	-	
$BaTiO_3$(B)		10.0	3400	0.03	9.5	3700	0.03	9.0	2900	0.09	4.0	-	
$BaTiO_3$(C)		10.5	3000	0.018	10.1	3500	0.019	10.0	3100	0.05	6.5	1900	0
$BaTiO_3(M_1)$		10.0	2600	0.03	9.0	2650	0.04	5.0	2140	0.15	3.5	-	
$BaTiO_3(M_2)$		10.2	2650	0.03	9.5	2800	0.04	8.2	2450	0.09	7.0	1975	0
$BaTiO_3(M_3)$		10.0	2540	0.041	9.1	2600	0.05	8.2	2520	0.07	7.5	2400	0
$BaTiO_3(M_4)$		10.5	2800	0.04	9.5	3000	0.04	9.0	2750	0.07	8.0	2520	0.
$BaTiO_3(M_5)$		10.5	3300	0.04	10.0	3750	0.04	9.0	3500	0.061	8.2	2600	0.

upto 900°C but not at 1100°C; among M_1, M_2, M_3, M_4 and M_5, M_4 and M_5 are showing the better properties at 1100°C compared to all the other samples. From the table one can conclude that to produce BME disc capacitors by using Ni-frit glass electrode, minimum concentration required to get the good properties of the $BaTiO_3$ dielectric is 0.6 mole percent of composition M_2 or 2.0 mole percent of composition C.

IV.3.7. Annealing and Quenching in Various P_{O_2} at 1100°C:

With the application of the multilayer capacitor in mind, in order to prevent the oxidation of Ni in a given P_{O_2} at 1100°C these studies were carried out. Hagemann (15) reported the similar sutides on the samples prepared from $BaCO_3$ and TiO_2. To prevent the oxidation of Ni the partial pressure P_{O_2} of oxygen at 1100°C should be lower than 10^{-10} bar. Table IV.14 shows the variation of the resistivity with P_{O_2}. With decreasing P_{O_2} (down to the lower partial pressure of oxygen) the resistivity of the undoped and Mn doped $BaTiO_3$ decreases, but the amount of decrease is higher in the case of 0 percent and lightly doped samples compared to the higher Mn doped samples. In the Ni/NiO partial pressure of oxygen, $P_{O_2} = 10^{-10}$ atm., the minimum concentration of Mn required to retain the high resistivity is 0.6 mol percent (M_2) in the case of Group III compositions, and 2 mol percent (C) in the case of Group I compositions. In this range undoped $BaTiO_3$ exhibits high conductivity.

Table IV.14

Variation of resistivity with P_{O_2} -samples annealed and quenched in various partial pressures oxygen at 1100°C/30 minutes: Sintered in air at 1350°C/2 hrs

Compositions	P_{O_2} (atm.): 9.0×10^{-15}	2.0×10^{-13}	1.0×10^{-10}	2.5×10^{-5}	2.1×10^{-1}	O_2 ($\frac{100}{sec}$
	Resistivity (ohm-cm)					
$BaTiO_3$(A)	5×10^{2}	1.1×10^{3}	5.0×10^{4}	1.2×10^{8}	2.0×10^{11}	5.0×10^{9}
$BaTiO_3$(B)	5.1×10^{5}	1.5×10^{7}	3.5×10^{7}	1.2×10^{9}	6.0×10^{10}	7.1×10^{1}
$BaTiO_3$(C)	2.0×10^{6}	1.0×10^{8}	4.2×10^{8}	1.0×10^{9}	8.0×10^{9}	8.5×10^{9}
$BaTiO_3(M_1)$	1.2×10^{3}	1.0×10^{5}	2.0×10^{5}	3.0×10^{8}	5.0×10^{10}	5.0×10^{1}
$BaTiO_3(M_2)$	1.0×10^{6}	1.1×10^{7}	1.08×10^{8}	5.0×10^{8}	1.2×10^{10}	1.6×10^{1}
$BaTiO_3(M_3)$	2.0×10^{7}	1.0×10^{8}	5.0×10^{8}	1.2×10^{9}	1.0×10^{10}	1.1×10^{1}
$BaTiO_3(M_4)$	1.2×10^{8}	1.5×10^{9}	3.0×10^{9}	8.11×10^{9}	9.0×10^{9}	1.1×10^{1}
$BaTiO_3(M_5)$	3.1×10^{8}	3.4×10^{9}	4.5×10^{9}	6.6×10^{9}	8.2×10^{9}	1.2×10^{1}

IV.3.8. Behaviour of the Ni Electroded Capacitors:

This study was done to measure the capacitance and the loss factor of the Ni electroded Mn-doped sample. Table IV.15(A) shows, the values of C and tanδ of the Ni electroded Mn compositions after treated in H_2 at 900°C for 1 hr. After the heat treatment in Hz, the continuity of the electrode was checked; the resistance is less than 0.7 ohms. Electrode adhered very well to the pellet samples.

Table IV.15(A)

Ni electroded samples: Treated in H_2 at 900°C for 60 minutes

Composition	Dielectric constant	Loss factor
$BaTiO_3(C_1)$	3200	0.070
$BaTiO_3(M_5)$	3500	0.082

In order to compare the behaviour of the Ni electrode, Ni was removed and Ag was applied. Their behaviour is, shown in Table IV.15(B).

Table IV.15(B)

Ag electroded on the samples which were previously coated with Ni electrode

Composition	Dielectric constant	Loss factor
$BaTiO_3(C_1)$	3200	0.050
$BaTiO_3(M_5)$	3500	0.061

Very little change in loss value proves the effectiveness of Ni electrode and also the doping.

IV.3.9. Temperature Dependence of Resistivity of Pure and Mn-doped $BaTiO_3$:

Figure IV.31 shows the variation of the resistivity of the samples with temperature. It is clear in the case of Group III, the resistivity at any temperature was found to decrease with Mn content. This indicates that acceptors are more or less fully ionized. But Samples B and C behaving in a different way.

IV.4. EFFECT OF THE STRONG REDUCING ATMOSPHERE ON THE PROPERTIES OF THE Mn-DOPED COMPOSITIONS:

The samples were sintered at 1350°C for 2 hrs. in dry H_2 (60 cc/sec). The partial pressure of oxygen which will be produced in this condition is approximately 10^{-18} atm. Table IV.16 summarizes the properties of the samples. The permittivity of the composition (C) is very high with low loss factor. In the strong reducing atmosphere $BaTiO_3$ will become semiconductive, and therefore the loss involved is very high.

In the strong reducing atmosphere Mn will be reduced to Mn^{+2} and a separate MnO phase start to appear (10).

This experiment shows that the strong reducing atmosphere is not advisable to sinter the Mn doped samples.

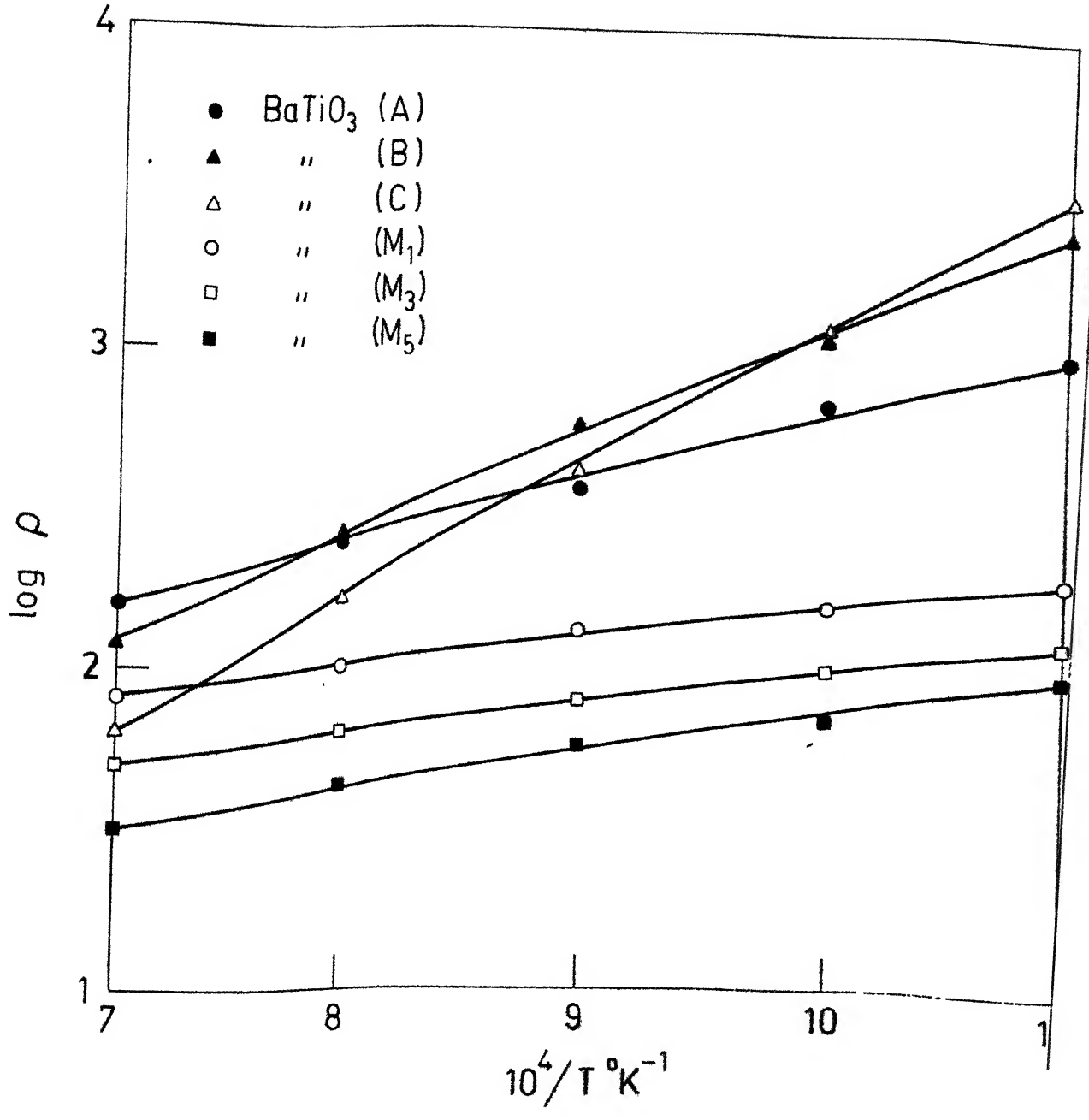

Fig. IV.31. Variation of resistivity with temperature for the und and Mn-doped BaTiO .

Table IV.16

Effect of strong reducing sintering on the properties of Mn-doped samples

Composition	ε	tanδ	at R.T. (ohm-cm)
$BaTiO_3$(A)	-	-	2.2×10^2
$BaTiO_3$(B)	26,000	0.4	3.0×10^5
$BaTiO_3$(C)	40,000	0.251	2.5×10^5
$BaTiO_3(M_1)$	-	-	1.25×10^3
$BaTiO_3(M_2)$	22,000	0.500	4.0×10^5
$BaTiO_3(M_3)$	30,000	0.65	5.0×10^5
$BaTiO_3(M_4)$	>1 million	0.99$^{\varphi}$	1.5×10^6
$BaTiO_3(M_5)$	>1.5 million	0.99$^{\varphi}$	5.1×10^6

φ The loss factor could be covered by GR 1615-A is 0.99. Approximate ε values, at tanδ = 0.99, are reported.

V. SUMMARY AND CONCLUSIONS

Mn-doped $BaTiO_3$ prepared by oxalate method (when Mn added to the Ba and Ti solutions and then precipitated as Mn-doped BTO) was studied thoroughly in order to understand the role of Mn. In this, Mn behaved both like a donor and an acceptor dope. $BaTiO_3$ samples of this kind do not have any regular trend like the acceptor doped $BaTiO_3$ prepared from $BaCO_3$ + TiO_2 mixtures. The domain stabilization behaviour of these samples were achieved by annealing them in the low partial pressure of oxygen. Samples of this kind shown very high dielectric constant (~50,000) with low loss (< 0.25), when they were sintered in strong reducing atmosphere at 1350°C for 2 hrs. These samples might help to develop the high value capacitors.

The role of Mn when precipitating along with the Barium Titanyl oxalates was studied and hence a reasonably good dielectric composition was developed for the BME technology. The suspected mechanism of reduction, oxidation and subsequent function of higher oxalate group of Mn was explained. The development of the doping was necessiated, because the doping procedure has a marked influence on the properties of Mn doped $BaTiO_3$. It is due to the fact that Mn has three important oxidation states (+2, +3 and +4) and in different oxidation states it may occupy different sites.

The influence of Mn on the decomposition of BTO was studied by DTA and TGA. Mn doped BTO's (samples of

Group III), show the decrease in the peak temperatures and this trend increases with increasing Mn concentration. Mn doping also affected the change in enthalpy peaks mainly the one which corresponds to the main oxalate decomposition. A decomposition scheme for the pure BTO has been proposed in order to calculate and compare with the observed weight losses. The comparison of the weight losses between the undoped and the one doped with 2 mol percent Mn (Group III), showed that (i) in the Mn doped BTO, the water of crystallization is less compared to the pure BTO; (ii) in the main oxalate decomposition, the evolution of CO group is large for Mn doped BTO, compared to the undoped BTO; (iii) in the final decomposition there is a slight decrease in amount of O_2 evolution in the doped case.

IR technique has been used successfully to detect the acceptance of Mn by BTO. The Ti-O peak has been shifted to higher frequency. This combined with the DTA and TGA analysis show indirectly that Mn got into the compound BTO with its higher oxidation oxalate group.

The dielectric constant and loss factor of the Mn-doped samples of group III showed the regular trend of decreasing nature and the Mn-doped samples of group I showed the unusal behaviour that the dielectric constant of doped samples are higher compared to the undoped one.

The domain stabilization studies of the Mn doped samples of Group III showed that (i) domain stabilization has been improved by the quenching from the higher

temperatures and it has been improved still further by carrying out the quenching in the low partial pressure of oxygen, and (ii) the change in permittivity and loss factor with ac field decreases with increasing concentration of Mn. The frequency dependence of the loss factor study showed that apart from the acceptor doped sample, pure $BaTiO_3$ of the present study (fine grain material) also showing the large variation of loss with frequency and the loss decreases with increasing frequency. But ceramic $BaTiO_3$ prepared from $BaCO_3$ and TiO_2 does not have this effect. Like in the case of Mn-doped samples, the fine grained $BaTiO_3$ ceramic also might have the low frequency relaxational response.

The electrical resistivity behaviour of the Mn-doped $BaTiO_3$, with the application of BME disk and multilayer capacitors in mind, was investigated (i) by annealing the material in hydrogen over a wide range of temperatures (500, 700, 900 and 1100°C) and (ii) by annealing and quenching the material at 1100°C in the various partial pressures of oxygen (P_{O_2}). These studies show that Mn-doped $BaTiO_3$ with higher Mn concentration retains its resistivity at the extreme temperature and P_{O_2} conditions, whereas undoped $BaTiO_3$ showed large conductivity. From these studies one can conclude that the minimum concentration of 0.6 mol percent Mn (M_2) and 2.0 mol percent Mn (C) doped $BaTiO_3$ can be used to produce BME disc capacitors and M_2 itself could be used to produce BME multilayer capacitors.

Nickel electroded capacitors with good dielectric properties were prepared.

APPENDIX I

CHEMICAL ANALYSIS

INTRODUCTION

To determine the Barium and Titanium in the $BaTiO_3$ which was prepared from Barium titanyl oxalate method the following procedure is used which is essentially the one Clabaugh (21) and Desu (6) followed. The preparation of $BaTiO_3$ is from BTO, so in the case of pure $BaTiO_3$, it is necessary to check the Ti to Ba mole ratio is unity and in the case of Mn-doped $BaTiO_3$, since Mn is expected to occupy Ti site, to know the respective Ti to Ba ratio that depends upon dopant concentration. The error involved in this method is negligibly small and care has been taken for the interference of Mn with Ba or Ti values.

EXPERIMENTAL PROCEDURE

About 0.5 g of barium titanate is accurately weighed and digested with 15 ml concentrated hydrochloric acid by heating gently until the yellow colour of the solution disappears. To this 15 ml of water is added and boiled gently until the sample dissolves completely. This is further diluted to 100 ml and to this 50 ml of a 3 percent solution of EDTA is added. The acidity is adjusted to pH 3.5 to 4.0 with diluted ammonium hydroxide. The resulting solution is boiled and the barium is precipitated as barium sulphate by adding 20 ml of a 25 percent

solution of ammonium sulphate. This is digested on the steam bath until the barium sulphate precipitates and the supernatant liquid becomes clear. The precipitate is removed by filtration, washed with water, ignited in a previously weighed silica crucible and weighed as $BaSO_4$. From this weight of $BaSO_4$ the percentage by weight of Ba is calculated.

The combined filtrate and washings are concentrated to about 100 ml, acidified with 20 ml concentrated sulphuric acid and cooled to $10^{\circ}C$. To the cooled solution a freshly prepared 5 percent aqueous cupferron solution is added slowly and with constant vigorous stirring. First a yellow precipitate of titanium cupferrate is formed and the addition of the cupferron reagent is continued till the formation of a white precipitate. The formation of a white precipitate indicates that the reagent is present in excess. The precipitate is removed by filtration while it is cold through a No. 41 filter paper. This is washed several times with 10 percent by volume of sulphuric acid containing 1.5 g of cupferron per litre, then twice with 5 N ammonia solution to remove excess of cupferron and finally once with water. The precipitate is ignited in a previously weighed silica crucible gently at first and then strongly. This is weighed as TiO_2. From this weight of TiO_2 the percentage by weight of Ti is calculated. The mole ratio Ba/Ti is calculated from the percentages of Ba and Ti.

In manganese doped barium titanate samples the manganese is also precipitated along with titanium and converted as Mn_2O_3 on ignition. The ignited sample is treated with concentrated hydrochloric acid, which will dissolve the Mn_2O_3. This is filtered, washed with water, ignited in a previously weighed silica crucible and weighed as TiO_2. The mole ratio Ba/Ti is calculated as mentioned above.

APPENDIX II

OXYGEN SENSOR

This is an oxygen sensor using a calcia stabilized zirconia solid state electrolyte with platinum electrodes to measure trace amounts of oxygen in a flowing argon-oxygen gas mixture (24). Figure AII.1 shows the schematic representation of the oxygen sensor unit.

PRINCIPLE:

In an oxygen concentration cell of the type

$$(-)\ Ar\text{-}O_2/ZrO_2\text{-}CaO/O_2\ (+)$$

in which the electrolyte has an average, ionic transport number, $\bar{t}_i = 1$, the electromotive force of the cell, E is given by

$$E = \frac{RT}{4F} \ln \frac{P''_{O_2}}{P'_{O_2}} \qquad \text{(AII.1)}$$

where P''_{O_2} and P'_{O_2} are the oxygen pressures at the cathode and anode, respectively. R the universal gas constant, T the absolute temperature in ^{o}K and F the Faraday's constant.

Ideal gas behaviour i.e. fugacity = pressure is assumed. In the present study $P''_{O_2} = 0.21$ atm, since air is used as the reference electrode. Taking R = 1.987 cal $mol^{-1}\ {}^{o}K^{-1}$ and F = 23061 cal per volt equivalent in

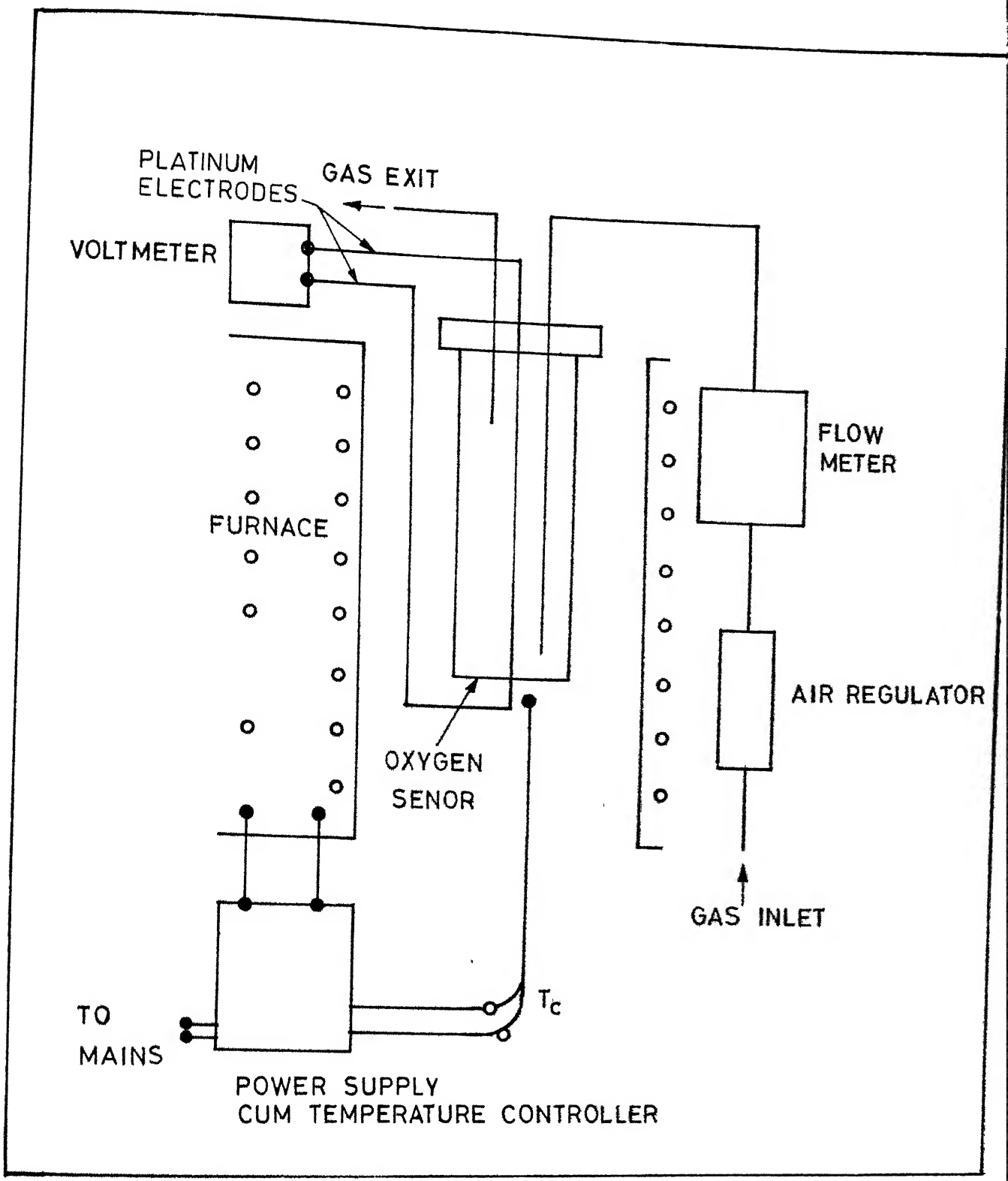

Fig. AII.1. Oxygen sensor unit.

equation (AII.1) yields

$$\log \frac{P'_{O_2}}{0.21} = -\frac{20.159\ E}{T} \qquad \text{(AII.2)}$$

or alternatively

$$E = 0.0496\ T \log \frac{0.21}{P'_{O_2}} \qquad \text{(AII.3)}$$

where E is in abs mV, T is in ^{o}K and P'_{O_2} in atm.

CALIBRATION:

By using the calibrated Flow meter known amount of Argon-Oxygen gas mixture could be passed into the oxygen sensor and the developed emf measured by using the platinum electrodes. The experimental value was very well agreed with the calculated one by using the eqn. (AII.3). Figure AII.2 shows the calibration of the oxygen sensor.

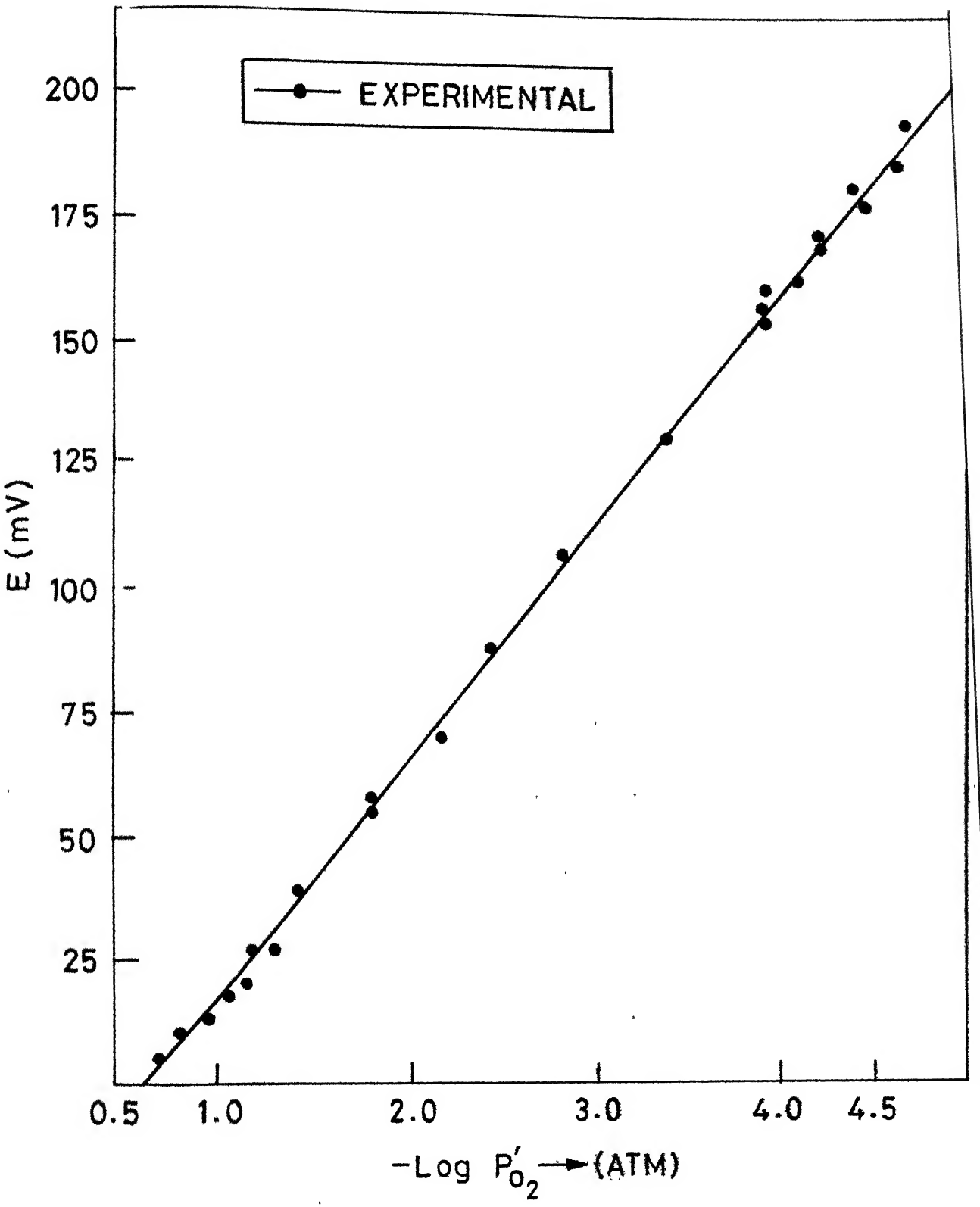

Fig. AII.2. E Vs $-\log P'_{O_2}$

APPENDIX III

FORMATION OF ELECTROCHEMICAL CELL TO STUDY THE DOPING MECHANISM OF Mn

While preparing Mn-doped BTO of Group II two main points were noticed.

(i) When Mn^{+2} was added to the barium oxalate solution with the excess of oxalic acid, the barium oxalate started to disappear;

(ii) In the same solution if $TiCl_4$ was added in drops, the solution turned into reddish brown colour immediately.

First point proves the reduction of Mn and the second, the oxidation.

To confirm, two electrochemical cells were formed:

(i) Barium oxalate solution with excess of oxalic acid and manganous solution were taken. Metallic Mn attached with Pt was dipped into the manganous solution and the other Pt-lead was dipped into the barium oxalate solution. The voltage of 900 mV was developed as soon as the sodium oxalate salt bridge connected the two solutions. After few hours, the voltage started to reduce and the metallic Mn was taken out. Gain in weight proved the reduction process of Mn in the presence of other cationic oxalate.

(ii) The same set up was taken again but instead of barium oxalate, dilute titanium tetrachloride with small

amount of oxalic acid was taken. The developed voltage in this case was 500 mV.

Here, the metallic Mn started to give bubbles. Moreover dull brown colouration was observed in Mn beaker. To check further, metallic Mn was treated with the following and various colourations were observed:

HCl	:	Enormous amount of bubbles and dull pink colouration due to Mn^{2+}.
Aqueous $TiCl_4$	:	Enormous amount of bubbles and intense purple or voilet colour due to Mn^{7+}.
Dilute $TiCl_4$ + Oxalic acid solution	:	Enormous amount of bubbles and reddish brown colour due to Mn^{3+}.

These results confirmed the existence of redox system in the experiment.

REFERENCES

1. W.R. Buessem and T.I. Prokopowicz, Ferroelectrics, 10, 255 (1976).
2. J.L. Mukherjee and H.S. Ravishankar, in Proc. Symp. on Sintering and Sintered Products, Bombay, 281 (1979).
3. D. Hennings, Ber. Dtsch. Keram. Ges. 55, 359 (1978).
4. K.R. Chowdary and E.C. Subbarao, Ferroelectrics, 35, 668 (1981).
5. E.C. Subbarao, in Proc. Symp. on Sintering and Sintered Products, Bombay, 1 (1979).
6. S.B. Desu, M.Tech. Thesis, I.I.T. Kanpur (1979).
7. P.H. Eisenberg and H.C. Schneider, Plating, 42, 1269 (1955).
8. I. Burn, Amer. Ceram. Soc. Bull. 57, 600 (1978).
9. J.M. Herbert, Proc. IEE 112(7), 1474 (1965).
10. F.W. Ainger and J.M. Herbert, Trans. Brit. Ceram. Soc. 58, 410 (1959).
11. J.M. Herbert, Trans. Brit. Ceram. Soc. 62, 645 (1963).
12. S.B. Desu and E.C. Subbarao, Ibid. 15[8], 2113 (1980).
13. J.M. Daniels, Philips Res. Repts. 31, 505 (1976).
14. H.J. Hagemann, J. Phys. C. Solid State Phys. 11, 3333 (1978).
15. I. Burn, J. Mat. Sci. 14, 2453 (1979).
16. S.A. Long and R.N. Blumenthal, J. Amer. Ceram. Soc. 54, 515 (1971); Ibid. 54, 577 (1971).
17. N.H. Chan and D.M. Smyth, J. Electrochem. Soc. 123, 1585 (1976).
18. N.G. Eror and D.M. Smyth, J. Solid State Chem. 24, 235 (1978).
19. H.J. Hagemann, Ber. Dt. Keram. Ges (Nr. 7), 55, 353 (1978).

21. W.S. Clabaugh, E.M. Swiggard and R. Gilchrist, J. Res. N.B.S., 56, 289 (1956).

22. H.M. Landis, J. App. Phys., 36, 2000 (1965).

23. A.I. Vogel, A Textbook of Qua. Ino. Anys., Longman, 525 (1975).

24. E.P. George and T. Arulmozhi, A project report of Oxygen Sensor Set up., Met. IIT (1982).

25. J. Hrizo and E.C. Subbarao, Rev. Sci. Instr., 34, 8 (1963).

26. B.V. Striztkov, A.V. Lapitskiv and L.G. Blasov, Zh. Prikla Khim., 33, 2009 (1960).

27. O. Saburi, Chem. Abstr. 202j (1962).

28. P.K. Gallagher and F. Schery, J. Amer. Ceram. Soc., 46, 567 (1963).

29. P.K. Gallagher and J. Thomson Jr., J. Amer. Ceram. Soc., 48, 644 (1965).

30. M.S.G.K. Murthy, M.S. Rao and T.R.N. Kutty, J. Inorg. Nucl. Chem., 37, 891 (1975).

31. L.V. Novika and I.N. Balyaev, Zh. Neorg. Khim., 10, 294 (1965).

32. R.J. Panlener and R.N. Blumenthal, J. Amer. Ceram. Soc., 54, 610 (1971).

33. EDI: G.C. Pimentel, Chemistry: An expl. sci., W.H.F. and Co., 199 (1963).

34. H.G. Unruh and H.E. Muser, Z. Angew. Phys., 14, 121 (1962).

35. C.H. Jonker, J. American Ceramic Soc., 55, 57 (1972).

36. K. Okada, J. Phys. Soc. Japan, 16, 414 (1961).

37. E.S. Kirkpatrick, K.A. Muller and R.J. Rubins, Phys. Rev., A135, 86 (1964).

38. R. Aserway, W. Berlinger and K.A. Muller, Proc. 18th Amp. Congress, 145 (1974).

39. M. Nakahara and T. Murakami, J. Appl. Phys., 45, 3795 (1974).

40. Cotton and Whilkinson, Qua. Ing.,Chemistry (1970).